Université du Québec en Abitibi-Témiscamingue

MODÉLISATION DES ÉPIDÉMIES DE LA TORDEUSE DES BOURGEONS DE L'ÉPINETTE EN FORÊT BORÉALE QUÉBÉCOISE : DÉVELOPPEMENT ET APPLICATION DE NOUVELLES APPROCHES STATISTIQUES

Thèse par articles
présentée
comme exigence partielle
du doctorat sur mesure en modélisation écologique

Par
Olaloudé Judicaël Franck OSSE

Septembre 2025

PRÉSENTATION DU JURY

Cette thèse a été évaluée par le jury composé des membres suivants :

- Prof. Flavia Braghiroli, présidente du jury
  Université du Québec en Abitibi-Témiscamingue
- Prof. Dominique Gravel, évaluateur externe
  Université de Sherbrooke
- Prof. Yan Boulanger, évaluateur externe
  Ressources naturelles Canada
- Prof. Miguel Montoro Girona, directeur de recherche
  Université du Québec en Abitibi-Témiscamingue

et a fait l'objet d'une soutenance le 02 septembre 2025 à l'Université du Québec en Abitibi-Témiscamingue.

REMERCIEMENTS

Il me paraît opportun d'exprimer, avec une profonde humilité et une sincère reconnaissance, l'ensemble de mes remerciements à l'égard de toutes les personnes ayant contribué de manière déterminante à l'élaboration de ce doctorat au cours des dernières années. Bien que les mots puissent paraître insuffisants pour traduire l'étendue de ma gratitude, il convient de souligner ici l'importance de votre soutien constant, de votre bienveillance et de la pertinence de vos conseils. La collaboration étroite avec chacun d'entre vous a constitué non seulement un privilège, mais également une expérience académique enrichissante, marquant durablement mon parcours de recherche.

Je souhaite tout particulièrement remercier le Professeur Philippe Marchand pour son encadrement exceptionnel et distingué. Sa rigueur scientifique, son expertise pointue dans le domaine des analyses statistiques et sa direction avisée ont constitué un véritable pilier tout au long de ce parcours doctoral. Son soutien constant et sa confiance inébranlable en mes capacités m'ont permis de surmonter les défis inhérents à cette entreprise académique, tout en m'inspirant à poursuivre mes ambitions avec détermination et humilité.

Je tiens également à exprimer ma profonde gratitude au Professeur Miguel Montoro Girona pour ses conseils éclairés et son soutien indéfectible. Sa vision scientifique, ses suggestions pertinentes et sa disponibilité ont enrichi mon travail de recherche en apportant une perspective complémentaire essentielle à l'élaboration de ce projet. Son accompagnement a été une source précieuse d'inspiration et a contribué de manière significative à la réussite de ce doctorat.

Je tiens à exprimer ma gratitude la plus chaleureuse envers Debaly Max, l'une des rencontres les plus marquantes que j'aie faites depuis la France, et qui m'a finalement rejoint en tant que postdoctorant au CEF. Les innombrables heures passées au téléphone à échanger sur nos parcours respectifs, à partager nos aventures et à mener des débats passionnés, tant politiques que scientifiques, ont été une source inestimable de joie et de réflexion. Notre fructueuse collaboration sur l'un de mes

articles, nos inoubliables excursions de pêche sur les lacs d'Abitibi, ainsi que nos soirées et week-ends à jouer à la belote, demeurent autant de moments ayant profondément marqué cette période de mon parcours. Son amitié et son enthousiasme ont assurément contribué à enrichir cette expérience.

La concrétisation de ce projet a été rendue possible grâce au soutien financier déterminant du Conseil de recherches en sciences naturelles et en génie du Canada (CRSNG), via son programme Alliance axé sur la compréhension de la dynamique de la tordeuse des bourgeons de l'épinette, ainsi que par l'entremise de la subvention Découverte visant à reconstituer le régime de perturbations naturelles dans les écosystèmes forestiers. À cela s'est ajouté le concours de la bourse d'excellence Jean-Jacques et Fernand Cossette (Chaire UQAT-UQAM en aménagement forestier durable). Leur conviction quant à l'importance de mes travaux a non seulement stimulé mon ambition et permis la concrétisation de mes recherches, mais a également soutenu mes participations à divers colloques et groupes de travail. Ces échanges et rencontres avec des experts de mon domaine ont, à leur tour, enrichi mon expérience académique et nourri ma réflexion, contribuant de manière significative à l'essor et à la diffusion de mes résultats.

Je tiens à exprimer ma profonde gratitude à la Fondation J.A. DeSève et à la Fondation de l'UQAT pour leur soutien financier à travers la bourse de soutien au dépôt de thèse doctorale. Cette aide précieuse m'a permis de me consacrer pleinement à la finalisation de mes travaux de recherche et à la rédaction de cette thèse dans des conditions optimales.

À l'achèvement de cette thèse, je demeure convaincue que l'aboutissement d'un tel projet repose sur une subtile alchimie de passion, d'audace, de travail assidu et, surtout, d'un précieux soutien moral. Bien que mes intérêts pour la modélisation et ses applications en écologie m'aient conduite à concrétiser ce projet doctoral, je n'aurais pu affronter seul les multiples épreuves qui ont jalonné ce parcours. J'adresse ainsi mes plus sincères remerciements à toutes les personnes qui se sont investies

dans cette aventure, contribuant à en révéler le meilleur, qu'elles soient ou non citées nommément dans ces pages.

Je souhaite dédier mes ultimes remerciements à mes proches, qui ont largement participé à la réussite de ce projet, malgré la distance géographique ou mes disponibilités parfois limitées. Je pense en particulier à mon frère, à mes sœurs, à Imelda ainsi qu'à mes parents, dont la bienveillance et la constance exemplaires m'ont sans cesse insufflé la confiance nécessaire pour viser mes objectifs et affronter chaque difficulté. Leur soutien infaillible, conjugué à leur amour et à la foi qu'ils ont toujours placée en mes capacités, a constitué le socle de mes réussites. C'est grâce à eux que j'ai pu puiser l'énergie indispensable pour persévérer et franchir de nouveaux paliers dans mon cheminement académique. Je leur témoigne ici toute ma reconnaissance. Je suis pleinement conscient que chacun de mes accomplissements leur doit une part essentielle.

ÉPIGRAPHE

« *La forêt précède les peuples, le désert les suit*. » -- François-René de Chateaubriand

AVANT-PROPOS

Cette thèse de doctorat a été réalisée à l'Université du Québec en Abitibi-Témiscamingue (UQAT) et s'inscrit dans le cadre des recherches sur la prédiction de la propagation des épidémies de tordeuse des bourgeons de l'épinette dans un contexte de changement climatique. Cette thèse est présentée sous la forme d'une introduction générale, de trois articles scientifiques rédigés en anglais et d'une conclusion. Ces trois articles, qui constituent le noyau central de ce travail doctoral, sont le résultat de collaborations scientifiques pluridisciplinaires. Toutefois, j'ai assumé la responsabilité principale de ces études, incluant la collecte et le traitement des données, les analyses statistiques, la rédaction des manuscrits et leur soumission pour publication. Ma direction et co-direction de recherche, ont apporté un soutien scientifique précieux à chaque étape du processus de recherche, l'équipement nécessaire pour le travail ainsi que le financement.

Le premier article (Chapitre II), intitulé *Adjacent-category model for ordinal time series with application to climate-dependent spruce budworm defoliation dynamics*, a été soumis à la revue Stochastic Environmental Research and Risk Assessment et est actuellement en cours de révision. Le second article (Chapitre III), intitulé *Spatial variability in defoliation dynamics during spruce budworm outbreaks: a landscape perspective,* est publié dans la revue Ecological Modelling. Le troisième article (Chapitre IV), intitulé *Drivers of Spruce Budworm Defoliation under Projected Climate-Change Scenarios*, a été soumis à la revue Climate Change Ecology.

RÉSUMÉ

Les insectes défoliateurs constituent l'une des principales sources de perturbation naturelle dans les écosystèmes forestiers boréaux. Parmi eux, la tordeuse des bourgeons de l'épinette (TBE) est responsable de cycles épidémiques récurrents qui provoquent des défoliations massives en Amérique du Nord. En plus de ses impacts écologiques sur la structure et la composition des peuplements, la TBE engendre d'importantes pertes économiques dans le secteur forestier. Dans un contexte de changement climatique, la dynamique de cette espèce et la vulnérabilité des forêts qu'elle affecte pourraient évoluer de manière significative, sous l'effet combiné de facteurs climatiques directs et de processus écologiques non linéaires encore mal compris. À ce jour, les interactions entre climat, structure du couvert forestier et intensité des épisodes de défoliation demeurent peu explorées dans une perspective temporelle intégrée. Il devient donc impératif de développer des outils statistiques adaptés afin de mieux caractériser et anticiper les réponses écosystémiques aux perturbations biotiques futures.

Cette thèse s'articule autour de trois chapitres complémentaires qui visent à mieux comprendre, modéliser et anticiper les dynamiques de défoliation causées par la TBE dans les forêts boréales du Québec. En mobilisant des approches statistiques novatrices, fondées sur la nature ordinale des données, la dépendance temporelle des épidémies et l'hétérogénéité spatiale des conditions écologiques, ce travail propose une lecture intégrée des processus qui structurent les régimes de perturbation à l'échelles de l'unité paysagère.

Le premier chapitre introduit le modèle autorégressif à catégories adjacentes (ACAR), spécifiquement adapté aux séries temporelles de données ordinales. Appliqué à des séries dendrochronologiques couvrant plus d'un demi-siècle, ce modèle a permis d'identifier des seuils climatiques critiques et des dynamiques régionales différenciées, mettant en lumière l'influence du climat saisonnier sur l'intensité et la persistance des épisodes de défoliation.

Le deuxième chapitre élargit l'analyse en intégrant la dimension spatiale à l'échelle des unités de paysage régional (UPR). Grâce à une classification fonctionnelle basée sur les effets climatiques estimés, ce volet révèle des regroupements de territoires partageant des profils similaires de sensibilité épidémique, offrant ainsi une base opérationnelle pour la gestion différenciée du risque à l'échelle du Québec boréal.

Enfin, le troisième chapitre explore les trajectoires futures de la défoliation sous trois scénarios climatiques RCP (Representative Concentration Pathways). En isolant les effets marginaux du climat futur, il met en évidence des gradients de vulnérabilité différenciés selon les UPR. Ces résultats confirment que les effets du changement climatique sur les perturbations biotiques ne seront ni uniformes ni linéaires, et soulignent la nécessité d'une planification territoriale adaptative.

En somme, cette thèse propose un cadre méthodologique rigoureux et extensible pour l'étude des perturbations écologiques, et fournit des outils d'aide à la décision pour

anticiper les effets du climat sur les forêts boréales. Elle contribue ainsi à une meilleure compréhension des risques épidémiques à long terme et à l'élaboration de stratégies de gestion forestière plus résilientes face aux changements globaux.

Mots-clés : Climat, défoliation, classification, perturbations forestières, modélisation écologique, modèle autorégressif à catégories adjacentes

ABSTRACT

Defoliating insects are among the main sources of disturbance in boreal forest ecosystems. Among them, the spruce budworm (SBW) is responsible for recurrent epidemic cycles that cause massive defoliation events across North America. In addition to its ecological impacts on forest stand structure and composition, SBW induces substantial economic losses in the forestry sector. Under climate change, both the dynamics of this species and the vulnerability of the forests it affects are likely to shift significantly due to the combined effects of direct climatic factors and poorly understood non-linear ecological processes. To date, interactions among climate, forest canopy structure, and the severity of defoliation events remain insufficiently explored from a temporally integrated perspective. It is therefore imperative to develop suitable statistical tools to better characterize and anticipate ecosystem responses to future biotic disturbances.

This dissertation is structured around three complementary chapters aimed at improving the understanding, modeling, and forecasting of SBW defoliation dynamics in Quebec's boreal forests. Using innovative statistical approaches that account for the ordinal nature of the data, the temporal dependence of outbreaks, and the spatial heterogeneity of ecological conditions, this work provides an integrated framework for analyzing the processes shaping disturbance regimes at the landscape unit scale.

The first chapter introduces the adjacent-category autoregressive (ACAR) model, specifically tailored for ordinal time series. Applied to dendrochronological series spanning over half a century, this model enabled the identification of critical climatic thresholds and region-specific dynamics, shedding light on the influence of seasonal climate on the intensity and persistence of defoliation episodes.

The second chapter extends the analysis by incorporating spatial structure at the level of regional landscape units (UPRs). Using a functional classification based on estimated climatic effects, this chapter reveals clusters of territories sharing similar epidemic sensitivity profiles, thereby offering an operational basis for risk-based forest management across Quebec’s boreal region.

Finally, the third chapter investigates future defoliation trajectories under three climate change scenarios (RCP 2.6, 4.5, and 8.5). By isolating the marginal effects of future climate, it highlights spatially differentiated vulnerability gradients among UPRs. These results confirm that the impacts of climate change on biotic disturbances will be neither uniform nor linear and emphasize the need for adaptive spatial planning.

In summary, this dissertation proposes a rigorous and extensible methodological framework for the study of ordinal ecological disturbances, and offers decision-support tools to anticipate the effects of climate change on boreal forests. It contributes to a deeper understanding of long-term epidemic risks and the development of more resilient forest management strategies in the face of global change.

Keywords: Climate, Defoliation, clustering, Forest disturbances, Ecological modeling, adjacent-category autoregressive model

TABLE DES MATIÈRES

LISTE DES FIGURES

LISTE DES TABLEAUX

INTRODUCTION

Contexte. Les régimes de perturbations naturelles et anthropiques constituent des forces motrices majeures des changements affectant la structure et le fonctionnement des écosystèmes forestiers (De Grandpré et al. 2018; Aakala et al. 2023; Watha-Ndoudy et al. 2022). Ces perturbations, qui incluent les feux de forêt, les épidémies d'insectes, les tempêtes, les sécheresses prolongées et les interventions humaines (exploitation forestière, aménagement du territoire, changements d'usage des sols), influencent profondément la dynamique des peuplements forestiers (Seidl et al. 2017; MacLean 2016). Elles modulent la biodiversité, modifient la composition spécifique des forêts et déterminent leur capacité à résister et à s'adapter aux changements environnementaux (Mackey et al. 2023). Dans un contexte de réchauffement climatique, la fréquence et l'intensité de ces perturbations sont amenées à évoluer, rendant plus incertaine la trajectoire des écosystèmes forestiers et compliquant la mise en place de stratégies de gestion durable (Pureswaran et al. 2015; Yonghe Wang 2024). Les projections climatiques pour l'Amérique du Nord suggèrent une augmentation significative des températures hivernales et estivales moyennes, ce qui pourrait modifier considérablement la phénologie de la TBE et exacerber la fréquence et l'intensité de ses épidémies (Pureswaran et al. 2015; Yonghe Wang 2024).

Parmi les perturbations biotiques affectant les forêts nord-américaines, la tordeuse des bourgeons de l'épinette (Choristoneura fumiferana, TBE) représente le principal agent de défoliation des conifères (Lavoie, Montoro Girona, and Morin 2019; Alvaro Fuentealba et al. 2022; Kayes and Mallik 2020; Jacques Régnière and Nealis 2019b). Son cycle biologique, étroitement lié aux conditions climatiques et à la phénologie de ses essences hôtes (Figure 1), favorise l'émergence de vastes épidémies pouvant s'étendre sur plusieurs décennies (Lavoie et al. 2021; Yataco et al. 2024). En phase épidémique, les larves de la TBE consomment massivement le feuillage des arbres hôtes, notamment le sapin baumier (Abies balsamea) ainsi que les épinettes blanche (Picea glauca) et noire (Picea mariana), ce qui provoque un stress physiologique important. La défoliation répétée sur plusieurs années engendre une réduction significative de la croissance radiale et peut conduire au dépérissement des arbres,

accroissant ainsi leur vulnérabilité aux maladies et aux agents pathogènes, jusqu'à entraîner leur mortalité (Lavoie et al. 2021; Z. Liu et al. 2022; Zinsou Max Debaly, Marchand, and Girona 2022; MacLean 2016). Cette dynamique des pertubations modifie la structure et la composition des peuplements forestiers et peut affecter durablement les forêts boréales.

L'impact écologique des épidémies de TBE ne se limite pas à la mortalité des arbres. La défoliation provoque une altération de nombreux services écosystémiques fournis par les forêts boréales (Subedi et al. 2023; Scott et al. 2023; Sato et al. 2023; Chagnon, Bouchard, and Pothier 2022). Parmi ces services, la séquestration du carbone est particulièrement affectée. En Amérique du Nord, la forêt boréale constitue l'un des puits de carbone essentiels, et la mortalité accrue des arbres réduit cette capacité, contribuant à l'augmentation des émissions de CO_2 dans l'atmosphère (Z. Liu et al. 2019, 2020; Ameray et al. 2021). Outre la perturbation du cycle du carbone et les pertes de biomasse associées, les épidémies de la TBE modifient la disponibilité des habitats pour la faune, perturbent les interactions écologiques au sein des écosystèmes forestiers et accroissent le risque d'incendies de grande ampleur (Watt et al. 2020; Mackey et al. 2023; Noor et al. 2025).

Les conséquences économiques des épidémies de TBE sont également considérables. La baisse de croissance et la mortalité des arbres engendrent des pertes substantielles pour l'industrie forestière, qui dépend de la qualité et de la quantité de bois disponible (Grondin et al. 1996; Lemay, Barrette, and Krause 2022). Les arbres sévèrement défoliés deviennent plus vulnérables aux champignons lignicoles et aux pathogènes, ce qui compromet la qualité du bois récolté et limite son utilisation pour des applications industrielles de haute valeur (MacLean 2016; Safranyik et al. 2010; Chang et al. 2012b; Alvaro Fuentealba et al. 2022). Cette dégradation de la ressource forestière peut avoir des répercussions directes sur les marchés du bois et sur la compétitivité du secteur forestier canadien. De plus, les coûts associés aux interventions sylvicoles, telles que l'aménagement des peuplements, la coupe sanitaire ou la lutte biologique contre la TBE, constituent une charge financière supplémentaire pour les gestionnaires forestiers.

Au cours des dernières décennies, la modélisation est devenue un outil central pour comprendre et prédire la dynamique des épidémies de la TBE. Les approches existantes se répartissent entre (i) des modèles empiriques corrélatifs, tels que les régressions paramétriques (Gray 2013), les GAM/GAMM semi-paramétriques (Eickenscheidt, Augustin, and Wellbrock 2019; Subedi et al. 2023) et les classifieurs d'apprentissage automatique (Candau and Fleming 2011a; Zhu et al. 2018), (ii) des modèles mécanistes individucentrés décrivant le cycle physiologique de l'insecte (Jacques Régnière, St-Amant, and Duval 2012; Jacques Régnière and Nealis 2019b), et (iii) des modèles spatialisés de paysage simulant l'interaction entre feu, récolte et épidémies (Sturtevant et al. 2015; James et al. 2011). Cependant, nombre de ces modèles simplifient la réponse de la défoliation en la convertissant en variable binaire ou continue, ignorant ainsi l'échelle ordinale utilisée dans les inventaires forestiers (Candau and Fleming 2011a). Cette simplification limite la détection de seuils écologiques critiques et la pertinence opérationnelle des prévisions.

La dynamique de propagation des épidémies de la TBE est un phénomène complexe, régi par une multitude de facteurs environnementaux, biotiques et climatiques (Bouchard and Auger 2014; Montoro Girona, Navarro, and Morin 2018). Ces épidémies peuvent s'étendre sur plusieurs décennies et couvrir de vastes superficies. Une épidémie typique de TBE est cyclique chaque 35 à 40 ans et peut affecter d'énormes surface (Boulanger and Arseneault 2004; Germain et al. 2021). L'ampleur de ces perturbations complique grandement leur gestion, nécessitant la mise en place de stratégies adaptées, combinant surveillance, modélisation et interventions ciblées. Comme illustré par le cycle biologique de la TBE (Figure 1), les phases critiques telles que l'émergence des larves et la synchronisation avec l'ouverture des bourgeons sont particulièrement vulnérables aux variations climatiques (Noor et al. 2025).

Au Canada, la forêt boréale représente un élément fondamental du patrimoine écologique, économique, culturel et historique (Kayes and Mallik 2020). Elle constitue une ressource vitale pour de nombreuses communautés, notamment pour les peuples autochtones qui en dépendent pour leur mode de vie traditionnel et leurs activités économiques (Natcher 2001; Wilson and Graham 2005; Wyatt 2008). Face aux défis

posés par l'augmentation des épidémies de TBE et les incertitudes liées aux changements climatiques, il est essentiel de développer des outils de modélisation permettant d'anticiper l'évolution des épidémies et d'optimiser les stratégies de gestion forestière (Boulanger, Taylor, et al. 2017). Une meilleure compréhension des facteurs qui influent sur la dynamique des épidémies et leur interaction avec le climat contribuera à renforcer la résilience des forêts boréales et à préserver leurs fonctions écologiques et économiques à long terme (Girardin et al. 2016).

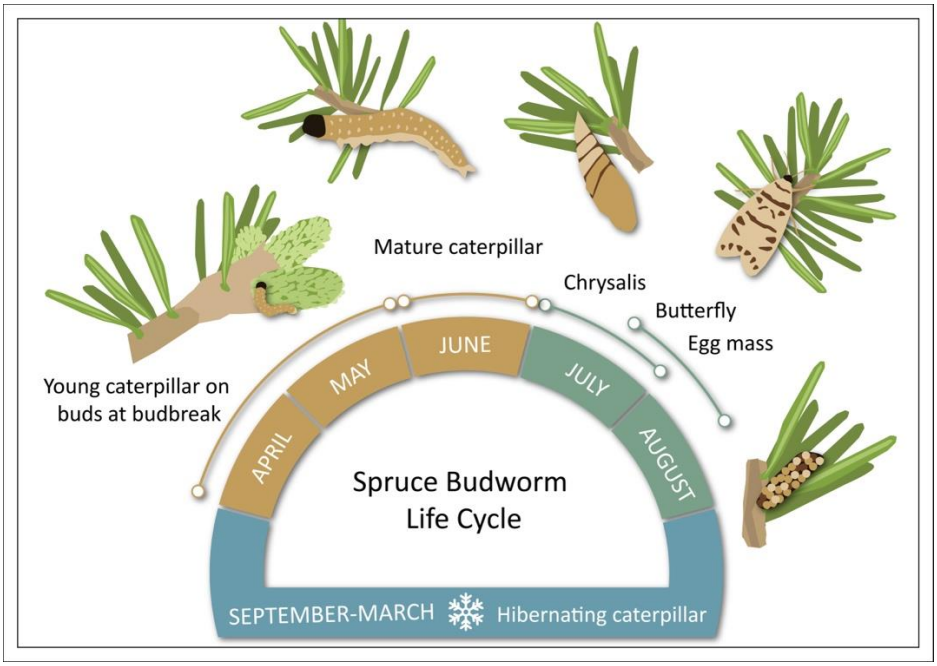

Figure 1
Cycle de développement de la TBE

La tordeuse des bourgeons de l'épinette (TBE). ***Biologie et écologie***. La tordeuse des bourgeons de l'épinette (*Choristoneura fumiferana*, TBE) est un lépidoptère Tortricidae et constitue le principal défoliateur des conifères du nord-est de l'Amérique du Nord (Blais 1983; Vincent Nealis and Régnière 2021). Par l'ampleur de ses épidémies, ses retombées économiques et son rôle structurant dans les trajectoires forestières, elle est devenue un organisme modèle en écologie des populations et en entomologie forestière (Volney and Fleming 2000; Pureswaran, Roques, and Battisti

2018; Royama 1984). Une littérature abondante en décrit la biologie, les interactions trophiques et les facteurs environnementaux qui gouvernent ses dynamiques.

Cycle vital et phénologie. La TBE présente un cycle vital annuel, fortement contraint par la phénologie de ses hôtes, notamment le sapin baumier (*Abies balsamea*) et diverses espèces d'épinettes (*Picea spp.*). Après l'émergence estivale des adultes (juillet–août), la ponte des femelles a lieu directement sur les aiguilles des conifères. Les œufs éclosent en août, donnant naissance à des larves néonates (L1), qui entrent rapidement en diapause au stade L2 dans des hibernacula soyeux fixés aux rameaux, où elles demeurent de septembre à mars. Cette phase de dormance, essentielle à la survie hivernale, confère à l'espèce une tolérance accrue aux conditions extrêmes des forêts boréales. La réactivation des larves au printemps, généralement en avril, coïncide avec le débourrement des hôtes. La synchronisation entre le développement larvaire et l'ouverture des bourgeons est cruciale : les chenilles consomment d'abord les bourgeons en expansion puis les jeunes pousses. Tout décalage phénologique défavorable compromet la survie larvaire et constitue un facteur de régulation clé des populations (Pureswaran et al. 2019; Noor et al. 2025; Tai and Carroll 2022). Entre mai et juin, les larves traversent six instars successifs (L1–L6) et atteignent leur maturité, marquée par une phase de consommation foliaire intensive. À la fin juin et au début juillet, elles se nymphosent en chrysalides (stade pupal), amorçant leur métamorphose. Après une à deux semaines, les adultes émergent (juillet–août), s'accouplent et pondent une nouvelle génération d'œufs, initiant ainsi le cycle suivant. Ce cycle, représenté dans la Figure 1.1, illustre la forte dépendance de la TBE à la phénologie de ses hôtes et souligne la sensibilité de l'espèce aux modifications climatiques. La phénologie constitue donc un maillon critique de la dynamique épidémique, en conditionnant à la fois la survie individuelle et le succès démographique des populations.

***Dynamique des populations*.** Les populations de la TBE se caractérisent par des cycles épidémiques récurrents, généralement observés à l'échelle régionale avec une périodicité moyenne de 30 à 40 ans et une durée de 25 à 40 ans, séparés par de longues phases endémiques à faible densité (Royama 1984; Jardon, Morin, and

Dutilleul 2003; Boulanger and Arseneault 2004). Ces cycles émergent de la combinaison d'interactions densité-dépendantes, incluant la compétition intra-spécifique et la régulation du recrutement, ainsi que de processus de dispersion. Pour ce qui est de la disperson, nous avons des épisodes de dispersion de masse chez les adultes, pouvant connecter des foyers distants et favoriser l'expansion spatiale des épidémies (Royama 1984; Sturtevant et al. 2015; Jacques Régnière and Nealis 2019a). À l'autre extrémité du spectre, des effets d'Allee peuvent limiter la croissance des populations en contexte de faible densité, contribuant au maintien prolongé des phases endémiques (Jacques Régnière and Nealis 2019a; M. Li et al. 2020). Parmi les facteurs abiotiques, les conditions climatiques printanières notamment les régimes de température et la disponibilité de feuillage au moment du débourrement, combinées à la densité des populations survivantes à l'issue de l'hivernation, constituent des prédicteurs majeurs de l'intensité annuelle de la défoliation (Candau and Fleming 2011a; Subedi et al. 2023). À plus grande échelle spatiale, la synchronie partielle des épidémies régionales peut être interprétée dans le cadre de l'effet Moran, c'est-à-dire l'influence de fluctuations climatiques corrélées spatialement, qui agissent en synergie avec les rétroactions biotiques internes pour générer des dynamiques cycliques complexes (Ranta et al. 1995; Liebhold, Koenig, and Bjørnstad 2004).

***Forçages « bottom-up » : hôtes et nutrition*.** La performance larvaire de la tordeuse des bourgeons de l'épinette est fortement conditionnée par la qualité et la disponibilité du feuillage de ses hôtes. Les caractéristiques biochimiques des aiguilles, telles que la teneur en azote, la concentration en sucres solubles et la proportion de composés phénoliques défensifs, exercent une influence directe sur la croissance, la fécondité et la survie des larves (Mattson et al. 1991; Kumbasli and Bauce 2013). De plus, des variables structurelles comme l'âge des aiguilles, la densité de la canopée et l'architecture du houppier modulent non seulement la quantité de ressources accessibles, mais également la micro-physiologie du feuillage (température, humidité), affectant ainsi l'efficacité de l'alimentation (Bauce, Crépin, and Carisey 1994; A. Fuentealba and Bauce 2012). La phénologie des hôtes constitue un facteur critique : les dates de débourrement déterminent la synchronie entre les stades

larvaires précoces et la disponibilité de tissus foliaires tendres, hautement nutritifs. Tout décalage entre l'émergence larvaire et le développement phénologique des hôtes se traduit par une réduction drastique de la survie et de la performance individuelle, influençant la dynamique des populations à des échelles plus larges (Pureswaran et al. 2019). À l'échelle interannuelle, la variabilité de ces facteurs nutritionnels et phénologiques contribue à déterminer l'intensité locale de la défoliation, ainsi que la capacité de tolérance et de résilience des peuplements forestiers soumis à une pression épidémique récurrente (Fuentealba and Bauce 2012).

Forçages « top-down » : ennemis naturels et régulation. Un réseau diversifié d'ennemis naturels, incluant parasitoïdes, pathogènes et prédateurs généralistes, contribue à la régulation des populations de tordeuse des bourgeons de l'épinette, en particulier durant les phases endémiques à faible densité (Jacques Régnière, Seehausen, and Martel 2020; Seehausen et al. 2014). Parmi les parasitoïdes les plus influents, Tranosema rostrale (Hymenoptera: Ichneumonidae) attaque préférentiellement les stades larvaires intermédiaires (L3–L4). Sa propre dynamique est cependant modulée par les conditions climatiques, ce qui illustre la complexité des interactions tri-trophiques dans ce système (Jacques Régnière, Seehausen, and Martel 2020; Seehausen et al. 2017). Au-delà de la régulation directe par la mortalité induite, d'autres processus comportementaux et démographiques interviennent. Ainsi, des biais de sex-ratio peuvent influencer le succès reproducteur et conditionner la dynamique de dispersion des adultes. De plus, la communication chimique via les phéromones sexuelles module non seulement l'accouplement, mais également la structure spatiale des populations, avec des implications pour la propagation des vagues épidémiques (Rhainds and Heard 2015; Ponder et al. 1986). Ces forçages « top-down » interagissent avec les contraintes abiotiques et les forçages « bottom-up », contribuant à la complexité des cycles épidémiques observés.

Impacts écologiques et socio-économiques. En phase épidémique, les larves consomment massivement les pousses de sapin baumier et d'épinettes (*Picea glauca*, *P. mariana*), entraînant (i) une forte réduction de la croissance radiale et de la

production de bois (pouvant dépasser 50 % dans les peuplements sévèrement touchés) (MacLean 2016; Chen et al. 2017b), (ii) une mortalité accrue sous défoliation répétée sur 3–5 ans, avec des changements durables de structure et de composition (Lavoie, Montoro Girona, and Morin 2019; MacLean et al. 2024), (iii) une diminution temporaire du puits de carbone, voire un basculement vers un état source de CO_2 (Z. Liu et al. 2019), et (iv) des pertes économiques majeures pour la filière forestière et les communautés dépendantes (Chang et al. 2012b; Alvaro Fuentealba et al. 2022). Ces effets, modulés par la composition et l'âge des peuplements, soulignent l'importance d'analyses intégrant structure, histoire des perturbations et gradients climatiques (Kneeshaw et al. 2022; Lavoie et al. 2021).

Facteurs régissant la dynamique épidémique. La dynamique résulte d'une interaction complexe entre abiotiques et biotiques :

1. ***Climat et phénologie***. Hivers doux et printemps chauds accroissent survie et synchronie; des extrêmes thermiques peuvent cependant réduire la performance (Jacques Régnière and Nealis 2019b; Pureswaran et al. 2019; O'Connell and Wiley 2024; Portalier, Candau, and Lutscher 2024).
2. ***Composition et structure des peuplements***. Proportion d'hôtes, densité de canopée et âge des peuplements conditionnent l'offre de feuillage et la tolérance à la défoliation (Lavoie et al. 2021; Kneeshaw et al. 2022).
3. ***Réseau trophique***. Parasitisme, prédation et pathogènes modulent la croissance démographique, avec des sensibilités au climat et à la configuration paysagère (L. Venier and Holmes 2010; Bouchard, Régnière, and Therrien 2018a; McNie, Kneeshaw, and Filotas 2024).
4. ***Processus spatiaux***. Dispersion, y compris déplacements de masse des adultes, connectivité forestière et hétérogénéité topographique gouvernent l'extension des foyers (D. P. Anderson and Sturtevant 2011; Chen, Rahimzadeh-Bajgiran, and Weiskittel 2021; Cooke 2022; Larroque, Wittische, and James 2022).

Patrons spatio-temporels de la TBE au Québec. Les archives dendrochronologiques, relevés aériens et données de télédétection documentent plusieurs siècles d'occurrence épidémique:

- ***Cycles récurrents***. Depuis le XVIIe siècle, de grandes vagues se répètent à un pas de 30–40 ans, durant 25–40 ans (Boulanger and Arseneault 2004; Jardon, Morin, and Dutilleul 2003).
- ***Ceinture épidémique***. Une ceinture de défoliation s'étend classiquement du Saguenay–Lac-Saint-Jean à la péninsule gaspésienne, où fréquence et sévérité sont élevées (Navarro et al. 2018; Berguet et al. 2021).
- ***Gradient et déplacement***. Des indices récents suggèrent un déplacement du noyau vers le nord-est, possiblement lié au réchauffement et à la migration bioclimatique (Boulanger, Taylor, et al. 2017; Navarro et al. 2018).

Ces constats plaident pour des modèles tenant compte (i) du caractère ordinal des niveaux de défoliation, (ii) de la mémoire interannuelle (autorégression) et (iii) des gradients climatiques et contextes paysagers.

Cadres classiques de la dynamique de la TBE. ***La perspective de Royama : rétroactions et délais.*** (Royama 1984) a proposé une lecture systémique de la TBE où les cycles émergent d'un jeu de rétroactions positives (ressource, fécondité) et négatives (ennemis naturels), modulées par des délais, des saturations et des non-linéarités qui gouvernent les transitions endémique–épidémique. Dans ce cadre, la dynamique n'est pas réductible à un seul facteur (climat ou ennemis), mais résulte d'une architecture causale où la qualité du feuillage, la densité larvaire et la régulation trophique interagissent. Les signatures temporelles observées (périodicités, déphasages, persistances) sont alors interprétées comme des propriétés émergentes d'un système à rétroactions avec mémoire.

Les reconstructions historiques de Blais et la périodicité multi-séculaire. Les travaux pionniers de Blais, fondés sur des analyses dendrochronologiques et l'exploitation des premières archives aériennes, ont révélé la récurrence remarquable des épidémies de tordeuse des bourgeons de l'épinette sur plusieurs siècles dans la

forêt boréale de l'est du Canada. Ces études ont mis en évidence un intervalle moyen de retour des épidémies de l'ordre de 30 à 40 ans (Blais 1983; Boulanger and Arseneault 2004; Berguet et al. 2021). En fournissant des séries temporelles continues et spatialement étendues, elles ont constitué un ancrage empirique essentiel pour évaluer les hypothèses relatives à la périodicité, à l'ampleur et au degré de synchronie des épidémies. Elles ont également permis de situer les variations régionales, en soulignant notamment l'existence d'une ceinture épidémique couvrant le domaine boréal méridional et des gradients de sévérité et de fréquence selon la latitude. Ces reconstructions multi-séculaires demeurent une référence incontournable pour comprendre les patrons à long terme et tester les cadres théoriques de la dynamique de la TBE.

Ces grands cadres se révèlent complémentaires dans l'analyse des dynamiques de la TBE. Les travaux de Royama ont permis de formaliser l'architecture endogène des populations, en insistant sur les rétroactions densité-dépendantes, les délais de réponse et la stabilité des cycles. En parallèle, les reconstructions historiques de Blais ont fourni une assise empirique multi-séculaire, révélant la périodicité et la récurrence des épidémies à l'échelle du paysage. Ensemble, ces apports ont constitué le socle conceptuel et empirique qui a nourri le développement ultérieur de modèles mécanistes et statistiques intégrant à la fois les mécanismes internes, les forçages climatiques et les contraintes spatiales.

Modélisation des interactions entre climat et défoliation par la TBE. La compréhension des interactions entre le climat et les perturbations naturelles est cruciale pour adapter l'aménagement forestier durable aux changements climatiques (Seidl et al. 2023; Gauthier et al. 2023). En raison de ses conséquences écologiques et économiques, la TBE constitue un enjeu prioritaire pour la foresterie québécoise (Messier, Puettmann, and Coates 2013). Toutefois, la TBE s'inscrit dans un système écologique complexe. En écologie, pour comprendre le fonctionnement de tels systèmes, en anticiper l'évolution et en saisir les interactions qui s'y déroulent, on recourt souvent à la modélisation (Nenzen et al. 2017). Plusieurs travaux récents se

sont ainsi attachés à modéliser la dynamique des épidémies de la TBE par différentes approches.

Modèles existants et limites. Il est à noter que les modèles existants concernant la TBE portent principalement sur la dynamique des populations de l'insecte (Baskerville and Kleinschmidt 1981; Dwyer, Dushoff, and Yee 2004; Hassell, Allwright, and Fowler 1999; Ludwig et al. 1978), sur l'impact du réchauffement climatique (surtout la température) sur le développement larvaire et la synchronisation entre l'émergence des larves et la phénologie des bourgeons (Crozier and Dwyer 2006; Pureswaran et al. 2019; Jacques Régnière and Nealis 2019b, 2019a; Jacques Régnière et al. 2012; Volney and Fleming 2007), ou encore sur l'effet de la densité et des caractéristiques du peuplement sur la présence ou l'absence de la TBE (Alvaro Fuentealba et al. 2017) ainsi que sa dispersion (Kabir 2021; Nenzén, Peres-Neto, and Gravel 2018; Yan Wang 2019). Les modèles décrivant la dynamique des populations de la TBE sont, pour la plupart, des modèles mécanistes, intégrant la disponibilité des ressources pour la survie de l'insecte, la compétition inter- et intraspécifique (présence de parasites ou de prédateurs) (Ludwig et al. 1978; Dwyer, Dushoff, and Yee 2004), ainsi que la variation aléatoire de l'environnement (Meng Liu and Zhu 2018), afin de déterminer les conditions d'équilibre stable de la population.

En outre, les modèles linéaires sont largement utilisés pour étudier la TBE et ses conséquences (Bouchard, Régnière, and Therrien 2018a; Bouchard and Auger 2014; Subedi et al. 2023). Ils servent notamment à analyser l'effet des facteurs climatiques sur la synchronisation de la dynamique des populations de la TBE (Bouchard, Régnière, and Therrien 2018a), la défoliation (Bouchard and Auger 2014) ou encore l'influence de la composition forestière sur la défoliation (Nie, MacLean, and Taylor 2018).

Parallèlement, les approches dendrochronologiques ont permis de reconstruire la dynamique spatiotemporelle des épidémies de la TBE au Québec. (Navarro et al. 2018) et (Berguet et al. 2021) ont ainsi identifié des regroupements (clusters) de trajectoires de défoliation via la méthode des k-moyennes, montrant une association

entre les basses températures annuelles et la sévérité des épidémies. Cependant, les tentatives pour relier directement la fréquence des épidémies aux variables climatiques par régression linéaire se sont révélées peu concluantes, soulignant la nécessité de méthodes plus adaptées (Navarro et al. 2018).

Dans une perspective prédictive, (Candau and Fleming 2011a) ont employé des forêts aléatoires (random forests) afin de modéliser la fréquence des épisodes de défoliation modérée à sévère en Ontario. Leurs résultats mettent en évidence l'influence des températures hivernales et des températures minimales estivales sur la dynamique de la TBE. De leur côté, des modèles additifs généralisés (GAM) appliqués à des données recueillies en Allemagne (Eickenscheidt, Augustin, and Wellbrock 2019) indiquent que les sécheresses cumulées ont un effet significatif sur la défoliation, avec un décalage temporel pouvant s'étendre sur plusieurs années. En Chine, l'analyse par régression de données Landsat a montré que l'accumulation de chaleur et les précipitations automnales inhibent les infestations de chenilles, tandis qu'une forte durée d'ensoleillement les favorise (Zhu et al. 2018). Si ces résultats concordent avec les caractéristiques biologiques des insectes, les limites inhérentes aux approches linéaires pour des données ordinales et dépendantes dans le temps demeurent problématiques. Par ailleurs, (M. Li et al. 2020) ont montré qu'en considérant à la fois l'état de l'épidémie l'année précédente et les conditions climatiques printanières, il est possible de prédire efficacement l'évolution des populations de TBE l'année suivante. Ceci met en lumière l'importance de l'effet autorégressif de la défoliation.

Nature des données de défoliation et problématique. Le processus de défoliation par la TBE est cumulatif et présente une autocorrélation temporelle marquée (J. Régnière and Nealis 2007; Chen et al. 2017b; M. Li et al. 2020). De plus, les données de défoliation sont souvent recueillies sous forme d'échelles ordinales (p. ex. : classes de sévérité), ce qui soulève des difficultés d'ordre méthodologique. Bien que ces échelles simplifient grandement les inventaires à large échelle, les approches actuelles — régressions linéaires (Bouchard, Régnière, and Therrien 2018a), modèles additifs généralisés (GAM) (Subedi et al. 2023) ou méthodes d'apprentissage automatique

- intégrant l'ordre des classes de défoliation et leur dépendance temporelle via une structure autorégressive ;
- permettant une modélisation individuelle par série temporelle, afin de capter l'hétérogénéité régionale des effets climatiques ;
- offrant une interprétabilité directe des effets des covariables (p. ex. températures, précipitations), contrairement aux méthodes de type boîte noire, telles que les forêts aléatoires.

En outre, plutôt que d'ajuster un modèle global à toutes les séries temporelles, une approche région-centrée, consistant à estimer un modèle distinct pour chaque région, permet de mieux cerner les spécificités locales du processus de défoliation et d'identifier des réponses climatiques particulières. Cette démarche s'avère d'autant plus pertinente dans un contexte de gestion forestière, car elle éclaire les interventions possibles en fonction des réalités écologiques et climatiques propres à chaque zone.

Objectifs. Ce travail de recherche vise à combler une lacune méthodologique en proposant une modélisation spécifiquement adaptée aux particularités des données de défoliation. L'objectif général de cette thèse est de développer et d'appliquer des approches statistiques novatrices pour modéliser la dynamique des épidémies de la tordeuse des bourgeons de l'épinette en forêt boréale québécoise. Plus précisément, notre but est de comprendre et de quantifier les interactions complexes entre le climat et la défoliation, en tenant compte de la nature ordinale des données et de leur caractère cumulatif. Les objectifs spécifiques, correspondants aux différents articles, sont structurés comme suit :

1. ***Développement d'un modèle autorégressif pour séries temporelles ordinales***. Élaborer et formaliser un modèle statistique autorégressif novateur permettant d'analyser les séries temporelles de défoliation, en intégrant simultanément leur nature ordinale et leur caractère cumulatif.
2. ***Application régionale, validation et analyse spatiale du modèle***. Implémenter le modèle sur des données empiriques de défoliation issues de différentes unités de paysage au Québec, afin d'évaluer l'impact des facteurs climatiques sur l'intensité et la dynamique des épidémies. Cette étape vise

également à comparer diverses configurations du modèle pour en vérifier la robustesse, et à mettre en évidence l'importance du contexte local (hétérogénéité du paysage, microclimat) dans la compréhension de la variabilité de la défoliation. Enfin, on combinera ces estimations régionales avec des méthodes de regroupement (clustering) afin de classifier les unités de paysage selon les similarités observées dans les effets climatiques estimés localement.

3. ***Évaluer l'influence future du climat sur la dynamique de défoliation par la TBE dans la forêt boréale québécoise***. Quantifier l'influence future du climat sur la dynamique de défoliation causée par la tordeuse des bourgeons de l'épinette (TBE) dans la forêt boréale québécoise. Intégrer des scénarios climatiques dans le cadre de l'analyse afin de projeter l'évolution spatiale et temporelle des effets marginaux de variables climatiques sur la défoliation. L'objectif est de proposer une perspective prospective permettant d'anticiper l'impact des changements climatiques sur la forêt boréale.

Ces objectifs permettent de fournir des recommandations opérationnelles directement exploitables par les gestionnaires forestiers, améliorant la planification des interventions adaptées au climat futur et renforçant la résilience des forêts boréales québécoises. Ces axes méthodologiques répondent à des besoins clairement identifiés dans la littérature et à la demande de techniques d'analyses plus fines, capables de tirer parti de la nature ordinale et temporelle des données de défoliation. L'approche région-centrée contribuera à mieux comprendre les processus épidémiques, tout en fournissant des informations utiles pour la gestion forestière à l'échelle locale dans un contexte de changement climatique.

1. ADJACENT-CATEGORY MODEL FOR ORDINAL TIME SERIES WITH APPLICATION TO CLIMATE-DEPENDENT SPRUCE BUDWORM DEFOLIATION DYNAMICS

Olaloudé Judicaël Franck Osse, Zinsou Max Debaly, Philippe Marchand et Miguel Montoro Girona

Une version de ce chapite a été soumis au journal Stochastic Environmental Research and Risk Assessment

1.1. Résumé

Les données catégorielles ordinales se composent de valeurs discrètes hiérarchisées et sont couramment rencontrées en biologie et en écologie. En écologie, elles apparaissent lorsqu'on classe des observations dans des catégories possédant un ordre naturel: stades de développement des végétaux, phases de comportement animal ou encore paliers d'un cycle de vie. Elles servent aussi à représenter des phénomènes continus mesurés sur une échelle ordinale afin de faciliter des inventaires de grande ampleur, par exemple les relevés aériens des perturbations forestières.

Dans cet article, nous généralisons le modèle ordinal à catégories adjacentes en y intégrant une dynamique autorégressive, afin de traiter des séries temporelles de données ordinales. Nous appliquons ensuite ce modèle pour analyser l'influence du climat sur l'intensité de la défoliation des arbres au cours des épidémies de tordeuse des bourgeons de l'épinette (TBE) dans l'est du Canada. Les paramètres sont estimés par maximum de vraisemblance et un test portemanteau d'adéquation est proposé. La performance de la méthode est d'abord évaluée sur de petites tailles d'échantillon simulées, puis sur des données réelles de défoliation (quatre classes ordinales) recueillies dans deux régions, le Témiscamingue et la Matawinie, assorties de variables climatiques explicatives.

Nos résultats montrent que l'effet de la température sur la défoliation est non linéaire et dépend de la saison : des termes quadratiques sont significatifs pour les températures estivales et printanières. Au Témiscamingue, une amplitude thermique estivale inférieure ou égale à 22,7 °C est associée à une défoliation moindre, tandis qu'en Matawinie le seuil correspondant est de 21,81 °C. De plus, des températures printanières plus élevées en Matawinie accentuent la défoliation, avec un seuil de 32,54 °C. Ces analyses révèlent également d'importantes différences régionales dans les processus de défoliation.

1.2. Abstract

Ordinal categorical data consist of ranked discrete values and are commonly found in fields like biology and ecology. In ecology, these data arise when observations are categorized into groups that have a natural order. They enable the study of transitions between different ecological categories, such as plant development stages, phases of animal behavior, or changes in species life cycles. They can also represent continuous phenomena recorded on an ordinal scale to facilitate efficient large-scale surveys, such as aerial observations of forest disturbances. In this paper, we extend the traditional adjacent-category ordinal model by introducing autoregressive dynamics to accommodate ordinal categorical time-series data. We then apply the model to study the effect of climate on the intensity of tree defoliation during spruce budworm (SBW) outbreaks periods in Eastern Canadian forests. The model's parameters are estimated via the maximum likelihood approach. A portmanteau test for goodness-of-fit is proposed. The quality of our method is shown with small numerical experiments for finite samples. Our method is then applied to real data consisting of defoliation levels in two regions (Témiscamingue and Matawinie) recorded as categorical data with four levels along with explanatory climate variables. Our study finds that the effect of temperature on defoliation is non-linear and varies by season, with quadratic effects observed for both summer and spring temperatures. In Témiscamingue, a summer temperature range up to 22.7°C is linked to lower defoliation, while in Matawinie, the threshold is 21.81°C. Additionally, higher spring temperatures in Matawinie correlate with increased defoliation, with a threshold of 32.54°C. The study also highlights regional differences in defoliation processes.

1.3. Introduction

Natural and anthropogenic disturbances regimes are major drivers of changes in the structure and function of forest ecosystems (De Grandpré et al. 2018; Aakala et al. 2023). The spruce budworm (SBW, *Choristoneura fumiferana* (Clemens, 1865)) is an insect pest responsible for widespread defoliation in North America's boreal forests, primarily affecting balsam fir (*Abies balsamea* (L.) Mill.), white spruce (*Picea glauca* (Moench) Voss) and black spruce (*Picea mariana* (Mill.) Britton, Sterns & Poggenb.) (Lavoie, Montoro Girona, and Morin 2019; Alvaro Fuentealba et al. 2022; Kayes and Mallik 2020; Anderegg et al. 2015). This defoliation and the subsequent tree mortality reduce many goods and services that these trees and forests provide (Subedi et al. 2023; Scott et al. 2023; Sato et al. 2023; Chagnon, Bouchard, and Pothier 2022), as well as the boreal forest's carbon sequestration capacity (Z. Liu et al. 2019, 2020). Forest damage occurs when SBW larvae repeatedly feed on the annual foliage of mature balsam fir, white spruce and black spruce which leads to radial growth suppression and tree mortality (Lavoie et al. 2021; Z. Liu et al. 2022; Zinsou Max Debaly, Marchand, and Girona 2022). SBW is therefore responsible for marked losses in forest productivity with an important effect on economic activities (Grondin et al. 1996). In addition, defoliated trees are more susceptible to fungi and diseases, which leads to a reduction in the quality of the wood available to the woodworking industries (MacLean 2016; Safranyik et al. 2010; Chang et al. 2012b; Alvaro Fuentealba et al. 2022). The spread of forest pest insect outbreaks is a complex phenomenon that can occur on a wide range of spatial scales (Bouchard and Auger 2014; Montoro Girona, Navarro, and Morin 2018). The surface area of defoliated forests during the 35 to 40 years that a SBW outbreak lasts (Boulanger and Arseneault 2004) can attain 130000 km^2(Germain et al. 2021), or around the size of Greece. In Eastern Canada, the boreal forest is an integral part of the environment, economy, culture and history (Kayes and Mallik 2020). Due to the ecological and economic consequences of SBW outbreaks, their study is a major topic in Canadian forestry.

Furthermore, the reconstruction of the dynamics of SBW outbreaks over the last centuries shows that the frequency, severity and spatial distribution of SBW outbreaks

have changed (Simard, Morin, and Lavoie 2006; Navarro et al. 2018; Berguet et al. 2021; Girona et al. 2023), with their distribution shifting towards the north-eastern sector of the country (Pureswaran, Roques, and Battisti 2018; Jactel, Koricheva, and Castagneyrol 2019; Navarro et al. 2018; Seidl et al. 2017; Jacques Régnière and Nealis 2019b). These changes can be explained by alterations in the spatial distribution of SBW hosts due to climate change and climate effects on SBW population dynamics (Jacques Régnière and Nealis 2019b; D'Amato et al. 2023; MacLean 2016; Schowalter 2022). Understanding the temporal dynamics of SBW outbreaks is crucial for developing effective forest management and intervention strategies (Pureswaran et al. 2015; Overpeck, Rind, and Goldberg 1990; Jacques Régnière and Nealis 2019b). The challenge, however, lies in the complex, nonlinear nature of these outbreaks, which evolve through distinct stages—from endemic (low) populations to epidemic (high) levels and eventual collapse. Defoliation data are most often analysed with predictive methods such as random forests (Candau and Fleming 2011b), parametric statistical models such as like linear regression (Zhu et al. 2018; Germain et al. 2021) and semi-parametric methods such as GAMs (Eickenscheidt, Augustin, and Wellbrock 2019; Perrier et al. 2021; Boakye et al. 2022; T. J. Hastie 2017; T. Hastie, Tibshirani, and Friedman 2009; Shalev-Shwartz and Ben-David 2014). However, all of these methods do not take into account either the ordinal time series nature of defoliation data, or the fact that the process of defoliation is cumulative across time (J. Régnière and Nealis 2007; Chen et al. 2017b; Sturtevant et al. 2015). This article aims to offer straightforward statistical tools that can easily accommodate the characteristics of most defoliation data, and more generally, time series of ordinal categorical data. These methodological limitations not only lead to reduced predictive accuracy but also limit forest managers' ability to precisely anticipate outbreaks, complicating targeted and economically viable management strategies.

Ordinal categorical data, i.e., data taking discrete values that can be ranked on a scale but do not represent precise numerical intervals, are common in many disciplines, including biology and ecology (Agresti 2010). They can be produced when the observed phenomenon occurs inherently on a series of discrete, qualitative states,

such as the phenological stages of flowering (Salisbury, Wareing, and Galston 2013). In other cases, the underlying phenomenon is continuous but is recorded on an ordinal scale to allow for the rapid surveying of a large area. Examples include regional surveys of weed density (Goodsell et al. 2021) or aerial surveys of defoliation from forest insect outbreaks (e.g., donnees Quebec surveys. If the ordinal variable being measured also depends on its own value at previous points in time, then the analysis of these data requires methods adapted to ordinal time series. Important developments have been made recently for discrete-valued time series (Weiß 2018; Davis et al. 2016). Many models exist for count data (Fokianos and Tjøstheim 2012; Fokianos et al. 2020), binary data (Moysiadis and Fokianos 2014), categorical data (Fokianos and Kedem 2003) and even multivariate mixed data (Zinsou-Max Debaly and Truquet 2023). Unfortunately, ordinal categorical time series have not received as much attention. Indeed, since about 1980, authors have distinguished between ordered- and unordered-scale categorical data. (Agresti 2010) detailed specific modeling approaches for individual response variables having ordered categories, which are based on different transformations of probabilities of each category. (Fokianos and Kedem 2003) introduced generalized linear-type models and distinguished models for ordinal and nominal time series. Ordinary time series (hereafter OTS) models are then formulated with the so-called cumulative-logit model. Their work was extended by (Moysiadis and Fokianos 2014) for nominal data only. The latter proposed a model nested in the broad class of observation-driven (Cox et al. 1981) models for time series data. Other methods for modeling nomimal categorical time series include (Weiß 2020) for advances in so-called discrete autoregressive–moving-average model (DARMA), presented in (Jacobs and Lewis 1978), and (Berchtold and Raftery 2002) for the mixture transition distribution model (MTD). More recently, new models have been proposed for ordered categorical processes based on a quantitative interpretation of the scales of time series. For example, (Mengya Liu, Li, and Zhu 2022) considered OTS as Poisson-bounded time series, while (Mengya Liu, Zhu, and Zhu 2022) studied the latter with inflated 0 and 1. (Jahn and Weiß 2024) used the interpretation of OTS as binomial processes. In doing so, one can deal with OTS as a univariate process and re-use existing materials for univariate time series

models, such as the INGARCH model (Ferland, Latour, and Oraichi 2006; Fokianos and Tjøstheim 2012) or models for binomial time series (Weiß 2018, example 4.2.5). Compared with usual methods for ordinal categorical data that consist of multivariate models, these models lower the number of parameters to be estimated, but the resulting parameters are harder to interpret.

In this research, we introduce the adjacent-category autoregressive model (ACAR), a new observation-driven framework for ordinal categorical time series. We propose diagnostic portmanteau tests (Akashi et al. 2021) to assess model adequacy and develop a test for comparing two ACAR models. The approach is applied to model the defoliation level of white spruce (Picea glauca) during spruce budworm (Choristoneura fumiferana) outbreaks in two regions of the Eastern Canadian boreal forest, incorporating both autoregressive dynamics and climate covariates.

While alternative methods for ordinal time series exist, a detailed empirical comparison is beyond the scope of this paper. Many available models target nominal data, counts, or latent continuous processes, and adapting them to the cumulative and ordinal nature of defoliation data would require extensive re-specification. We focus instead on developing a simple, interpretable, and problem-specific model tailored to practical forest management applications.

1.4. Methods

1.4.1. Statistical methodology

The details regarding notations and conventions used throughout this document are provided in the Appendix 6.1 for reference.

General formulation. The ACAR is a type of generalized linear model specifically designed for ordinal data, where the outcome variable has a natural order but no numerical interpretation of the distances between categories. The ACAR focuses on modeling the odds of transitioning between adjacent categories in a time series framework. For SBW outbreaks, these categories can represent different severity levels of defoliation. The log odds of being in a higher outbreak category versus the immediately lower category are modeled as a function of both covariates (e.g., climate

variables, forest composition) and autoregressive terms (e.g., the outbreak severity in the previous time step). We denote by Y_t the ordinal response variable (e.g., outbreak severity level) at time t. It corresponds to the defoliation level for each area classified on a scale of 0 to 3 corresponding to no defoliation, a low, moderate, and high fraction of the year's foliage defoliated by SBW. More generally, Y_t can take K + 1 values indexed from 0 to K.

For any sequence $(u_n)_{n\in\mathbb{N}}$, we adopt the convention $\sum_{i=0}^{-1} u_i = 0$. Mathematically, our model is given by:

$$Y_{j,t} = \mathbb{1}\left\{\sum_{k=0}^{j-1} \pi_{k,t} \le U_t < \sum_{k=0}^{j} \pi_{k,t}\right\}, \qquad 0 \le j \le K,$$

$$\pi_{0,0} = \cdots = \pi_{K,0} = 1/(K+1),$$

$$\log\frac{\pi_{j,t}}{\pi_{j-1,t}} =: \eta_{j,t} = \omega_j + \gamma^\top X_{t-1} + \alpha^\top \overline{Y}_{t-1} + \beta_j \eta_{j,t-1}, \qquad 1 \le j \le K, t > 0.$$

$$\text{where } \omega_j \in \mathbb{R}, \gamma \in \mathbb{R}^P, \alpha \in \mathbb{R}^K \text{ and } \beta_j \in \mathbb{R}^* \text{ for } j = 1, \dots, K.$$

In Eq. ([model]), $\pi_{k,t}$ is the probability that $Y_t = k$ and U_t is a uniform random variable. The vector $(Y_{0,t}, \dots, Y_{K,t}) \in \{0,1\}^K$, where for $0 \le j \le K$, $Y_{k,t} = 1$ when $Y_t = k$, is thus the one-hot encoding of the ordinal response Y_t. The vector $\overline{Y}_t = (Y_{1,t}, \dots, Y_{K,t})$ in Eq. ([eq::model_recursion]) is the same encoding without its first element $Y_{0,t}$. In this model, ω_j is the intercept for category j, γ represents the effect of covariates (e.g., temperature, precipitation), and α captures the autoregressive effect of the previous year's defoliation. The parameters $\beta_j, j = 1, \dots, K$ act as feedback parameters that allow us to extend the memory of model [model]-[model_recursion] beyond lag 1; the effect of lagged values decreases exponentially if $|\beta_j| < 1$ for $j = 1, \dots, K$.

Others specifications for probabilities. At least two others ratios can be considered in place of $\frac{\pi_{j,t}}{\pi_{j-1,t}}$ in equation [model_recursion]. For example, $\frac{\sum_{i=1}^{j}\pi_{i,t}}{\sum_{i=j+1}^{K}\pi_{i,t}}, j = 0, \dots, K-1$ corresponds to cumulative-logit model (Agresti 2010; Fokianos and Kedem 2003)

while $\frac{\pi_{j,t}}{\sum_{i=j+1}^{K}\pi_{i,t}}, j = 0, \ldots, K-1$ is known as continuation-ratio logit model (Agresti 2010). For an ordinal response, the most popular of these three models is the cumulative-logit model. However, the adjacent-category model presents some advantages for interpretability, as described in detail below. Specifically, in the context of SBW defoliation data, this model allows for clear interpretation of the transition probabilities between successive defoliation categories, facilitating direct insights into outbreak dynamics.

Let us denote by $X_{p,t}$ the p-th covariate and $X_{-p,t}$ the remaining and set for simplicity $\beta_j = 0, \forall j$. If we define

$$R\left(X_{p,t}, X_{-p,t}, \overline{Y}_{t-1}\right) = \frac{\pi_{j,t}}{\pi_{j-1,t}} \text{ and } R_k\left(X_{p,t}, X_{-p,t}, \overline{Y}_{t-1}\right) = \frac{\pi_{j+k,t}}{\pi_{j-1,t}},$$

respectively the ratio of probabilities of two successive levels of Y_t, and the ratio of probabilities for a difference of $k+1$ levels, then for two different values $X_{p,t}$ and ${X_{p,t}}'$ we have

$$\frac{R\left(X_{p,t}, X_{-p,t}, \overline{Y}_{t-1}\right)}{R\left({X_{p,t}}', X_{-p,t}, \overline{Y}_{t-1}\right)} = \exp\left(\gamma_p\left(X_{p,t} - {X_{p,t}}'\right)\right) \text{ and } \frac{R_k\left(X_{p,t}, X_{-p,t}, \overline{Y}_{t-1}\right)}{R_k\left({X_{p,t}}', X_{-p,t}, \overline{Y}_{t-1}\right)} = \left[\frac{R\left(X_{p,t}, X_{-p,t}, \overline{Y}_{t-1}\right)}{R\left({X_{p,t}}', X_{-p,t}, \overline{Y}_{t-1}\right)}\right]^{k+1}$$

where γ_p is the regression parameter of the covariate $\left(X_{p,t}\right)_{t\in\mathbb{Z}}$ and these quantities do not depend on the category j.

Moreover, larger values of $X_{p,t}$ are associated with lower values of Y_t for the covariates with $\gamma_p < 0$, and with higher values of Y_t for the covariates where $\gamma_p > 0$.

Finally, model [model]-[model_recursion] is similar to the baseline-category logistic model for nominal data since

$$\lambda_{j,t} := \log\frac{\pi_{j,t}}{\pi_{0,t}} = \sum_{k=0}^{j-1} \log\frac{\pi_{k+1,t}}{\pi_{k,t}} = \sum_{k=0}^{j-1} \eta_{j+1}.$$

$$\text{For } k = 1, \dots, K,$$

$$\pi_{k,t} = \frac{e^{\sum_{j=1}^{k} \eta_{j,t}}}{1 + \sum_{i=1}^{K} e^{\sum_{j=1}^{i} \eta_{j,t}}}, \quad \pi_{0,t} = 1 - \sum_{k=1}^{K} \pi_{k,t}.$$

Equal slopes model. Equations [eq::model]-[eq::model_recursion] coincide with the equal slopes model in multinomial regression since the parameters α and γ in [eq::model_recursion] do not depend on j. However, the coefficients for the latent processes β_j are indexed with the categories. It would be possible to build a full equal slopes model by replacing $\beta_j \eta_j$ in [eq::model_recursion] by $\sum_{k=1}^{K} \beta_k \eta_k$. The latter model is not a nested model of the one considered here and therefore cannot be compared to this one with nullity coefficients tests (see for example (Heyde 2013) chap. 9). Some arguments can be made in favour of models with category-specific effects, *i.e*

$$\log\frac{\pi_{j,t}}{\pi_{j-1,t}} =: \eta_{j,t} = \omega_j + \gamma_j^\top X_{t-1} + \alpha_j^\top \overline{Y}_{t-1} + \beta_j \eta_{j,t-1}, \qquad 1 \le j \le K.$$

For the application under consideration here, this model would allow us to disentangle the effect of climate on different phases of SBW outbreaks. In this case, the parameters γ_1 stand for the effect of covariates on the initial phase of outbreaks and $\gamma_j, j > 1$ the outbreaks' development. Such a study appears in (Bouchard, Kneeshaw, and Bergeron 2006) where the authors employed Bayesian model averaging (D. Anderson and Burnham 2004; Soti et al. 2019).

Model for more lags. For a more general model, [eq::model_recursion] can be replaced by

$$\log\frac{\pi_{j,t}}{\pi_{j-1,t}} =: \eta_{j,t} = \omega_j + \gamma^\top X_{t-1} + \sum_{i=1}^{r} \alpha_i^\top \overline{Y}_{t-i} + \sum_{i=1}^{r} \beta_{j,i}\, \eta_{j,t-i}, \quad 1 \le j \le K$$

for a fixed r.

However, a model with lag 1 is often sufficient to capture the properties of time series. A detailed discussion of the model's stability properties and statistical inference is provided in Appendix 6.2. Conditions for stationarity and ergodicity are outlined in Proposition 6.1 based on the (Truquet 2020), while Proposition 6.2 addresses the asymptotic properties of the maximum likelihood estimator for the parameters using standard existing results. Proposition 6.3 (Appendix 6.2) investigates the goodness-of-fit test. As we will see below, we are also interested in comparing the dynamics across different sites, with results on this topic provided in Section 6.2.2 of the appendix 6.2. We intentionally assume certain high-level conditions and omit some technical details to make this paper accessible to the ecological audience for which it is written. For a thorough explanation and additional context, please refer to that section.

Model implementation. Numerical implementation of model [eq::model]-[eq::model_recursion] and statistical inference methods are implemented in the R language (R Core Team 2022). We choose $\beta_{j,0} = 0.5, j = 1, \dots, K$ for initial values of the latent processes, whereas the first observations of paths acts as initial values for the sequence $(Y_t)_{t\in\mathbb{Z}}$. The initial value of the score sequence is set to 0_{3K+P}, where for any integer d, 0_d represents the d-dimensional vector with all elements equal to 0. The loss function [eq::cmle] is optimized for 20 different random initializations with the built-in R function optim using the L-BFGS-B method (Byrd et al. 1995), a derivative-free optimization routine that allows box constraints. For the parameter vector $\beta_j, j = 1, \dots, K$, the box constraints are represented as follows $-0.999999 \leq \beta_j \leq 0.999999$. The estimated θ vector is the one corresponding to the minimum loss function value over all initializations. Let us define θ_j as the j-th element of the parameter vector θ, the set $\Theta \ni \theta$ is :

$$\Theta =: \Theta_\varepsilon = \{\theta \in \mathbb{R}^{3K+P} : \theta_{3K+P-j} \in [-1+\varepsilon, 1-\varepsilon], j = 1,2,3 \text{ and } \theta_j \in [-1/\varepsilon, 1/\varepsilon], j = 1, \dots, 2K+P\}$$

for a fixed and known $\varepsilon > 0$. Here we fixed $\varepsilon = 1\mathrm{e}^{-6}$. All methods are make available *via* two top-level functions *poly_autoregression* and *comparison_test_dependent*. The first one takes as arguments the observed paths of sequences $\left(\overline{Y_t}\right)_{t\in\mathbb{Z}}$ and $(X_t)_{t\in\mathbb{Z}}$ and returns among others the estimated values of the parameters θ, their standard errors and the result of the Portmanteau test in proposition 6.3. The second function takes as arguments the returned values of two models fitted with *poly_autoregression* and gives the statistics and the p-values of the test in Proposition 6.4.

Numerical experimentation. We recall that the parameter vector is denoted by $\theta = (\omega^\top, \mathrm{vec}(\Gamma)^\top, \alpha^\top, \beta_1, \dots, \beta_K)^\top$. For numerical experimentation, we used a simulated adjacent categorial response variable with four levels, as in our real data example, and five simulated covariates. We will consider parameter sets in Table 2.1, which were chosen to meet the condition $\left|\beta_j\right| < 1, j = 1, \dots K$ in proposition 6.1.

Table 1
Parameter sets for numerical experimentation

	$\boldsymbol{\omega_1}$	$\boldsymbol{\omega_2}$	$\boldsymbol{\omega_3}$	$\boldsymbol{\gamma_1}$	$\boldsymbol{\gamma_2}$	$\boldsymbol{\gamma_3}$	$\boldsymbol{\gamma_4}$	$\boldsymbol{\gamma_5}$	$\boldsymbol{\alpha_1}$	$\boldsymbol{\alpha_2}$	$\boldsymbol{\alpha_3}$	$\boldsymbol{\beta_1}$	$\boldsymbol{\beta_2}$	$\boldsymbol{\beta_3}$
$\theta_0^{(1)}$	1.2	0.7	0.5	-0.8	1.5	-1.5	2.0	2.0	0.3	-0.3	0.5	0.8	-0.2	0.3
$\theta_0^{(2)}$	1.2	0.7	0.5	0.8	-1.5	1.5	-2.0	-2.0	-0.3	0.3	-0.5	-0.8	0.2	-0.3
$\theta_0^{(3)}$	1.2	0.7	1.5	0.8	-1.5	-1.5	2.0	-2.0	0.3	-0.3	-0.5	-0.8	0.2	-0.3

Finite sample performance of the maximum likehood estimator. We investigate the finite sample performance of the estimator [eq::cmle] for the parameter sets $\theta_0^{(1)}, \theta_0^{(2)}$ and $\theta_0^{(3)}$. For each vector θ_0, the data genaration process consists in drawing the covariates $(X_t)_{t=1..n}$ from a standard Gaussian random distribution on $\mathbb{R}^5$ and $(Y_t)_{t=1..n}$ according to [eq::model]. Four sample sizes are considered: $n = 70{,}100{,}300{,}500$. We repeat this process $B = 499$ times and for each sample, we compute the estimate $\hat{\theta}_n$ and the covariance matrix of estimator 6.2. Table 6.1 in supplementary materials 6.4.7 presents the simulation results. In those results, CMLE refers to the average value of the parameter estimates and TSE refers to the average value of the theoretical standard errors :

$$\text{CMLE} = B^{-1}\sum_{b=1}^{B}\hat{\theta}_T^{(b)} \text{ and } \text{TSE} = B^{-1}\sum_{b=1}^{B}\text{diag}\left\{\hat{J}^{-1(b)}\hat{L}^{(b)}\hat{J}^{-\top(b)}\right\}^{1/2}$$

where the superscript b stands for the index of replication and $\text{diag}M$ is the vector of diagonal elements of a matrix M. MAE and MSE refer to the mean absolute error and mean squared error of the estimator. It appears that the model parameters are well estimated even for $n = 100$. For $n = 70$, the estimates are less precise based on our estimated standard errors. Nethertheless, the true values of parameters are recovered in many cases by the confidence interval at level 0.95 (refer to Table 6.4.7).

Comparison tests. We set four scenarios to access the quality of the comparison test in Proposition 6.4. (1) The processes $\left(X_t^{(1)}, U_t^{(1)}\right)_{t\in\mathbb{Z}}$ and $\left(X_t^{(2)}, U_t^{(2)}\right)_{t\in\mathbb{Z}}$ are independent and their true parameter values are both equal to $\theta_0^{(1)}$. (2) The processes $\left(X_t^{(1)}, U_t^{(1)}\right)_{t\in\mathbb{Z}}$ and $\left(X_t^{(2)}, U_t^{(2)}\right)_{t\in\mathbb{Z}}$ are independent and their true parameter values are different, i.e. $\theta_0^{(1)}$ and $\theta_0^{(3)}$, respectively. (3) The processes $\left(X_t^{(1)}\right)_{t\in\mathbb{Z}}$ and $\left(X_t^{(2)}\right)_{t\in\mathbb{Z}}$ are independent, $U_0^{(2)} = 1 - U_0^{(1)}$ and their true parameter values are both equal to $\theta_0^{(1)}$. (4) The processes $\left(X_t^{(1)}\right)_{t\in\mathbb{Z}}$ and $\left(X_t^{(2)}\right)_{t\in\mathbb{Z}}$ are independent, $U_0^{(2)} = U_0^{(1)}$ and their true parameter values are $\theta_0^{(1)}$ and $\theta_0^{(3)}$, respectively.

For each of theses scenarios, we simulated $B = 1000$ pairs of paths of length $n = 500$ and performed the comparison tests on each simulated pair. For scenarios 2 and 4, the null hypothesis is rejected for all $B = 1000$ tests, showing a power of test near 1. For scenerio 1, the null hypothesis is accepted in 65% cases and this rate drops to 60% for scenario 3.

1.4.2. Study area

The study area is located in the northern temperate zone of eastern North America , in the temperate forests of the province of Québec, Canada. The two study sites (Témiscamingue and Matawinie) were selected based on the availability of long time series of dendrological and weather data, as described in the following sections.

With an area of 64,656 km^2, Abitibi-Témiscamingue is located in the extreme west of province of Quebec. The region is cold and dry (Dfc type, according to the Köppen-Geiger classification) (Kottek et al. 2006) and the rainfall is about 900 mm per year (*MDDEP, 2012*). The region of Abitibi-Témiscamingue overlaps three contrasting Canadian ecoregions: the highlands of Mistassini, the lowlands of Abitibi and James Bay, and the Southern Laurentides (Tiné et al. 2019). The sampled forest of this region sits at 46°34' North and 78°50' West in the boreal zone of Témiscamingue. It is located in the Sugar maple - yellow birch bioclimatic zone (Figure 2), in the northern temperate zone which is made up of deciduous and mixed forests (a mixture of deciduous and coniferous trees).

Matawinie is located in the Lanaudière administrative region of Québec. With an area of 13 515 km^2, this region is cold (Dfb type according to the Köppen-Geiger classification) (Kottek et al. 2006) and the rainfall is about 1000 mm per year (*MDDEP, 2012*). The sampled forest of this region sits at 46°26' North and 73°30' West in the wooded hills zone of Matawinie. Like Témiscamingue, It is located in Sugar maple - yellow birch bioclimatic zone (Figure 2)

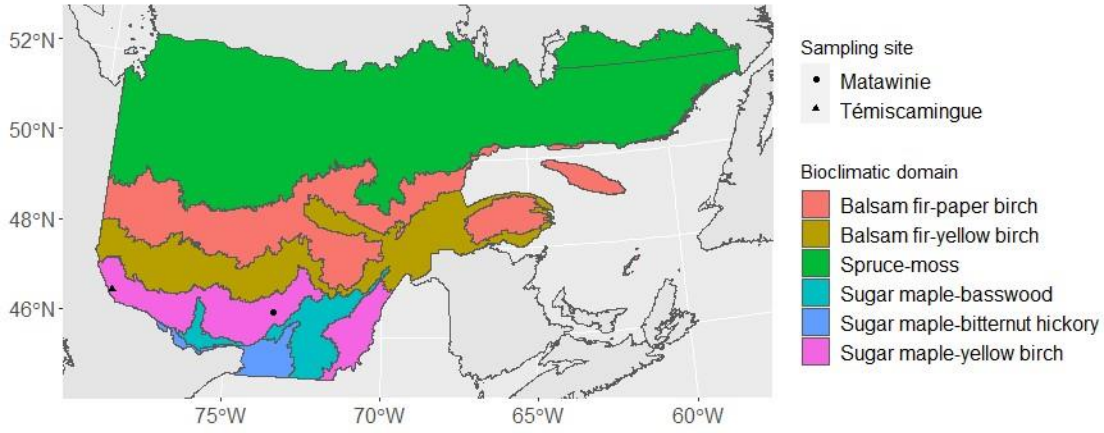

Figure 2
Location of sites of study area in Quebec boreal ecoregions.

1.4.3. Data description

Defoliation Data. We obtained dendrological data for the two study sites for a 75-year period (1920-1995) from the study of (Navarro et al. 2018). This database incorporated sites from an original study by (Jardon, Morin, and Dutilleul 2003). In this survey, a 400 m^2 plot was sampled at each site. In each plot, wood disks were collected from seven dominant living trees and three dominant living saplings. The time period selected for this study guarantees that tree samples were able to register multiple insect outbreaks during the 20th century providing long chronologies across the study area. Authors employed dendrochronology methods (Krause and Morin 1995) to reconstruct SBW outbreaks at each site. It should be noted that reduced growth is an indirect indicator of defoliation. We refer interested readers to (Navarro et al. 2018) for details the methodology for detecting defoliation events. Briefly, a tree was considered as defoliated when its growth was at least 1.28 sd under the mean of the detrended dendrochronology over multiple years. The severity of the insect outbreak at a site was defined by the proportion of trees at the site that presented such a pattern of growth reduction for a given year. For the purpose of the present study, the proportion of defoliated trees at each site was converted to an ordinal variable as follows: level 0 (null defoliation) If less than 1% or no tree experiences a reduction in growth based on the above criteria; 1 (light defoliation) if 1 to 35% of trees had reduced growth; 2 (moderate defoliation) if more than 35 to 70% of trees had reduced growth and 3 (severe defoliation) if 70 to 100% *i.e* of trees had reduced growth reduction. The data collections are available on figshare.

Note that for the purpose of this study, we convert the proportion of defoliated trees to a less precise ordinal scale, the model presented here will be applied to defoliation data collected on an ordinal scale, i.e. from the Quebec Ministry of Natural Resources and Forests aerial surveys (MFFP 2022) in future studies, and the defoliation thresholds chosen here match the ordinal scale used for those surveys. The dendrological data was chosen for this initial demonstration of the method, since it provides longer time series as mentioned above.

Climate data sets. Climate data were obtained from the National Centers for Environmental Information (NCEI). The weather station in Témiscamingue is located 25 km away from the forest site and the distance between the forest in Matawinie and the weather station is about 35 km. The data sets from the two measuring stations contain daily maximum and minimum temperatures, the amount of precipitation and snow depth from 1920 to 1995 (75 years of daily data). The daily climate data for 1928 contains a lot of missing data. We have therefore excluded 1928 from our analysis. From this raw data, we computed seasonal covariates in summer and spring as suggested by the biological characteristics of SBW and many previous studies (Zinsou Max Debaly, Marchand, and Girona 2022; Volney and Fleming 2007, 2000). The specific covariates used are described in the following section. We considered the months of April, May and June as the spring season and the months of July, August and September as the summer season. Since the effect of defoliation on growth is delayed, the model will include the effect of climate covariates with a lag of two years.

1.4.4. Data analysis

We considered two sets of temperature-related covariates and one set of precipitation-related covariates for the models. The first set of temperature covariates included inter-annual differences (current year - previous year) in the mean daily maximum and mean daily minimum temperatures for the spring and summer. The second set of temperature covariates included the seasonal range (maximum - minimum across all days) of daily minimum and daily maximum temperatures for the spring and summer. The set of precipitation covariates included annual precipitation, annual snowfall, and the log values of the two. For all temperature-related covariates, we included a quadratic term to the model in addition to the linear effect. The threshold at which the effect of temperature shifts from positive to negative or vice versa was estimated as described in supplementary material.

For both sites of interest, we fit the model [eq::model]-[eq::model_recursion] with all the possible combinations of the covariates, except that only one of the two sets of temperature-related covariates (inter-annual differences or seasonal ranges) was used in each model. For each fitted model, the Portmanteau goodness-of-fit test (see

Appendix 6.2.2) with a lag of one was performed. Only the models for which H_0 was not rejected were considered for our analysis. In order to demonstrate the use of the comparison test between analogous models at each site (Proposition 6.4), we selected the best model at the Témiscamingue site based on the Akaike information criterion (AIC) and compared it to model with the same covariates for Matawinie. If the null hypothesis was rejected at the global level (i.e. the two models differed), we performed the covariate-level test (Proposition 6.4) to determine which covariate(s) were responsible for the difference.

1.5. Results

The best model (according to AIC) for Témiscamingue is the one including the seasonal range of daily maximum and minimum temperature as covariates (see Table 2.2). That model suggests not only that the effect of temperature on defoliation dynamics is non-linear, but also that this effect varies according to season (summer and spring). The estimated coefficients for summer temperature and spring temperature show a quadratic effect of temperature with a maximum and minimum respectively for summer temperature and spring temperature. Results from both regions show that up to a certain threshold (see details in Appendix 6.4.6) estimated at 23°C (CI of 0-40°C at 95%) in Témiscamingue and 22°C (CI of 0-54°C at 95%) for Matawinie, a greater range of the daily maximum temperatures during the summer is associated with lower levels of defoliation. Over the entire period covered by our study, the range of the daily maximum temperatures during the summer used for modelling is between 15°C and 30°C with a median of 23°C for Témiscamingue and between 15°C and 28°C with a median of 21°C for Matawinie.

For Matawinie, the model shows that a greater range in temperature for the spring is associated with a higher level of defoliation. We estimated a threshold of 32°C (CI of 0-80°C) under which an increase in range of spring temperatures promotes defoliation. The range of the daily maximum temperatures during the spring in Matawinie is between 25°C and 37°C, with a median of 31°C. Indeed, hot springs are characterized by premature emergence from dormancy of larvae (Volney and Fleming 2000, 2007).

A comparison between these regions reveals that defoliation processes differ from one region to another. This difference lies in their autoregressive structure. The model for Témiscamingue is close to a parameter-driven model (*i.e.* the latent process does not depend on previous values of observed process) since the p-value of the test $H_0: \alpha_1 = \alpha_2 = \alpha_3 = 0$ is 0.512; this is not the case for Matawinie. We also note the statistical significance of the feedback parameters, in particular β_2 for both regions, indicating a link between Y_t and its all history. This result is consistent with the known cumulative effect of the defoliation on tree growth (Chen et al. 2017b; Houndode, Krause, and Morin 2021).

Table 2
Estimates of the selected model for Témiscamingue and Matawinie

	number of parameters = 14 n = 72			
	Témiscamingue	Matawinie	Comparison of both models	
	parameters (t-stat)	parameters (t-stat)	t-statistics	sig. code
ω_1	-0.684 (-0.005)	17.808 (0.635)	0.144	
ω_2	-35.239 (-0.160)	-2.233 (-0.084)	0.149	
ω_3	-35.745 (-0.163)	-6.407 (-0.244)	0.133	
Δ*temp. max. spring*	56.351 (0.564)	31.206* (2.299)	0.254	
Δ*temp. min. summer*	-2.454 (-0.366)	1.248 (1.061)	0.543	
Δ*temp. max. summer*	-58.714*** (-3.820)	-67.179* (-2.198)	0.253	
Square of Δ*temp. max. spring*	-10.742 (-0.568)	-4.794* (-2.203)	0.317	
Square of Δ*temp. max. summer*	12.927*** (4.966)	15.404* (2.219)	0.338	
α_1	34.638 (0.341)	3.201* (2.004)	0.310	
α_2	40.594 (0.357)	25.209*** (3.264)	0.136	
α_3	42.134 (0.367)	27.066*** (3.111)	0.132	
β_1	0.839 (1.348)	0.263 (0.669)	0.824	
β_2	0.811*** (4.212)	-0.985*** (-52.428)	9.288	***
β_3	0.693*** (3.614)	-0.009 (-0.005)	0.460	
portmanteau stat :	2.238	0.082	comparison stat : 12006.0***	
portmanteau p-value :	0.524	0.994	comparison p-value : $< 10^{-5}$	

Δtemp. : range of temperature over season
sig. code : 0.90 . 0.95 * 0.99 ** 0.999 *** 1

1.6. Discussion and perspectives

Ecological studies that involve time series are generally based on intensive studies of restricted populations or small-scale ecosystem recovery. In fact, variations often occur in few places and under relatively static conditions (Goodsell et al. 2021). It is

therefore advantageous to cover a larger area more quickly, simply by estimating the data on an ordinal scale. In this paper, we propose a statistical tool for modeling adjacent-categories time series. Using the intensity of defoliation data as a case study, we related the impact of climate variation on intensity of SBW defoliation in Eastern Canadian forests through an adjacent-category autoregressive model. The model we are proposing is a useful tool to analyze the impact of climate on defoliation, since each of the successive defoliation levels can be influenced differently by environmental factors during a SBW outbreak (Bouchard and Auger 2014; Jepsen et al. 2009) and SBW development is also dependent of the previous year's defoliation (Bouchard and Auger 2014).

Our paper presents two majors findings. The first one is a non-linear effect of temperature on defoliation. Although several studies show that with increasing temperatures (caused by climate change), there is an increase in the frequency and severity of SBW outbreaks (Overpeck, Rind, and Goldberg 1990; J. Régnière and Nealis 2007; Pureswaran et al. 2015, 2019; Bouchard and Auger 2014; Bouchard, Régnière, and Therrien 2018a; Moise, Lavigne, and Johns 2019), our results suggest that a greater range of summer temperatures increases defoliation up to a certain threshold beyond which the effect is reversed. It can be explained by the fact that extreme temperatures reduce SBW fecundity, increase mortality and affect the sex ratio via an impact on endosymbionts by favouring the production of male individuals (Hance et al. 2007). Summer temperature had a much greater influence on SBW population recruitment. Summer marks the development of larvae and the reproduction of adult SBWs, processes which are closely linked to a number of climatic factors, including temperature (Bouchard and Auger 2014; Pureswaran et al. 2015, 2019; Volney and Fleming 2000). Indeed, summer corresponds to the period when female deposits her eggs (see Figure 6.1). Our results suggest that high variations of temperature induce low survival egg rate. The growth of SBW population density is the combination of its egg recruitment rate and generation survival rate (see. (Royama et al. 2005)). The success of SBW in establishing itself on sites depends on reproduction, the initial weight of the eggs and the synchronization of their

development with that of the buds of their hosts, which is strongly influenced by climatic factors (Volney and Fleming 2000, 2007).

We also denote that a greater range of spring temperatures has a negative effect on defoliation levels. Spring is a critical period for defoliation, as it marks the emergence of SBW larvae from hibernation and the start of needle mining by SBW hosts. Early spring is generally marked by mild temperatures, which favour cohabitation between SBW and its parasitoids(Bouchard, Régnière, and Therrien 2018a; Royama et al. 2005). This cohabitation could explain the negative effect of spring temperature. The SBW benefits from the negative synergistic effects of temperature pressures on its natural enemies, particularly its parasitoids. For example, the overall performance of some parasitoids is severely reduced at high temperatures. (Jacques Régnière, Seehausen, and Martel 2020; Hébert and Cloutier 1990; Seehausen et al. 2017; Smith, Hubbes, and Carrow 1986; Royama et al. 2005). This is the case for *T. rostrale* (an SBW parasitoid), whose survival is negatively correlated with temperatures above 20°C (Jacques Régnière, Seehausen, and Martel 2020; Seehausen et al. 2017). Although the uncertainty around the threshold value for the spring temperature is high, our results clearly illustrate the dynamics of the interaction between SBW and its parasitoids under the temperature effect and its consequences on defoliation levels.

We have shown how the comparison test associated with our models can reveal differences between the defoliation processes for two distinct sites. However, more work is needed to extend that comparison to greater number of sites. A possible approach would be to perform clustering analyses based on a measure of model dissimilarity between sites. Another limitation of this study is that the intensity of defoliation was reconstructed from tree growth data rather than directly observed. Bayesian models could be used to combine evidence from the longer, but indirect time-series measurements from dendrochronology to the shorter time series (a few decades) of aerial surveys of defoliation (MFFP 2022).

The ACAR model presented here could be applied in ecology beyond the topic of forest insect outbreaks; for example, the dynamics of agricultural weed density as

studied by (Goodsell et al. 2021) using an ordinal scale to quickly collect data over larger regions. Since many dynamic ecological processes that are autocorrelated over time also show spatial dependence (e.g., due to dispersion/migration of individuals), further development of the ACAR model could focus on incorporating this spatial dependence. This spatio-temporal extension of the model would be particularly important to leverage one of the main advantages of ordinal scale ecological data such as the aerial surveys of defoliation: that is, their availability over large, contiguous regions of space instead of point sampling sites. Future research could therefore prioritize the integration of spatial autocorrelation into the ACAR framework, allowing simultaneous consideration of spatial and temporal dynamics, thus maximizing the utility of large-scale ordinal ecological data such as aerial defoliation surveys.

Ethics approval and consent to participate. Not applicable

Consent for publication. Not applicable

Availability of data and material. The datasets and R scripts used and/or analyzed during the current study are available from the corresponding author upon request.

Competing interest. The authors have no conflict of interest to declare.

Funding. PM and MMG obtained funding from the Natural Sciences and Engineering Research Council of Canada (NSERC) Alliance and the Québec Ministry of Natural Resources and Forests (MRNF) to understand the dynamics of spruce budworm (ALLRP 558267-20). MMG obtained additional funding from an NSERC Discovery grant to reconstruct the regime of natural disturbances in forest ecosystems (RGPIN-2022-05423). ZMD received support from the Fonds de recherche du Québec – Nature et technologies (FRQNT) (PBEEE Scholarship DEBZI-334569) and a CY Initiative of Excellence (grant ”Investissements d’Avenir” ANR-16-IDEX-0008), Project ”EcoDep” PSI-AAP2020-0000000013.

Authors’ contributions. Design and conceptualization: OJFO, ZMD, PM and MMG. R software programming: OJFO and ZMD. Models and data analysis: OJFO, ZMD

and PM. Writing first draft: OJFO. Supervision and validation: PM and MMG. All authors provided input for the manuscript, contributed critically to the drafts and gave final approval for publication.

Acknowledgments. We acknowledge all the previous projects and researchers from which we compiled the dendrochronological data. We thank Professor Paul Doukhan from Paris University for his valuable comments. We also wish to thank Murray Hay, whose proofreading greatly improved the quality of the manuscript.

2. SPATIAL VARIABILITY IN DEFOLIATION DYNAMICS DURING SPRUCE BUDWORM OUTBREAKS: A LANDSCAPE PERSPECTIVE

Olaloudé Judicaël Franck Osse, Philippe Marchand et Miguel Montoro Girona

Une version de ce chapite a été publié dans le journal *Ecological Modelling* en 2025
https://www.sciencedirect.com/science/article/pii/S0304380025003230

2.1. Highlights

Seasonal temperatures, particularly in spring and summer, exhibit significant non-linear effects on defoliation dynamics.

Strong autoregressive feedback reveals the cumulative effect of past defoliation, which weakens trees over time. This creates feedback loops that increase vulnerability to subsequent outbreaks, affecting forest health and resilience.

Homogeneous zones can benefit from region-specific interventions, while transitional areas necessitate nuanced approaches to optimize resource allocation and mitigate the ecological and economic impacts of SBW outbreaks

2.2. Résumé

Notre étude examine les dynamiques spatio-temporelles de la défoliation causée par la tordeuse des bourgeons de l'épinette (TBE) dans les forêts boréales du Québec, en mettant en lumière les interactions entre les facteurs climatiques, les antécédents de défoliation et l'hétérogénéité du paysage. Les épidémies de TBE constituent l'une des principales perturbations naturelles dans ces écosystèmes, avec des répercussions écologiques et économiques majeures — d'où la nécessité de mieux comprendre les mécanismes sous-jacents à leur déclenchement et à leur intensification. Si des travaux antérieurs ont mis en évidence un lien entre le réchauffement climatique, l'historique des défoliations et l'amplification des épidémies, les effets localisés de ces facteurs demeurent encore insuffisamment caractérisés. L'objectif de cette recherche est donc de clarifier ces processus locaux afin d'orienter des stratégies de gestion forestière plus ciblées et adaptatives.

Pour ce faire, nous avons utilisé un modèle autorégressif à catégories adjacentes (ACAR), spécifiquement conçu pour des données ordinales de défoliation collectées entre 1992 et 2022. La défoliation y est classée en trois niveaux de sévérité : nulle, légère, et modérée/sévère. Les variables climatiques clés, notamment les températures printanières et estivales, ainsi que les précipitations, ont été obtenues via BioSIM et associées à chaque unité de paysage (UP). Après avoir ajusté un modèle ACAR distinct pour chaque UP et validé leur adéquation à l'aide du test de Portmanteau, les meilleurs modèles ont été sélectionnés sur la base du critère d'information d'Akaike (AIC). Une analyse de regroupement a ensuite permis de classifier les UP selon la similarité de leurs paramètres modèles, révélant des regroupements écologiques cohérents.

Nos résultats indiquent que la température exerce une influence non linéaire sur la défoliation par la TBE : si des conditions printanières et estivales plus chaudes favorisent initialement la survie larvaire, des températures excessives peuvent au contraire réduire l'intensité de la défoliation en dépassant les seuils de tolérance thermique des larves ou en perturbant la synchronisation phénologique avec les essences hôtes. De plus, les coefficients autorégressifs élevés (β_1, β_2) révèlent des

effets cumulatifs significatifs : les arbres affaiblis par les infestations précédentes deviennent plus vulnérables aux attaques ultérieures, ce qui enclenche des boucles de rétroaction susceptibles de compromettre la résilience des forêts à long terme. L'analyse de regroupement a mis en évidence cinq groupes distincts d'unités de paysage. Les groupes les plus homogènes (clusters 4 et 5) se distinguent soit par une stabilité relative des précipitations, soit par une forte variabilité thermique, et présentent des scores de silhouette élevés (0,55 et 0,24 respectivement), ce qui suggère des opportunités claires pour une gestion différenciée. À l'inverse, des regroupements plus hétérogènes comme le cluster 1 (score de silhouette : $-0{,}43$) présentent des caractéristiques écologiques chevauchantes, appelant à des analyses plus approfondies.

Dans l'ensemble, ces résultats soulignent la pertinence de stratégies de gestion forestière localisées, fondées sur l'identification de seuils climatiques critiques et la prise en compte des effets cumulatifs de la défoliation. L'identification des extrêmes thermiques et l'intégration des antécédents de défoliation dans les plans d'intervention pourraient améliorer à la fois le moment et l'intensité des actions de lutte ou d'adaptation. Des recherches futures pourraient incorporer d'autres facteurs spatiaux, tels que la composition forestière ou la connectivité des massifs, afin d'affiner les prédictions d'épidémies. À terme, une gestion adaptative, multi-échelle et fondée sur les données est essentielle pour préserver la résilience des forêts boréales face aux perturbations liées aux changements climatiques.

2.3. Abstract

Our study explored the spatiotemporal dynamics of spruce budworm (SBW) defoliation in Quebec's boreal forests, highlighting how climatic factors, historical defoliation, and landscape heterogeneity intersect. SBW outbreaks are a major disturbance in these ecosystems, with significant ecological and economic repercussions—underscoring the need to understand the mechanisms that drive them. Although previous research has linked warming temperatures and past defoliation patterns to more severe outbreaks, their localized effects remain poorly characterized. Our aim is to clarify these localized processes and support more targeted forest management strategies.

We employed an adjacent-category autoregressive (ACAR) model specifically designed for ordinal defoliation data spanning 1992–2022. Defoliation was categorized into three severity levels: none, light, and moderate/severe. Key climate variables—most notably spring and summer temperatures, as well as precipitation—were obtained from BioSIM and assigned to each landscape unit (LU). After fitting individual ACAR models to each LU and confirming their adequacy via the Portmanteau test, we identified the best models using the Akaike Information Criterion (AIC). A clustering analysis then grouped LUs with comparable model parameters into distinct ecological response clusters.

Our findings reveal that temperature exerts a non-linear influence on SBW defoliation: while warmer spring and summer conditions can initially facilitate larval survival, exceedingly high temperatures reduce defoliation by surpassing larval thermal tolerance and disrupting phenological synchrony with host trees. Additionally, strong autoregressive feedback values (β_1, β_2) underscore the cumulative effect of past defoliation—trees weakened by previous outbreaks become more susceptible to subsequent infestations, triggering feedback loops that endanger long-term forest health. Through clustering, we identified five distinct landscape groups. The more homogeneous clusters (Clusters 4 and 5) displayed either relatively stable precipitation patterns or pronounced temperature variability, each with high silhouette scores (0.55 and 0.24, respectively), indicating clear opportunities for targeted

management. Meanwhile, heterogeneous clusters like Cluster 1 (silhouette score: -0.43) exhibited overlapping characteristics that warrant further investigation.

Overall, these results emphasize the importance of localized management approaches that account for climatic thresholds and historical defoliation patterns. Pinpointing temperature extremes and incorporating the impacts of cumulative defoliation can guide both the timing and intensity of interventions. Future research may integrate additional spatial factors, such as forest composition and connectivity, to refine outbreak predictions further. Ultimately, adaptive, multi-scale management is essential for maintaining the resilience of boreal forests in a changing climate.

2.4. Introduction

The boreal forest, which extends across vast regions of North America, is a complex ecosystem that supports a wide range of plant, animal, and microbial life (Hansen, Stehman, and Potapov 2010; Brockerhoff et al. 2017). This biome plays an essential role in global carbon storage and climate regulation, making it a crucial element in the ecological balance of the Earth (Pan et al. 2011; Xu and Hisano 2024; Gauthier et al. 2023). However, the boreal forest is particularly vulnerable to natural and anthropogenic disturbances (Frelich, Johnstone, and Kuuluvainen 2024; Seidl et al. 2020, 2023). One of the most significant threats is the periodic outbreak of the spruce budworm (Choristoneura fumiferana Clem.), a native insect that specifically targets coniferous trees (Sidhu et al. 2024). Recurring every 30 to 40 years, SBW outbreaks involve massive larval populations that feed on host tree foliage of host trees. During these infestations, trees suffer extensive defoliation, which not only weakens their overall health but also compromises their growth and resilience (Zinsou Max Debaly, Marchand, and Girona 2022; Doran, MacLean, and Kershaw 2017). Extending our earlier work on the adjacent-category autoregressive (ACAR) model (Osse et al. 2023), we now delve deeper into how spatial heterogeneity influences SBW defoliation dynamics across the boreal landscape. When defoliation persists for multiple years (on average five), tree mortality rates can become alarmingly high (Houndode, Krause, and Morin 2021; Fierravanti et al. 2019; MacLean et al. 2024), especially in stands dominated by balsam fir (Abies balsamea) and white spruce (Picea glauca) (Lemay, Barrette, and Krause 2022; Kneeshaw et al. 2022). Despite ongoing research on the ecological and economic consequences of SBW outbreaks, the boreal forest's vulnerability is compounded by its limited ability to recover quickly under increasingly variable climatic conditions (Seidl et al. 2017).

Although numerous studies have already demonstrated the critical influence of temperature, precipitation, and landscape factors on the severity of SBW outbreaks (M. Li et al. 2020; Jacques Régnière and Nealis 2019b; Subedi et al. 2023; Bouchard and Auger 2014; Bouchard, Régnière, and Therrien 2018a; Fierravanti et al. 2015), the methods commonly used to model their effects on outbreak development present several limitations. On the one hand, most current approaches focus on the broad-

scale effects of climate (Gray 2013; Navarro et al. 2018; Bouchard, Régnière, and Therrien 2018a), often neglecting the fine-scale integration of spatiotemporal heterogeneity in models. This omission limits the capacity to account for local specificities, such as microclimatic variability, that play a determining role in the dynamics of defoliation. On the other hand, the cumulative effects of defoliation, which progressively weaken trees (Zinsou Max Debaly, Marchand, and Girona 2022; Paixao et al. 2019; Chen et al. 2017a) and can amplify the magnitude of subsequent outbreaks, remain relatively underexplored, making it difficult to identify management strategies that are well-adapted to real conditions. Moreover, the cumulative and lagged nature of defoliation damage, wherein each outbreak cycle builds on the weakened state induced by preceding cycles, demands advanced modeling techniques that simultaneously account for autocorrelation and spatial heterogeneity (Chen et al. 2017a; Zinsou Max Debaly, Marchand, and Girona 2022). Furthermore, the impact of extreme climate events, such as heatwaves and prolonged droughts, on SBW biology and the resulting defoliation of host species requires further research. These phenomena may initiate or reinforce medium to long-term feedback loops, affecting both outbreaks dynamics and the resilience of forest stands (Moise, Lavigne, and Johns 2019; Flower et al. 2014; Balducci et al. 2020). In light of these findings, an integrated approach is paramount. Employing models that capture the multiple levels of landscape heterogeneity, coupled with targeted studies conducted under varied conditions, will help develop more robust and effective management and adaptation strategies for SBW outbreaks.

The primary objective of this study is to investigate the dynamics of SBW-induced defoliation by exploring the interplay between climatic factors and landscape heterogeneity through the application of an adjacent-category autoregressive (ACAR) model for ordinal time series (Osse et al. 2023). This approach is particularly well-suited to capture the inherent characteristics of most defoliation data, notably its ordinal structure. We hypothesize that even when two spatially distinct sites exhibit the same level of defoliation, the underlying processes may diverge, thus warranting a departure from the conventional global modeling strategy. Instead of imposing a

single, uniform model across the entire study region with shared parameters (Subedi et al. 2023; Navarro et al. 2018; Zhu et al. 2018; Eickenscheidt, Augustin, and Wellbrock 2019; Berguet et al. 2021), we analyze multiple landscape units, each subjected to distinct environmental conditions. This localized modeling approach improves our understanding of how site-specific ecological and climatic drivers influence defoliation dynamics. By comparing outcomes across these varied units, we gain insights into localized patterns of forest health and resilience, as well as the context-dependent effects of environmental stressors. We further employ clustering techniques to group landscape units based on similarities in the locally fitted models, thereby facilitating more targeted forest management strategies that address the unique needs and conditions of each cluster. Consequently, the proposed framework offers a region-specific decision-making tool for forest resource management, enhancing the effectiveness of interventions aimed at mitigating SBW-induced defoliation. Through these clusters, forest managers can prioritize interventions in landscape units where climatic pressure and defoliation trajectories are most severe, optimizing resource allocation and potentially mitigating future SBW damage.

2.5. Materials and methods

2.5.1. Study area

The study area is located within the boreal forests of Quebec, encompassing approximately 840,000 km^2. This region is characterized by vast coniferous forests, predominantly composed of balsam fir (*Abies balsamea*) and white spruce (*Picea glauca*), extending across latitudes 45 to 51 N and longitudes 65 to 80 W (Figure 3). The regional climate is subpolar-subhumid continental, characterized by long, cold winters and short, cool summers. The north is colder and drier (mean annual temperature $-7.5\,^{\circ}\mathrm{C}$, mean annual precipitation $500\,\mathrm{mm/year}$), while the south is warmer and wetter ($1\,^{\circ}\mathrm{C}$, $1000\,\mathrm{mm/year}$). (Subedi et al. 2023). This region exhibits high vulnerability to periodic SBW outbreaks (Cooke 2024; Black, Pureswaran, and Marshall 2024; Boulanger and Arseneault 2004). The ecological classification of (Saucier et al. 2010) segments the study area into landscape units, defined as territories characterized by ecological homogeneity, shaped by factors such as

topography, climate, and soil. Our investigation encompassed the totality of landscape units affected by the defoliation attributable to the SBW during the study period 1992-2022 (see Figure 3). By focusing on all affected landscape units, we aimed to capture the variability of the severity dynamics and patterns of defoliation in different landscape units, thus providing a comprehensive understanding of the climatic impacts on the local dynamics of defoliation.

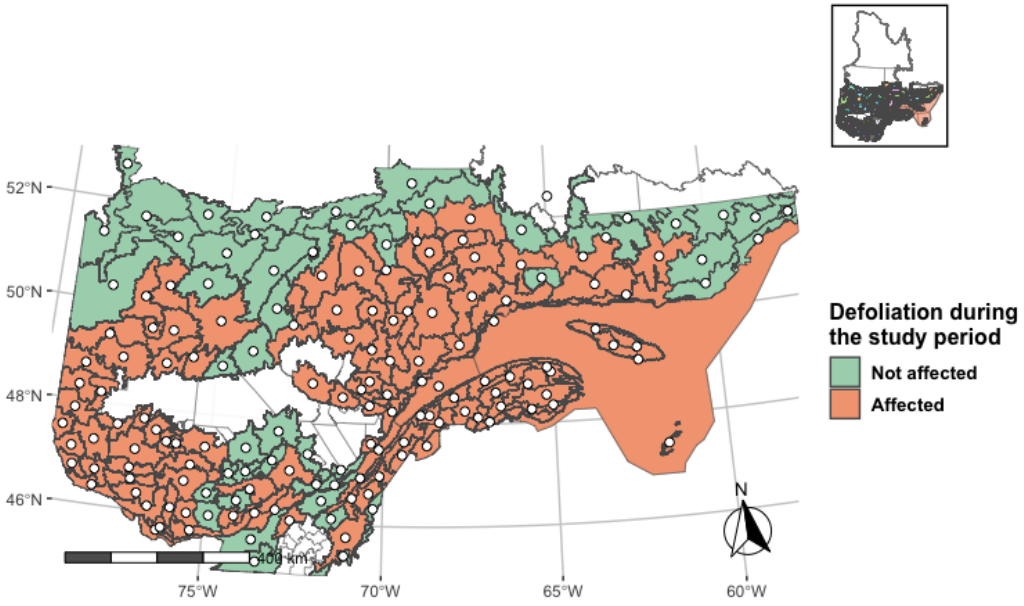

Figure 3
Landscape units of the Quebec boreal forest included in this study

2.5.2. Data description

Defoliation data. The defoliation data used for this study consist of georeferenced polygons, which were delineated during aerial surveys of the defoliation damage caused by the SBW. These surveys are conducted annually across the province of Quebec. Each polygon is associated with defoliation class defined on the following ordinal scale: no defoliation (none), defoliation of the upper few tiers (light), defoliation of the upper half (moderate), and almost complete defoliation (severe). The collected defoliation data span each year from 1992 to 2022, inclusively, and are freely

accessible through the Quebec Ministry of Natural Resources and Forests ((MRNF 2022)).

For the purposes of this study, models were developed at the landscape unit scale. To obtain a single value of defoliation for each landscape unit on a given year, a spatial intersection was performed between the defoliation polygons and the georeferenced polygons representing the landscape units, using the sf package (Pebesma 2018). When multiple defoliation levels were present in a landscape unit on a given year, the defoliation level with the largest area within the landscape unit was chosen. Some landscape units experienced minimal defoliation, while in others, certain defoliation levels were absent during the study period. For the modeling process, we excluded landscape units that experienced no defoliation during the study period; for the remaining units, moderate and severe defoliation levels were amalgamated into a single category to increase the number of observations for each defoliation level. Consequently, three defoliation levels (none, light defoliation, and moderate/severe defoliation) were analyzed instead of the initially mentioned four.

Climate data sets. We used climate data derived from BioSIM (Fortin et al. 2022), a software tool designed to generate interpolated climate information from meteorological records adjusted to specific geographic locations and elevation. BioSIM integrates long-term climate normals with short-term weather data from meteorological stations, along with digital elevation data, to interpolate climate variables. BioSIM (version 11) was configured to retrieve climate data from nearby weather stations managed by meteorological agencies (e.g., Environment and Climate Change Canada). For each landscape unit (using the centroid of the landscape unit), it selected the nearest weather stations. Elevation data were incorporated from high-resolution digital elevation models to adjust for topographic variation in temperature and precipitation, improving the accuracy of localized climate estimates.

We extracted elevation and a suite of key climate variables for each study location, including daily maximum and minimum temperatures, daily precipitation, daily relative humidity, daily solar radiation, daily wind speeds at 2 m and 10 m above ground, and

daily snow data. To reflect the biological characteristics of the spruce budworm (SBW) and align with prior studies (Zinsou Max Debaly, Marchand, and Girona 2022; Volney and Fleming 2007, 2000; Osse et al. 2023), daily maximum and minimum temperatures were seasonally aggregated for spring and summer. Given the high correlation between daily relative humidity and daily precipitation, as well as between daily wind speeds at 2 m and 10 m, we aggregated these variables to simplify subsequent analyses. Specifically, daily precipitation was aggregated as total annual precipitation, and daily wind speed at 10 m was represented as annual wind speed variation at the same height. Spring was defined as April, May, and June, while summer comprised July, August, and September.

For the purposes of this study, we focused on the following climate variables: the range (maximum - minimum) of daily maximum temperature during the summer (Tmax. summer), the range of daily maximum temperature during spring (Tmax. spring), the range of daily minimum temperature during summer (Tmin. summer), the range of daily minimum temperature during spring (Tmin. spring), the logarithm of total annual precipitation (logTotprec), the annual range of wind speed at 10 m (Wind speed at 10 m), the average annual solar radiation (Solar radiation), and the total annual snowfall (Snow). Quadratic terms were included for temperature-related variables (Tmax. summer, Tmax. spring, Tmin. summer, and Tmin. spring) to account for potential non-linear climate effects.

2.5.3. Modelling

For each landscape unit, we fitted an adjacent-category autoregressive model (Osse et al. 2023) with all possible combinations of our covariates. The model is defined as:

$$Y_{k,t} = \mathbb{1}\left\{\sum_{k=0}^{j-1} \pi_{k,t} \leq U_t < \sum_{k=0}^{j} \pi_{k,t}\right\}, \quad 0 \leq j \leq K,$$

$$\log\frac{\pi_{j,t}}{\pi_{j-1,t}} =: \eta_{j,t} = \omega_j + \gamma^\top X_{t-1} + \alpha^\top \overline{Y}_{t-1} + \beta_j \eta_{j,t-1}, \quad 1 \leq j \leq K, t \in \mathbb{Z},$$

where:

$\omega_j \in \mathbb{R}, \gamma \in \mathbb{R}^P, \alpha \in \mathbb{R}^K$ and $\beta_j \in \mathbb{R}^*$ for $j = 1, \ldots, K$.

ω_j: is the intercept for category j,

γ: represents the effect of covariates (e.g., temperature, precipitation),

α: captures the autoregressive influence of severity from the prior year and

β_j: extends the autoregression beyond a lag of 1.

Model adequacy was assessed using a Portmanteau test with lag 1, as described in (Osse et al. 2023). The test tests whether the first-order residual autocorrelations are jointly zero—i.e., whether the fitted model has left any serial dependence unexplained. Only models for which the Portmanteau test did not reject the adequacy were considered. We selected the best model for each landscape unit using the information criterion AIC.

2.5.4. Clustering

For any landscape unit i, we denote as $(X_t^{(i)}, Y_t^{(i)})$ the dataset that yielded the best model U_i with the estimated values of the parameters $\theta^{(i)} = (\omega^\top, \mathrm{vec}(\Gamma)^\top, \alpha^\top, \beta_1, \ldots, \beta_K)^\top$, k_i the number of estimated parameters in the model U_i and AIC_i its Akaike information criterion. Given two landscape units a and b, we have:

- for the dataset $X_t^{(a)}$ of landscape unit a, the best model is U_a with its Akaike Information Criterion AIC_a;
- for the dataset $X_t^{(b)}$ of landscape unit b, we have a different model U_b with its Akaike Information Criterion AIC_b;
- using model U_a as-is (same values of the parameters $\theta^{(a)}$, without re-fitting the model), we calculate its likelihood ($\mathcal{L}$) with the data $X_t^{(b)}$ to obtain the

corresponding Akaike Information Criterion, denoted AIC_{ba} denoted $AIC_{ba} = 2k_a - 2\ln\left(\mathcal{L}\left(\theta^{(a)}|X_t^{(b)}\right)\right)$;

similarly, we take model U_b and calculate its likelihood with the data $X_t^{(a)}$, resulting in the corresponding Akaike Information Criterion AIC_{ab} denoted $AIC_{ab} = 2k_b - 2\ln\left(\mathcal{L}\left(U_b|X_t^{(a)}\right)\right)$.

We also denote as $d_{a,b}$ the distance between U_a and U_b the respective best models of landscape units a and b. Our distance is given by:

$$d_{a,b} = \sqrt{(AIC_{ba} - AIC_b)^2 + (AIC_{ab} - AIC_a)^2}$$

In other words, we define a distance between models such that the distance is small if the best model for landscape unit a provides a good fit to the data of landscape unit b and vice versa. Clusters of landscape units were then identified from the pairwise distance matrix $d_{a,b}$ using hierarchical clustering with Ward's minimum-variance method (Murtagh and Legendre 2014).

2.5.5. Statistical characteristics of clusters and assessment of clustering quality

Statistical characteristics of clusters. The optimal number of clusters was determined by inspecting the Ward-linkage dendrogram. To discern the distinguishing features of each group, a comprehensive statistical analysis of the environmental and climatic variables was executed. Key variables such as elevation, seasonal temperature ranges (both maximum and minimum), humidity, wind speed, solar radiation, precipitation, and snow cover were chosen due to their ecological significance and potential impact on SBW defoliation dynamics. For each group, the means and standard deviations of these variables were computed to encapsulate the central tendencies and variability. A boxplot was constructed to visualize the mean values of these variables across clusters, facilitating direct comparisons. To evaluate the statistical significance of differences between the groups, we employed Analysis of Variance (ANOVA) (Stahle, Wold, et al. 1989) for each variable, using the cluster

assignments as the grouping factor. Variables exhibiting a p-value below the significance threshold of 0.05 were considered significantly different between groups. For these variables, a post hoc Tukey's Honest Significant Difference (HSD) test (Abdi and Williams 2010) was conducted to identify which clusters differed in a pairwise manner.

Assessment of clustering quality. The clustering quality was evaluated employing the silhouette method (Dudek 2020), which assesses cluster cohesion and separation. Initially, a Euclidean distance matrix was computed for the scaled numerical variables to quantify the dissimilarities among the landscape units. Subsequently, for each observation, the silhouette coefficient was computed using the formula:

$$S(i) = \frac{b(i) - a(i)}{\max\big(a(i), b(i)\big)}$$

where $a(i)$ signifies the average distance between observation i and all other points within the same cluster, and $b(i)$ indicates the minimum average distance between observation i and all other groups. The silhouette coefficient ranges from -1 to 1, where values approaching 1 denote strong clustering, values near 0 indicate boundary observations, and negative values suggest potential misclassification. The average silhouette width was determined as a global measure of cluster quality, with higher values indicating better-defined clusters. To visualize the results, a silhouette plot was generated, with each cluster represented by a distinct color, and the average silhouette width marked by a vertical dashed line. This visualization offered insights into the cohesion within clusters and the separation between clusters, thereby facilitating the identification of poorly defined or overlapping clusters.

2.5.6. Implementation and tools

All statistical analyses and inference methods were implemented in *R language version 4.4.2* (R Core Team 2022). The following packages were used for data manipulation, analysis, and visualization: dplyr (Wickham et al. 2023), tidyr, tibble, and ggplot2 for data handling and creating boxplots; cluster (Maechler et al. 2013) for silhouette analysis; factoextra (Kassambara and Mundt 2017) and dendextend for

cluster visualization and customization; sf (Pebesma 2018) and ggspatial for geospatial data handling and mapping; raster for raster data manipulation; multcompView to display multiple comparisons with letter-based grouping; ggthemes and viridis for additional themes and color palettes; grid and cowplot for advanced plot layout manipulation; and conflicted to manage naming conflicts between packages. The significance of the results was evaluated at the 5% threshold ($\alpha = 0.05$). All scripts and data sets are available in the repositories mentioned in the Data Availability Statement, ensuring reproducibility.

2.6. Results

This section presents how landscape-level models of SBW defoliation were fitted and then clustered based on their similarity, highlighting both the influential climatic covariates identified and the resulting spatial patterns of defoliation. In this study, the ACAR model was implemented on individual landscape units, which were subsequently aggregated into clusters based on similarities of the fitted models. Models in the same cluster thus show similar defoliation dynamics, including the effects of environmental variables on defoliation.

2.6.1. Climatic influences and defoliation dynamics

The coefficients of the best model for each landscape unit are presented in Table 3. The variation in minimum temperature during summer is the most influential climatic variable across the majority of landscape units (Figure 4). In numerous units, these models integrate parameters associated with the seasonal range of daily maximum and minimum temperatures, thus highlighting not only the non-linear relationship between temperature and defoliation but also the seasonal specificity of these effects. This underscores the diverse interactions between climatic factors and ecological processes dependent on the season. For example, in regions such as Lac la Blanche and Mont-Laurier, the coefficients for spring and summer temperatures exhibit a quadratic effect. For summer temperatures, a maximum threshold becomes apparent, indicating that elevated temperatures beyond a particular range correlate with reduced defoliation. For certain units (for example, Lac Mékinac and Réservoir Pipmuacan), significant feedback parameters, particularly β, indicate strong autoregressive

dependencies. This implies that the dynamics of defoliation in these landscape units are influenced by antecedent conditions, suggesting the cumulative impact of defoliation over time on forest health. In Port-Menier, the models demonstrate a pronounced effect of spring temperatures, where a wider range of spring temperatures leads to increased defoliation. Moreover, in Monts Groulx and Petit Lac Manicouagan, summer temperature thresholds exhibit a nuanced relationship: increased variability in summer temperatures is linked to reduced defoliation up to a certain threshold, beyond which the trend reverses, resulting in increased defoliation.

We also found that wind speed and precipitation exert contrasting, generally milder impacts on defoliation compared to temperature, yet they vary substantially across different landscape units. For instance, when wind speed at 10 meters emerges as a significant factor, it can either increase (e.g., Mont-Laurier) or decrease (e.g., Lac du Poisson Blanc) the probability of defoliation depending on local conditions. Precipitation likewise exhibits notable variability: positive effects are observed in certain units (e.g., Saint-Jérôme) and negative effects in others (e.g., Réservoir Pipmuacan). Overall, these results underscore the need to consider wind speed and precipitation locally in defoliation models, given that their impacts are strongly tied to each landscape’s distinct ecological context.

Table 3
Estimation of the best selected models for each landscape unit

Landscape Units	Parameters																		portemanteau stat	portemanteau p-value
	ω_1 (sd)	ω_2 (sd)	Tmax. spring (sd)	Tmax. summer (sd)	Tmin. spring (sd)	Tmin. summer (sd)	wind speed at 10m (sd)	$logTotprec$ (sd)	$Tmin.^2$ spring (sd)	$Tmax.^2$ spring (sd)	$Tmin.^2$ summer (sd)	$Tmax.^2$ summer (sd)	α_1 (sd)	α_2 (sd)	β_1 (sd)	β_2 (sd)				
Lac la Blanche	-10.68 (3.48)	-11.48 (3.34)	0.82 (0.30)	-1.70 (0.62)	-	-	-	-	-	-	0.30 (0.11)	-	2.25 (1.19)	4.45 (2.46)	0.76 (0.20)	-0.14 (2.14)			1.03	0.60
Mont-Laurier	-60.89 (29.14)	-64.43 (29.56)	-3.55 (0.53)	-	-	-	179.94 (47.21)	-	-	-	-0.37 (0.10)	-0.62 (0.11)	7.56 (5.61)	-6.77 (1.76)	0.94 (0.05)	0.25 (0.14)			0.32	0.85
Lac du Poisson Blanc	-181.5 (11.92	-284.5 (12.97	5.47 (0.54)	-	-	126.85 (10.23	-326.2 (49.38	-	-0.57 (0.05)	-	-11.52 (0.93)	-	208.96 (18.21	327.46 (29.44	-0.97 (0.01)	-0.49 (0.04)			0.05	0.97
Saint-Jérôme	-61.48 (12.05)	-179.28 (10.32)	-	-53.84 (3.84)	-	-	-	206.14 (9.96)	-0.17 (0.02)	-	-	3.36 (0.28)	30.85 (2.28)	138.36 (9.72)	0.39 (0.03)	-0.99 (0.01)			0.03	0.98
Lac Mékinac	-530.1 (141.0	-532.0 (141.4	-	-10.50 (3.67)	-	11.24 (2.62)	434.7 (105.2	37.31 (26.57	-0.08 (0.08)	-	-	-	103.98 (44.25	98.05 (37.54	0.76 (0.02)	-0.83 (0.29)			0.42	0.81
Tadoussac	-41.20 (56.82)	-49.25 (66.14)	7.15 (0.70)	-	-	-190.06 (61.62)	298.97 (165.18	47.66 (14.39)	-	-	17.03 (5.21)	-	-14.56 (6.80)	13.98 (33.59)	0.81 (0.14)	0.80 (0.18)			0.00	1.00
Plaine du lac Saint-Jean	-37.40 (4.12)	-194.4 (4.76)	-	-34.60 (2.43)	-7.65 (0.19)	-	143.72 (2.98)	-	-	-	-1.57 (0.06)	3.70 (0.17)	151.79 (3.43)	317.82 (5.66)	-0.60 (0.04)	-0.93 (0.01)			0.01	0.99
Réservoir Pipmua-can	9.08 (4.45)	-0.33 (2.74)	-	-	-	-	-	-10.09 (4.51)	-	0.01 (0.02)	-	-	16.60 (7.91)	25.80 (9.44)	0.87 (0.32)	0.54 (0.21)			0.04	0.98
Lac des Savanes	-2.78 (28.25	-9.22 (32.51	-	-27.50 (6.17)	-	-	56.10 (27.59	-	-	-	-	2.22 (0.49)	-2.97 (3.92)	-2.74 (4.63)	0.82 (0.13)	0.70 (0.27)			0.31	0.85
Forestville	-166.40 (44.53)	-168.37 (46.28)	5.98 (1.40)	-	-	-	58.77 (15.36)	-	-	-	-	-	25.52 (9.16)	-1.43 (5.77)	0.85 (0.07)	0.95 (0.05)			0.00	1.00
Lac au Loup Marin	-419.1 (51.48	-426.8 (48.77	-	-	-12.95 (1.21)	227.09 (13.45	-	-	-	-	-20.26 (1.02)	-	1.88 (10.12	0.44 (12.30	0.91 (0.03)	0.88 (0.06)			0.00	1.00
Lac Dionne	-321.89 (47.14)	-404.73 (52.07)	2.54 (0.72)	-	-	-1.23 (0.46)	-	199.37 (35.38)	-	-	-	-	132.10 (12.59)	212.41 (18.62)	-0.61 (0.11)	-0.89 (0.02)			0.00	1.00
Sept-Îles	-387.4 (22.31	-494.4 (31.78	-	-6.00 (0.67)	13.66 (1.04)	-6.56 (0.61)	-	-	-	-	-	-	419.57 (26.84	459.55 (29.17	-0.91 (0.01)	-0.80 (0.02)			0.03	0.99

Table 3
Estimation of the best selected models for each landscape unit

Landscape Units	ω_1 (sd)	ω_2 (sd)	Tmax. spring (sd)	Tmax. summer (sd)	Tmin. spring (sd)	Tmin. summer (sd)	wind speed at 10m (sd)	$logTotprec$ (sd)	$Tmin.^2$ spring (sd)	$Tmax.^2$ spring (sd)	$Tmin.^2$ summer (sd)	$Tmax.^2$ summer (sd)	α_1 (sd)	α_2 (sd)	β_1 (sd)	β_2 (sd)	portemanteau stat	portemanteau p-value
Port-Menier	36.61 (12.60)	23.29 (13.51)	-	30.79 (4.49)	0.69 (0.94)	-	-	-150.09 (8.00)	-	-	-	-	-128.43 (11.14)	-31.06 (2.27)	0.98 (0.01)	0.67 (0.02)	0.16	0.92
Rivière Jupiter	-1190.: (80.0!	-1193. (80.11	-	297.07 (22.05	-14.05 (1.44)	8.88 (0.66)	399.43 (23.43	-	-	-	-	-28.46 (1.98)	27.86 (1.83)	8.48 (3.54)	0.79 (0.02)	0.81 (0.01)	0.23	0.89
Rivière aux Saumons	-725.05 (87.94)	-741.87 (89.87)	5.36 (0.53)	278.55 (39.54)	-4.28 (0.61)	-42.05 (7.84)	43.13 (8.18)	-26.65 (13.45)	-	-	3.95 (0.74)	-24.35 (3.42)	13.31 (1.93)	9.56 (2.41)	0.42 (0.03)	-0.31 (0.07)	0.20	0.90
Lac Manouane	-328.6 (9.22)	-372.3 (10.32	32.28 (1.40)	-123.4 (11.34	-	-33.43 (2.54)	-	-	-	-	13.43 (0.50)	2.06 (0.39)	448.88 (24.91	259.49 (23.18	-0.47 (0.01)	-0.64 (0.01)	0.00	1.00
Lac Rouvray	-409.58 (57.16)	-477.51 (67.36)	-	-	-	137.83 (18.99)	-	-	-	-	-11.13 (1.54)	-	65.44 (10.82)	112.44 (21.33)	0.49 (0.07)	0.31 (0.08)	0.01	0.99
Lac du Sault aux Cochons	-119.1 (10.68	-234.6 (13.43	-8.87 (0.48)	-	-	-	-	112.53 (9.62)	-	-	-	-	207.59 (10.03	331.01 (16.76	-0.96 (0.01)	-0.98 0.01	0.00	1.00
Lac Dissimieux	43.47 (9.69)	-23.77 (2.33)	-	-	-	-	-	-	-0.24 (0.04)	-	0.32 (0.02)	-0.43 (0.09)	11.28 (1.84)	111.81 (15.78)	0.71 (0.05)	-0.95 (0.03)	0.15	0.93
Lac Guinecourt	-167.0 (79.27	-257.7 (103.9	-	-	-	92.24 (36.58	-	-40.63 (11.67	-	-	-9.77 (3.64)	-	98.36 (36.90	119.1 (220.9	0.86 (0.02)	-0.99 (0.02)	0.13	0.94
Lac Carteret	141.00 (22.66)	-87.15 (46.12)	-24.85 (2.33)	-	-	-	-116.35 (17.47)	-	0.99 (0.08)	-	-	-	483.52 (16.02)	352.34 (17.67)	-0.85 (0.03)	0.66 (0.02)	0.00	1.00
Réservoir Manic 3	-478.3 (15.81	-542.2 (15.28	-	-	-	164.05 (5.83)	174.32 (6.21)	-285.5 (12.36	-	-	-12.68 (0.49)	-1.59 (0.06)	156.11 (8.62)	308.27 (11.81	-0.83 (0.01)	-0.63 (0.01)	0.00	1.00
Lac Berté	47.36 (16.02)	-46.78 (6.93)	-	-	-	-	-	-	-0.50 (0.16)	-	-	-	249.51 (64.14)	111.57 (35.65)	-0.06 (0.33)	0.69 (0.01)	0.14	0.93
Lac Sainte-Anne	62.19 (6.92)	29.24 (23.04	-	-	-	-	-	-80.16 (6.32)	-	-	0.50 (0.07)	-0.71 (0.14)	221.90 (42.66	78.50 (18.19	-0.79 (0.03)	0.83 (0.02)	0.00	1.00
Lac Walker	-22.11 (5.17)	-73.64 (4.59)	-	-	0.79 (0.28)	-12.06 (0.73)	-	-	-	-	-	-	317.19 (13.91)	127.36 (6.82)	-0.80 -	0.77 (0.01)	0.00	1.00
Réservoir Manicouagan	-7.04 (3.26)	-14.66 (6.93)	-	-	-	-	-	-	-	-0.22 (0.09)	-	0.89 (0.23)	55.46 (21.95	-1.36 (10.09	0.59 (0.20)	0.73 (0.12)	0.09	0.95

Table 3
Estimation of the best selected models for each landscape unit

Landscape Units	ω_1 (sd)	ω_2 (sd)	**Tmax. spring** (sd)	**Tmax. summer** (sd)	**Tmin. spring** (sd)	**Tmin. summer** (sd)	**wind speed at 10m** (sd)	$logTotprec$ (sd)	$Tmin.^2$ **spring** (sd)	$Tmax.^2$ **spring** (sd)	$Tmin.^2$ **summer** (sd)	$Tmax.^2$ **summer** (sd)	α_1 (sd)	α_2 (sd)	β_1 (sd)	β_2 (sd)	**portemanteau stat**	**portemanteau p-value**
Monts Groulx	-767.70 (52.66)	-924.03 (66.89)	70.55 (5.13)	-	-32.81 (2.48)	-	-	-	-	-	-	-	366.70 (28.28)	422.45 (33.86)	-0.39 (0.03)	-0.79 (0.01)	0.01	1.00
Lac Grand-mesnil	-40.43 (5.71)	-459.2 (46.59	-	-	-	-	-	-	-	-0.45 (0.02)	-	-0.78 (0.05)	412.74 (46.96	670.93 (87.56	-0.95 (0.01)	-0.95 (0.01)	0.00	1.00
Lac Nipissis	132.71 (150.66	108.48 (134.40)	-	6.65 (5.38)	-29.89 (14.40)	32.10 (7.80)	-	-	-	-	-	-	10.06 (7.86)	16.17 (31.54)	0.96 (0.07)	0.74 (0.27)	0.00	1.00
Havre-Saint Pierre	-15.10 (1.09)	-155.1 (11.64	-	-	-	-	-	-	-0.16 (0.01)	-	-0.65 (0.05)	-	384.12 (31.84	176.94 (11.38	-0.86 (0.02)	0.84 (0.03)	0.21	0.90
Lac Pécaudy	10.49 (2.79)	-64.54 (7.96)	-	-	8.10 (1.10)	-11.96 (1.37)	-	-	-	-0.53 (0.06)	-	-	108.74 (10.55)	122.39 (11.26)	-0.50 (0.04)	-0.98 0.01	0.00	1.00
Petit lac Mani-couagan	35.41 (2.69)	33.35 (5.46)	-	-	-	-	-	-	-	-0.53 (0.02)	-1.18 (0.05)	-	171.20 (7.68)	-19.80 (1.83)	-0.90 (0.02)	0.62 (0.02)	0.24	0.89

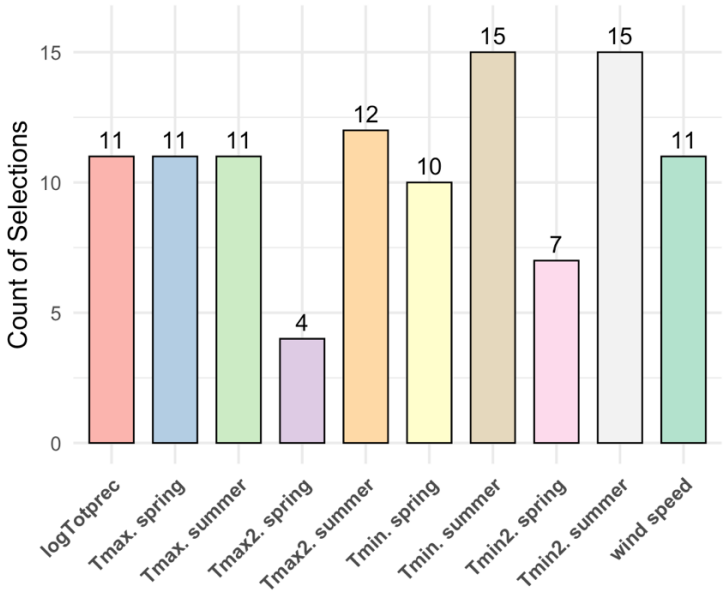

Figure 4
Frequency of Variable Selection

2.6.2. Cluster heterogeneity

The clustering of landscape units based on their models of defoliation dynamics (Figure [cluster]) and the characterization of these clusters (Figure [fig:anova_results]) have revealed a broad spectrum of SBW-induced defoliation patterns in boreal forests, intricately shaped by different environmental factors. Among the five identified clusters, clusters 4 and 5 stand out for their homogeneous climatic and topographic conditions, with positive silhouette scores (0.55 and 0.24, see Figure [silhouette]). Cluster 4, located in low-altitude zones with minimal thermal variation and high precipitation, indicates stable climatic conditions that reduce the vulnerability of SBW. Conversely, cluster 5, characterized by high altitudes, significant thermal variation, high solar exposure, and low snow cover, reflects extreme conditions where SBW activity is less predictable, requiring tailored adaptive management strategies. Figure 6 depicts the spatial distribution of landscape units, highlighting their arrangement across the study area.

In contrast, clusters 1, 2, and 3 exhibit negative silhouette scores (-0.43, -0.32, and -0.24, Figure [silhouette]), suggesting overlaps and heterogeneous characteristics. These clusters represent intermediate conditions, ranging from areas with significant wind exposure and moderate humidity (cluster 1), to low-altitude zones with low precipitation and humidity (cluster 2), to highly diverse landscapes that need further segmentation (cluster 3). These findings highlight the critical role of climatic factors such as altitude, thermal amplitude, humidity, and wind in shaping SBW defoliation patterns and provide actionable insights for developing differentiated forest management strategies.

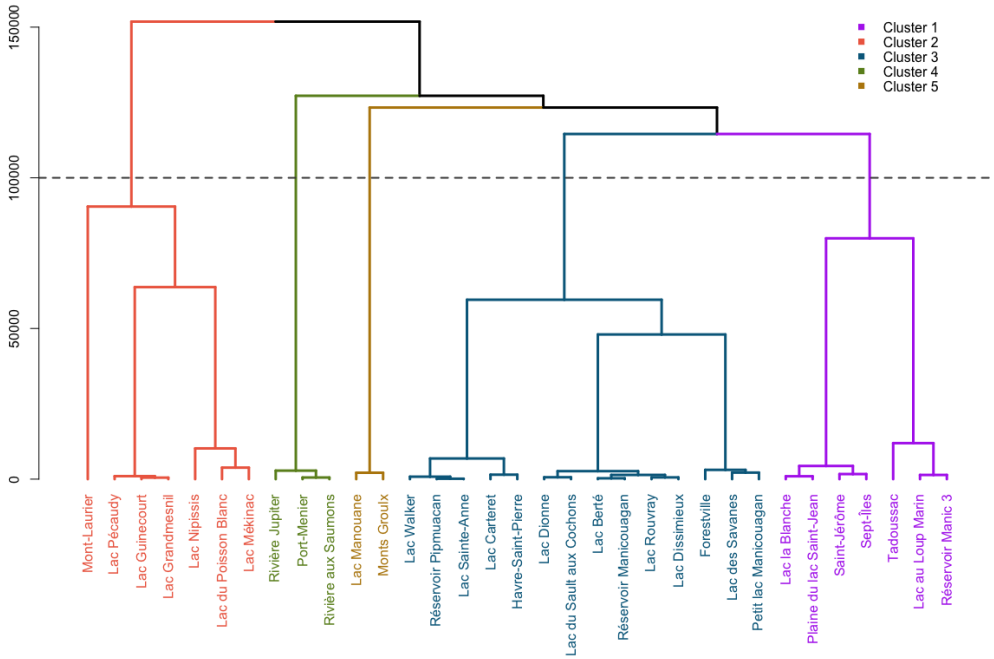

Figure 5
Dendrogram of landscape units hierarchical clustering

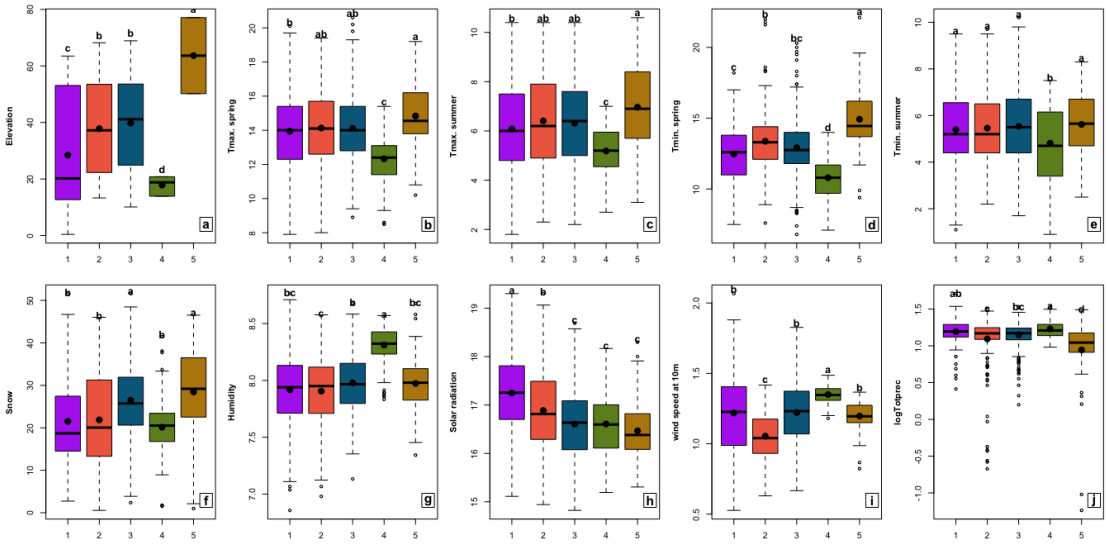

Figure 6
The distribution of significant environmental variables across clusters. Each boxplot represents a specific variable's variation among the five clusters. The black points within each box denote the mean values of the variable for the corresponding cluster. Compact letter displays (above the boxes) indicate significant differences between clusters based on post-hoc Tukey tests.

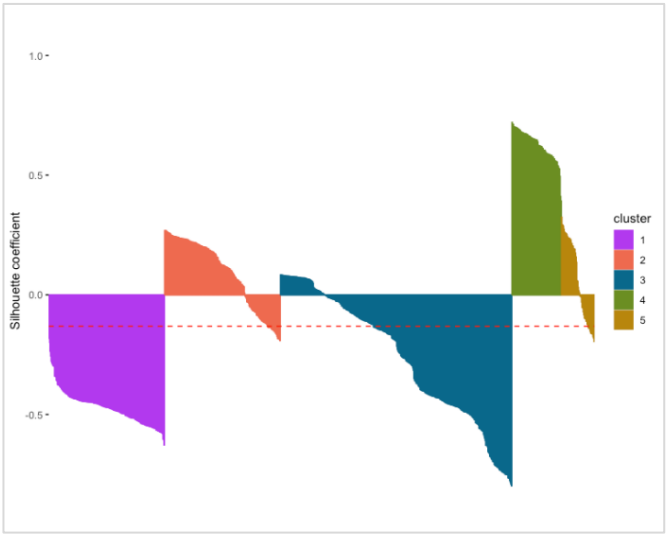

Figure 7
Silhouette analysis of cluster performance

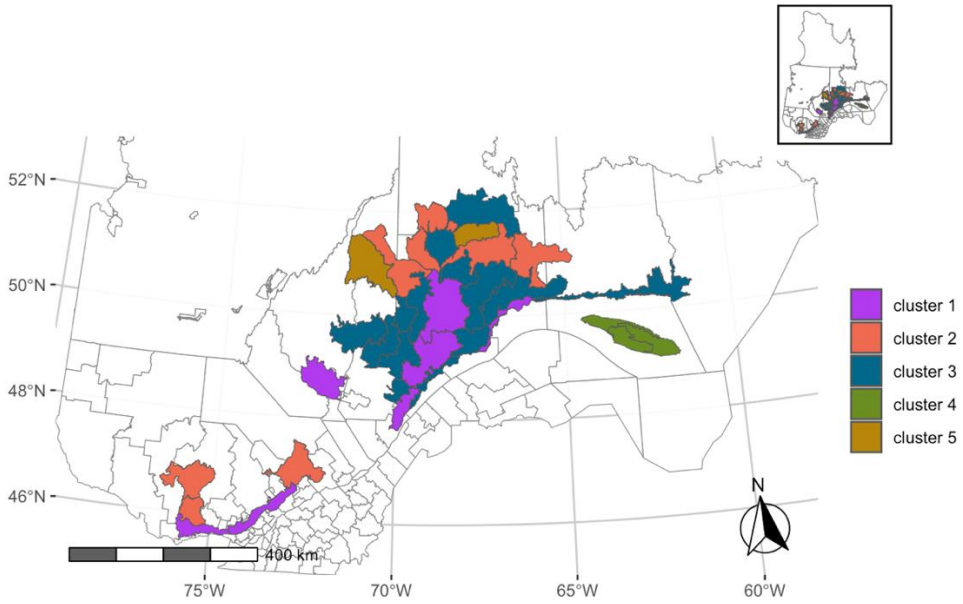

Figure 8
Mapping clustered landscape units

2.7. Discussion

2.7.1. The multifaceted impacts of climat on the defoliation dynamics

While numerous studies have shown that rising temperatures attributable to climate change are correlated with increases in both the frequency and intensity of SBW outbreaks (Overpeck, Rind, and Goldberg 1990; J. Régnière and Nealis 2007; Pureswaran et al. 2015, 2019; Bouchard and Auger 2014; Bouchard, Régnière, and Therrien 2018a; Moise, Lavigne, and Johns 2019), our model results demonstrate a complex and non-linear association between temperature and SBW defoliation dynamics. This complex relationship may arise from the combined influence of physiological (Bellemin-Noël et al. 2021; Deslauriers et al. 2019; Howe, Hart, and Trowbridge 2024), phenological (Eveleigh and Johns 2014; Deslauriers et al. 2019), and ecological factors (Zhang et al. 2018) that drive SBW behavior, highlighting the importance of understanding how climate change modifies defoliation patterns during SBW outbreaks. Existing ecological literature associated warmer summers with increased larval mortality or delays in defoliation cycles (Abarca and Lill 2015; Ward,

Moon, and Aukema 2019; Portalier, Candau, and Lutscher 2024; Delisle, Bernier-Cardou, and Labrecque 2022). Our results emphasize the complex role that temperature plays in shaping the defoliation dynamics. In specific landscape units, the models offer supplementary insights. Although initially beneficial to SBW populations (Jacques Régnière and Nealis 2019b; Bellemin-Noël et al. 2021), rising temperatures can precipitate a series of physiological stresses and ecological mismatches that ultimately constrain their success (Howe, Hart, and Trowbridge 2024; Portalier, Candau, and Lutscher 2024). These findings suggest that temperature-related variables (e.g., *Tmin. summer*) play a dual role: they can promote SBW development up to a threshold but can also hinder larval survival beyond it. This threshold-like behavior further reflects the non-linear impact of extreme temperatures on physiological processes (e.g., dehydration, metabolic stress) in SBW larvae.

A pivotal mechanism affecting SBW dynamics under increasing temperatures is the disruption of phenological synchrony between the budworm's life stages and the bud burst of its host trees. Premature bud bursts in species such as black spruce (*Picea mariana*) and balsam fir (*Abies balsamea*) may not coincide with larval emergence, leading to mismatches that diminish larval survival (Pureswaran et al. 2019; Portalier, Candau, and Lutscher 2024; Howe, Hart, and Trowbridge 2024). Black spruce, due to its inherently delayed bud burst, becomes less susceptible to defoliation in warmer climates, as larvae may emerge before adequate foliage becomes available for consumption (Pureswaran et al. 2015). This phenomenon highlights the existence of a defoliation threshold, wherein excessive warming reduces defoliation rates due to disrupted synchrony. This interpretation provides a compelling explanation for the quadratic effects observed in our model, emphasizing the complex and non-linear relationships among key variables.

In parallel to the effect of temperature on SBW-host synchrony, temperature-induced physiological stress emerges as a critical factor limiting SBW populations (Jacques Régnière and Nealis 2019b; Bouchard, Régnière, and Therrien 2018a). As temperatures rise, metabolic rates in ectothermic organisms such as the SBW accelerate, thereby increasing energy demands that may not be sustainable under

suboptimal conditions (Goodhue et al. 2017; Reichenbach and Stairs 1985; Hayes et al. 2015). This is particularly evident during critical life stages, such as larval feeding, where high temperatures lead to reduced nutrient absorption, dehydration, and impaired growth (Bellemin-Noël et al. 2021; VG Nealis and Régnière 2004). Additionally, extreme temperatures disrupt reproductive success by diminishing egg viability and altering timing, further constraining population growth (Candau, Fleming, and Wang 2018; Ren et al. 2020). Furthermore, the responses of host trees to rising temperatures significantly influence SBW survival and development. Elevated temperatures expedite foliage maturation, resulting in tougher and less nutritious leaves, thereby reducing their suitability for larvae (Eveleigh and Johns 2014). Compounding this effect, temperature-induced changes in foliage chemistry, such as increased levels of secondary metabolites like phenolics and terpenes, degrade food quality even further, intensifying physiological stress in larvae (Despland et al. 2011). Consequently, these nutritional limitations hinder larval growth and survival, ultimately reducing population viability.

Localized microclimatic conditions further exacerbate SBW outbreak dynamics. For instance, drier or warmer microclimates intensify water stress in host trees, accelerating the decline in foliage quality and availability (Zhang et al. 2018). This spatial variability in habitat suitability not only alters the geographical extent and intensity of outbreaks but also contributes to regional variations in the processes driving defoliation dynamics, as reflected in different landscape-based models. Taken together, these findings emphasize the urgent need for adaptive forest management strategies to mitigate the impacts of SBW outbreaks in the context of a changing climate. On one hand, monitoring phenological shifts in host trees is essential to enhance forest resilience; on the other hand, identifying temperature thresholds that constrain SBW populations is equally critical for refining predictive models. In some landscape units, spring temperatures lead to increased defoliation. This pattern agrees with the hypothesis that warmer springs may precipitate the early emergence of larvae, thereby exacerbating damage from defoliation (Jacques Régnière, St-

Amant, and Duval 2012; Bellemin-Noël et al. 2021; Delisle, Bernier-Cardou, and Labrecque 2022; Rose and Blais 1954; Moise, Warren, and Bowden 2024).

Our findings also underscore that, while temperature is widely recognized as a fundamental determinant of SBW dynamics (Pureswaran et al. 2015; Jacques Régnière and Nealis 2019b), additional climatic factors such as wind speed and precipitation can play a significant context-dependent role (Royama 1984). Higher wind speeds often facilitate the dispersal of first instar larvae by allowing them to bridge between host trees (Beckwith and Burnell 1982; Ramachandran 1987; D. P. Anderson and Sturtevant 2011), but strong gusts can also dislodge larvae, reducing their chances of survival (Jennings, Houseweart, and Dimond 1983). This dual effect is clearly illustrated by the contrasting coefficients in Mont-Laurier (positive effect) and Lac du Poisson Blanc (negative effect). Precipitation similarly exerts a range of impacts: excessive rainfall can reduce larval feeding efficiency or encourage entomopathogenic fungal outbreaks (Subedi et al. 2023), whereas heightened humidity can in some contexts bolster larval survival (Bouchard, Régnière, and Therrien 2018a). Given that these variables demonstrate markedly different influences across landscape units—positive in Saint-Jérôme vs. negative in Réservoir Pipmuacan—local ecological factors such as stand composition, topography, and microclimatic conditions likely mediate these processes. Consequently, incorporating wind speed and precipitation into defoliation models on a site-by-site basis is essential for accurately predicting SBW outbreaks and tailoring more effective forest management strategies.

2.7.2. Legacy effects of historical defoliation events

Our findings indicate that defoliation dynamics within a given landscape unit depend not only on the current year’s climatic conditions but also on the cumulative defoliation that occurred earlier in the same outbreak cycle. The significant autoregressive terms reflect this legacy effect: each successive year of moderate or severe defoliation further weakens host trees, thereby increasing their likelihood of sustaining additional damage as the epidemic wave progresses (Vincent Nealis and Régnière 2021; Zinsou Max Debaly, Marchand, and Girona 2022; Osse et al. 2023). Persistent defoliation can

lead to a reduction in the photosynthetic capacity of a tree, the depletion of its energy reserves, and the limitation of its recovery capabilities, increasing its vulnerability to additional stressors such as drought, secondary pests, or diseases (Z. Wang, Zhou, and Wang 2021; O'Connell and Wiley 2024; Deslauriers et al. 2019). In addition, this cumulative effect can trigger a feedback loop in which declining forest health increases the likelihood of further defoliation, thus amplifying the long-term effects on forest structure and composition (J. Régnière and Nealis 2007; Chen et al. 2017b; Sturtevant et al. 2015). These results highlight the need to integrate temporal factors and the legacy of historical disturbances into models of defoliation dynamics and forest management strategies. By appreciating the impact of previous conditions, managers can more effectively predict the severity of outbreaks, prioritize intervention strategies, and work towards preserving the ecological integrity of forest ecosystems over time. Such a cumulative effect aligns with previous research indicating that repeated defoliation episodes gradually erode a tree's vigor, increasing subsequent infestation risks (J. Régnière and Nealis 2007; Sturtevant et al. 2015). By capturing these feedback loops, the ACAR model thus provides a more realistic representation of defoliation trajectories in these vulnerable forest stands.

2.7.3. Advancements in management strategies

Although our findings support prior research advocating for differentiated management strategies in boreal forests (Park et al. 2014; MacLean 2016; James et al. 2011; Hennigar and MacLean 2010; L. Venier and Holmes 2010; Chavardès et al. 2021), they also provide significant advancements for managing SBW outbreaks in these ecosystems. Modeling using the ACAR framework, which accounts for both cumulative and autoregressive effects of defoliation, followed by clustering, emerges as a valuable tool for environmental segmentation to inform targeted strategies, identify complex and transitional zones, and optimize resource allocation. Homogeneous clusters, such as clusters 4 and 5 identified in our analysis, enable the recognition of specific climatic zones where long-term management strategies can be effectively planned. By tailoring management approaches to the unique characteristics of each cluster, resource allocation can be optimized, prioritizing interventions in the most vulnerable or unstable areas. The heterogeneous outcomes highlight the role of

local environmental conditions, such as topography, microclimate, and more, in shaping SBW outbreak dynamics. Consequently, they underscore the need for nuanced, site-specific modeling approaches rather than generic prescriptions, ensuring that forest management strategies can be better aligned with the particular climatic and ecological contexts of each landscape.

2.8. Conclusion

This study enhances our comprehension of the non-linear and region-specific dynamics associated with SBW outbreaks. The clustering analysis of landscape units further highlights the critical significance of accounting for local heterogeneity, as certain clusters reveal distinct opportunities for targeted interventions, whereas others exhibit more intricate, overlapping characteristics that necessitate further investigation. By assimilating these insights, it becomes apparent that adaptive and differentiated management strategies, tailored to the specific conditions of each cluster, are vital to alleviating both the ecological and economic repercussions of SBW outbreaks. Utilizing spatially explicit and temporally sensitive modeling approaches, future research can refine predictions regarding the temporal and spatial occurrence of outbreaks. Incorporating spatial dependencies into these models will effectively capture the influence of forest composition, geographic features, and climate on both the initiation and propagation of outbreaks, thereby improving predictive accuracy and facilitating proactive, region-specific interventions. Finally, while the present approach treats each landscape unit independently, many ecological processes, such as larval dispersal and host connectivity, operate spatially. Incorporating spatial autocorrelation into the ACAR framework in future work could further enhance outbreak predictions and better account for cross-boundary SBW spread. In conclusion, this study highlights the need for integrated research and management approaches that address the complex challenges of climate change in boreal forests. By identifying key links between SBW outbreaks and climate, we improve our understanding of these ecosystems and our ability to protect their health and resilience. These findings provide a strong foundation for creating sustainable and adaptive strategies that balance ecological conservation with the practical demands of forest resource management in an uncertain future.

Author contributions. OJFO: Conceptualization, Model development and data analysis, Software, Visualization, Writing – original draft, Writing – review and editing. PM: Conceptualization, Model development and data analysis, Funding acquisition, Software, Supervision, Validation, Writing – review and editing. MMG: Funding acquisition, Supervision, Writing – review and editing. All authors gave their final approval for publication.

Ethics approval and consent to participate. Not applicable

Consent for publication. Not applicable

Availability of data and material. The datasets and R scripts used and/or analyzed during the current study are available from the corresponding author upon request.

Competing interest. The authors have no conflict of interest to declare.

Funding. PM and MMG obtained funding from the Natural Sciences and Engineering Research Council of Canada (NSERC) Alliance and the Québec Ministry of Natural Resources and Forests (MRNF) to understand the dynamics of spruce budworm (ALLRP 558267-20). MMG obtained additional funding from an NSERC Discovery grant to reconstruct the regime of natural disturbances in forest ecosystems (RGPIN-2022-05423).

3. DRIVERS OF SPRUCE BUDWORM DEFOLIATION UNDER PROJECTED CLIMATE-CHANGE SCENARIOS

Olaloudé Judicaël Franck Osse, Philippe Marchand et Miguel Montoro Girona

Une version de ce chapite est en phase finale et soumis au journal *Climate Change Ecology*

3.1. Highlights

Simulations over more than 50 years reveal strong spatial heterogeneity in climate-driven defoliation dynamics.

RCP 8.5 intensifies defoliation risks in multiple boreal forest landscape.

Climate effects under RCP 4.5 can locally outpace those under RCP 8.5, revealing nonlinear climate–SBW interactions.

Results advocate for spatially adapted forest-management strategies under climate change.

3.2. Résumé

Le changement climatique a modifié les régimes de perturbation dans l'ensemble du biome boréal, mais son influence isolée sur les insectes défoliateurs demeure encore mal quantifiée. Dans cette étude, nous cherchons à projeter l'effet du climat futur sur la dynamique des épidémies de tordeuse des bourgeons de l'épinette (*Choristoneura fumiferana*, TBE) pour 33 unités de paysage écologique (UPR) couvrant environ 154 000 km^2 de forêts boréales au Québec, Canada. En combinant les effets climatiques estimés à partir d'un modèle autorégressif à catégories adjacentes (ACAR), ajusté sur des séries historiques de défoliation, avec des projections climatiques à haute résolution pour la période 2040–2100 (scénarios RCP 2.6, 4.5 et 8.5), nous avons isolé les effets marginaux du climat pour chaque unité de paysage, selon chaque scénario.

Ces effets projetés révèlent une hétérogénéité spatiale marquée. Une analyse de variance à trois facteurs (ANOVA) a mis en évidence des effets principaux significatifs du paysage, du scénario climatique et de la période temporelle, ainsi que des interactions fortes entre les UPR et les scénarios climatiques ($p < 0,001$), soulignant le caractère fortement contextuel du lien entre climat et défoliation. En conséquence, une approche uniforme de gestion forestière s'avère peu appropriée. Une gestion adaptée aux spécificités spatiales des territoires sera essentielle pour maintenir la résilience des forêts face à l'intensification des forçages climatiques.

Plus largement, cette étude met en évidence la valeur des modèles de séries temporelles ordinales pour dissocier les forçages climatiques exogènes des dynamiques endogènes des épidémies, fournissant ainsi un cadre transférable pour intégrer le risque entomologique dans la planification régionale de l'adaptation aux changements climatiques. Les recherches futures devraient réintégrer les processus de rétroaction et les interactions feu-insectes afin de mieux capter l'ensemble du spectre des perturbations composées dans un climat en mutation.

3.3. Abstract

Climate change has modified disturbance regimes across the boreal biome, yet its isolated influence on insect defoliators remains poorly quantified. Here, we aim to project how future climate would affect the dynamics of spruce budworm (*Choristoneura fumiferana*, SBW) outbreaks for 33 ecological landscape units (UPRs) spanning 154 000 km^2 of boreal forests in Quebec, Canada. Combining the estimated climate effects from a time-series (adjacent-category autoregressive, or ACAR) model fitted to historical data of SBW defoliation with down-scaled climate projections for 2040 – 2100 (RCP 2.6, 4.5, 8.5), we isolated the marginal effects of climate for each landscape unit under each climate scenario. These projected effects revealed pronounced spatial heterogeneity. A three-way ANOVA confirmed significant main effects of landscape, scenario and time, as well as strong UPR × climatic scenario interactions ($p < 0.001$), underscoring the context-dependent nature of climate–defoliation linkages. Consequently, a “one-size-fits-all” approach is unlikely to succeed. Instead, spatially adapted management will be essential to maintain forest resilience as climate forcing intensifies. More broadly, our study demonstrates the value of ordinal time-series models for disentangling exogenous climate forcing from endogenous outbreak dynamics, providing a transferable framework for integrating insect risk into regional climate-adaptation planning. Future research should reintegrate feedback processes and fire-insect interactions to capture the full spectrum of compound disturbance risk under climate change.

3.4. Introduction

The boreal forest, a vast biome encircling the Northern Hemisphere across Alaska, Canada, Scandinavia, and Siberia, represents approximately 30% of the world's forested area (Brandt et al. 2013) and stores between 30% and 40% of terrestrial carbon, primarily in its soils (MacCarthy et al. 2023), making it a linchpin in global climate regulation.(Pan et al. 2011; Ameray et al. 2024). Beyond its role as a carbon sink, this ecosystem harbors unique biodiversity, including iconic species such as caribou (*Rangifer tarandus*), boreal chickadees (*Poecile hudsonicus*), and lichen-dependent woodland ecosystems. It also sustains Indigenous communities and forestry economies reliant on timber and non-timber resources (Gauthier et al. 2015; L. A. Venier et al. 2014). However, anthropogenic climate change is destabilizing boreal ecosystems at an unprecedented pace (Girona et al. 2023). Rising temperatures, shifting precipitation regimes, and intensifying disturbance cycles—including wildfires, insect outbreaks, and droughts—threaten to transform these forests from carbon sinks into sources (Seidl et al. 2017; Walker et al. 2019).

Among these insect epidemics, cyclical outbreaks of the spruce budworm (*Choristoneura fumiferana*; SBW) stand out due to their historical recurrence and escalating impacts under climate change. SBW outbreaks are intrinsic to boreal forest dynamics, typically recurring every 30–40 years (Aakala et al. 2023). During epidemic phases, larvae voraciously feed on the needles of balsam fir (*Abies balsamea*) and spruce (*Picea spp.*), triggering defoliation that can persist for 10–15 years, leading to tree mortality, reduced timber yields, and carbon release (MacLean 2016; Q. Liu et al. 2023; Lavoie et al. 2021). Québec's 20th-century spruce budworm outbreaks were massive in scale, with the most significant event (1970s–80s) defoliating over 50 million hectares and causing hundreds of millions of cubic meters of timber loss (Chang et al. 2012a; Luo and Chen 2015; M. Li et al. 2020). Other eastern provinces also suffered serious outbreaks – especially New Brunswick (E. Y. Liu et al. 2019) – but none surpassed the sheer scope of Québec's experience. While these events are natural, climate change is altering their drivers. Warmer winters enhance larval survival by reducing mortality from extreme cold, while earlier springs accelerate larval emergence, potentially disrupting synchrony with budburst of host trees (Boulanger,

Fabry, et al. 2017; Jacques Régnière, St-Amant, and Duval 2012; Osse et al. 2023). Such phenological mismatches may initially reduce defoliation but could also extend outbreak durations as SBW adapts to shifting thermal niches (Pureswaran et al. 2015). Concurrently, climate-driven range expansions are enabling SBW to invade previously inhospitable northern and high-elevation forests, threatening naïve tree populations (Pureswaran et al. 2015).

The interplay between SBW biology and climate variables is multifaceted (Osse et al. 2023). Temperature directly affects SBW development: for example, larvae require ĩ,300 degree-days above 7°C to complete their life cycle, a threshold increasingly met earlier in the season under warming scenarios (Jacques Régnière et al. 2019). This accelerates population growth, potentially shortening intervals between outbreaks (Moise, Warren, and Bowden 2024; Boulanger et al. 2025). Conversely, extreme climatic events introduce nonlinearities. Drought stress compromises tree defenses by reducing resin production, rendering hosts more susceptible to SBW feeding (Subedi et al. 2023; Zinsou Max Debaly, Marchand, and Girona 2022). Unseasonal frosts, paradoxically exacerbated by climate-induced temperature variability, can damage young shoots, forcing larvae to consume older, less nutritious foliage, thereby prolonging larval stages and increasing tree exposure to defoliation (Battisti et al. 2005). Furthermore, elevated atmospheric CO_2 may alter foliar chemistry, though impacts on SBW remain debated (Jamieson et al. 2015). These cascading effects create feedback loops that defy simplistic cause-effect relationships, complicating outbreak forecasting.

Existing models of SBW defoliation often simplify outbreak dynamics by treating defoliation as a binary or continuous variable, despite empirical data typically being collected on ordinal severity scales (Candau and Fleming 2005; Bouchard and Auger 2014; Nenzen et al. 2017). This mismatch limits the utility of predictions for adaptive management. Furthermore, few studies account for the cumulative, autoregressive nature of defoliation, where outbreak severity in one year depends on prior defoliation and climatic conditions (Osse et al. 2023). Recent advancements in ordinal time series modeling, particularly the development of adjacent-category autoregressive (ACAR)

(Osse et al. 2023) frameworks, offer promising tools to address these limitations by explicitly incorporating temporal dependencies and the hierarchical nature of categorical responses. These models facilitate the isolation of the specific contributions of climatic variables to annual transitions between defoliation classes—a task that has historically been challenging due to temporal autocorrelation and internal feedback mechanisms inherent in outbreak dynamics. While future climate projections indicate significant environmental changes likely to influence SBW outbreak dynamics, the spatial variability of these climate effects across Quebec's ecological landscape units (*unité de paysage régional*, or UPR) remains underexplored.

This study examines how climate change scenarios are expected to influence SBW defoliation in eastern Canadian boreal forests. To evaluate this projected influence of climate change, we analyzed the temporal trajectories of the ACAR model's marginal climate effects across 33 UPRs from 2040 to 2100 under three emissions scenarios (RCP2.6, RCP4.5, and RCP8.5). Specifically, we aim to:

- quantify the marginal effects of climatic variables on the annual probabilities of transition between spruce budworm defoliation classes, employing a "time-slicing" approach to isolate climate impacts from endogenous outbreak dynamics;
- characterize the spatial variability of these climate-driven effects across the 33 UPRs.

3.5. Materials and methods

3.5.1. Study area

The study area is located in the boreal forest zone of Quebec, eastern Canada. This encompasses a large portion of Quebec's boreal region (on the order of 153,821 km^2) characterized by continuous forest cover across more than two major bioclimatic domains (Sugar maple – yellow birch, Balsam fir – yellow birch, Balsam fir – paper birch, Spruce moss) (Thiffault et al. 2015). The 33 landscape units selected for this study (Figure 4.1) extend from the confluence of the Ottawa and Gatineau rivers to the southwest (between 45 and 46 N), to Quebec's Côte-Nord region near the Gulf of

St. Lawrence and Labrador border to the northeast (around 50 N). Thus, the selected sites extend from southern boreal shield landscapes in western Quebec to the eastern boreal shield adjacent to the Atlantic-influenced coast, providing a representative geographic cross-section of Quebec's boreal ecosystem.

33 landscapes units of the Quebec boreal forest included in this study. Each colored polygon on the map represents a distinct UPR. UPRs are large-scale landscape divisions defined by relatively uniform ecological conditions – including climate, landforms, soils, and dominant vegetation – within Quebec's ecological classification framework (Gauthier, De Grandpré, and Bergeron 2000)

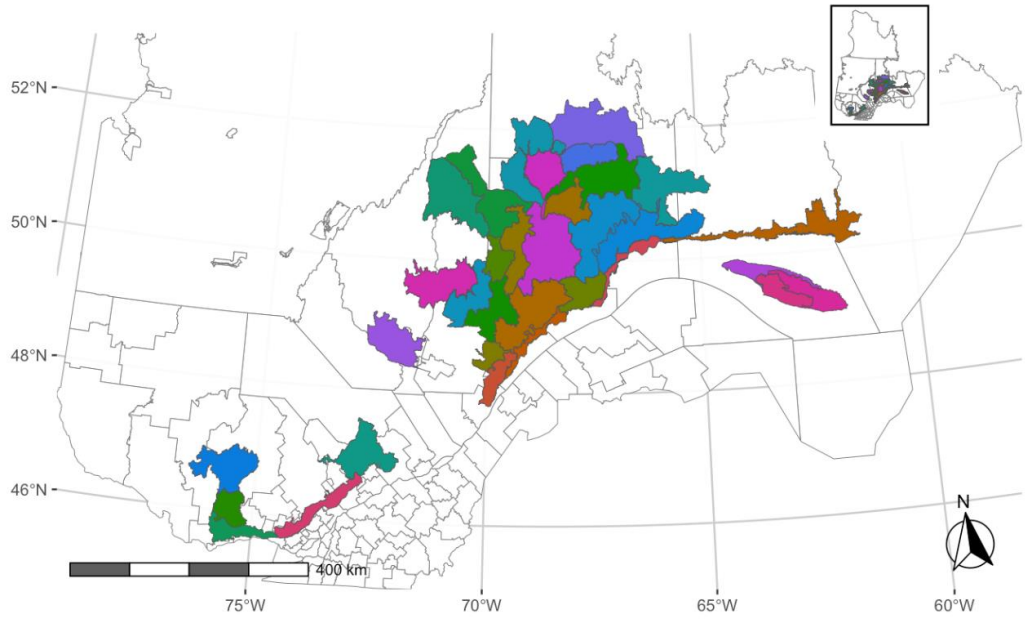

Figure 9
33 landscapes units of the Quebec boreal forest included in this study. Each colored polygon on the map represents a distinct UPR. UPRs are large-scale landscape divisions defined by relatively uniform ecological conditions – including climate, landforms, soils, and dominant vegetation – within Quebec's ecological classification framework (Gauthier et al., 2000)

3.5.2. Climate data sets

The climate data for this study were obtained from BioSIM, a climate interpolation and downscaling model developed by Natural Resources Canada's Canadian Forest Service (Fortin et al. 2022). It generates geographically specific daily weather time series by combining observations from nearby meteorological stations with long-term climate normals, while adjusting for local differences in elevation, latitude, and longitude. We used BioSIM to downscale climate projections under three Representative Concentration Pathway (RCP) emission scenarios: RCP2.6, RCP4.5, and RCP8.5. These RCPs correspond to standardized greenhouse gas concentration trajectories used in climate modeling, spanning a low, intermediate, and high future emission case, respectively. The inclusion of all three scenarios allows us to capture a broad range of plausible future climate conditions – from a stringent mitigation scenario (RCP2.6) to a mid-range stabilizing scenario (RCP4.5) and an unmitigated high-emission scenario (RCP8.5). All climate projections were generated for the period 2040–2100, providing daily climate data from the mid-21st century through the end of the century. The downscaled BioSIM outputs include daily values for the key meteorological variables that were significant in the ACAR models fitted to historical defoliation data for each landscape unit. In this study, we extracted the following daily climate variables from the BioSIM projections:

- Daily maximum air temperature, T_{max} (°C)
- Daily minimum air temperature, T_{min} (°C)
- Daily total precipitation (mm)
- Daily wind speed at 10 m height (m s^{-1})

These four variables represent the fundamental climate inputs used. BioSIM's framework is built around providing such daily weather variables, temperature (min/max), precipitation, and wind speed among others, as the core of its meteorological time series. The data have a daily temporal resolution, which means each variable is available as a continuous daily time series for 2040–2100 under each RCP scenario. The resolution of these downscaled projections is on the order of kilometers covering the study area. Daily maximum and minimum temperatures were

seasonally aggregated for spring and summer. Spring was defined as April, May, and June, while summer comprised July, August, and September.

3.5.3. Quantitative assessment and analysis of climate effects

The Adjacent-Category Autoregressive (ACAR) model (Osse et al. 2023) describes the log-odds of transitioning between adjacent defoliation severity classes as follows:

$$\log \frac{\pi_{j,t}}{\pi_{j-1,t}} = \omega_j + \boldsymbol{\gamma}^{\top} \mathbf{X}_{t-1} + \alpha\, Y_{t-1} + \beta_j\, \eta_{j,t-1},$$

where $\pi_{j,t}$ denotes the probability of being in class j at time t, $\mathbf{X}_{t-1}$ is a vector of climatic covariates (e.g., spring maximum temperature range, log-transformed total precipitation), and Y_{t-1} and $\eta_{j,t-1}$ represent the defoliation level and spatial structure from the previous year, respectively. The coefficients $(\omega_j, \boldsymbol{\gamma}, \alpha, \beta_j)$ were previously estimated for each UPR via maximum likelihood and selected based on rigorous model fit diagnostics (Osse, Marchand, and Girona 2025).

The ACAR models used for this prospective analysis were initially fitted by (Osse, Marchand, and Girona 2025) using annual defoliation data attributed to SBW from 1992 to 2022, aggregated across 33 ecological landscape units. These data, derived from standardized aerial survey observations. For each UPR, an adjacent-category autoregressive (ACAR) model was fitted, incorporating the effects of seasonal temperatures (spring, summer) and precipitation. Model fitting was performed using maximum likelihood estimation, and model adequacy was assessed using the Portmanteau test on residuals. The best-fitting model for each UPR was selected based on the Akaike Information Criterion (AIC). In the present study, these parameter estimates are treated as fixed. To project future defoliation responses under climate change, the historical covariates $\mathbf{X}_t$ are replaced with downscaled climate projections derived under three Representative Concentration Pathways (RCP 2.6, RCP 4.5, and RCP 8.5). We used the estimated coefficients $\boldsymbol{\gamma}$— which quantify the sensitivity of defoliation dynamics to individual climatic variables—from (Osse, Marchand, and Girona 2025) (Table 4).

To isolate the impact of climate alone, we calculate the term $\boldsymbol{\gamma}^{\top}\mathbf{X}_{t-1}$ in the model above, that is, the sum of all climate effects obtained by multiplying one of the model's climate covariate by its coefficient. The resulting output represents the *projected marginal climatic effect*, that is, the increase or decrease in SBW defoliation driven solely by future climate forcing. From the fitted model for each landscape unit, this marginal climate effect is calculated for every year of simulated climate data (2040 – 2100) under each RCP scenario.

To determine the overall contribution of each factor and their interactions, we carried out a Type-II sum-of-squares analysis of variance (Stahle, Wold, et al. 1989). The resulting F-tests indicated whether differences in the projected climatic effect were attributable to (i) spatial heterogeneity among landscape units, (ii) temporal trends, (iii) emission scenario, or (iv) interaction effects such as unit-specific temporal responses under a given RCP. All analyses were executed in R (R Core Team 2022).

Table 4
Estimated effects (γ) of climatic variables on defoliation dynamics, as included in the best-fitting ACAR models per landscape unit. Covariates include spring/summer temperatures, wind speed, and total precipitation (log-transformed), with linear and quadratic terms.

Landscape Units	**Tmax. spring** (sd)	**Tmax. summer** (sd)	**Tmin. spring** (sd)	**Tmin. summer** (sd)	**Wind speed at 10m** (sd)	*logTotprec* (sd)	$Tmin.^2$ **spring** (sd)	$Tmax.^2$ **spring** (sd)	$Tmin.^2$ **summer** (sd)	$Tmax.^2$ **summer** (sd)
Lac la Blanche	0.82 (0.30)	-1.70 (0.62)	-	-	-	-	-	-	0.30 (0.11)	-
Mont-Laurier	-3.55 (0.53)	-	-	-	179.94 (47.21)	-	-	-	-0.37 (0.10)	-0.62 (0.11)
Lac du Poisson Blanc	5.47 (0.54)	-	-	126.85 (10.23)	-326.21 (49.38)	-	-0.57 (0.05)	-	-11.52 (0.93)	-
Saint-Jérôme	-	-53.84 (3.84)	-	-	-	206.14 (9.96)	-0.17 (0.02)	-	-	3.36 (0.28)
Lac Mékinac	-	-10.50 (3.67)	-	11.24 (2.62)	434.70 (105.22)	37.31 (26.57)	-0.08 (0.08)	-	-	-
Tadoussac	7.15 (0.70)	-	-	-190.06 (61.62)	298.97 (165.18)	47.66 (14.39)	-	-	17.03 (5.21)	-
Plaine du lac Saint-Jean	-	-34.60 (2.43)	-7.65 (0.19)	-	143.72 (2.98)	-	-	-	-1.57 (0.06)	3.70 (0.17)
Réservoir Pipmuacan	-	-	-	-	-	-10.09 (4.51)	-	0.01 (0.02)	-	-
Lac des Savanes	-	-27.50 (6.17)	-	-	56.10 (27.59)	-	-	-	-	2.22 (0.49)
Forestville	5.98 (1.40)	-	-	-	58.77 (15.36)	-	-	-	-	-
Lac au Loup Marin	-	-	-12.95 (1.21)	227.09 (13.45)	-	-	-	-	-20.26 (1.02)	-
Lac Dionne	2.54 (0.72)	-	-	-1.23 (0.46)	-	199.37 (35.38)	-	-	-	-
Sept-Îles	-	-6.00 (0.67)	13.66 (1.04)	-6.56 (0.61)	-	-	-	-	-	-
Port-Menier	-	30.79 (4.49)	0.69 (0.94)	-	-	-150.09 (8.00)	-	-	-	-
Rivière Jupiter	-	297.07 (22.05)	-14.05 (1.44)	8.88 (0.66)	399.43 (23.43)	-	-	-	-	-28.46 (1.98)
Rivière aux Saumons	5.36 (0.53)	278.55 (39.54)	-4.28 (0.61)	-42.05 (7.84)	43.13 (8.18)	-26.65 (13.45)	-	-	3.95 (0.74)	-24.35 (3.42)

Source : Osse et al. (2025)

Table 4
Estimated effects (γ) of climatic variables on defoliation dynamics, as included in the best-fitting ACAR models per landscape unit. Covariates include spring/summer temperatures, wind speed, and total precipitation (log-transformed), with linear and quadratic terms.

Landscape Units	**Tmax. spring** (sd)	**Tmax. summer** (sd)	**Tmin. spring** (sd)	**Tmin. summer** (sd)	**Wind speed at 10m** (sd)	*logTotprec* (sd)	$Tmin.^2$ **spring** (sd)	$Tmax.^2$ **spring** (sd)	$Tmin.^2$ **summer** (sd)	$Tmax.^2$ **summer** (sd)
Lac Manouane	32.28 (1.40)	-123.49 (11.34)	-	-33.43 (2.54)	-	-	-	-	13.43 (0.50)	2.06 (0.39)
Lac Rouvray	-	-	-	137.83 (18.99)	-	-	-	-	-11.13 (1.54)	-
Lac du Sault aux Cochons	-8.87 (0.48)	-	-	-	-	112.53 (9.62)	-	-	-	-
Lac Dissimieux	-	-	-	-	-	-	-0.24 (0.04)	-	0.32 (0.02)	-0.43 (0.09)
Lac Guinecourt	-	-	-	92.24 (36.58)	-	-40.63 (11.67)	-	-	-9.77 (3.64)	-
Lac Carteret	-24.85 (2.33)	-	-	-	-116.35 (17.47)	-	0.99 (0.08)	-	-	-
Réservoir Manic 3	-	-	-	164.05 (5.83)	174.32 (6.21)	-285.53 (12.36)	-	-	-12.68 (0.49)	-1.59 (0.06)
Lac Berté	-	-	-	-	-	-	-0.50 (0.16)	-	-	-
Lac Sainte-Anne	-	-	-	-	-	-80.16 (6.32)	-	-	0.50 (0.07)	-0.71 (0.14)
Lac Walker	-	-	0.79 (0.28)	-12.06 (0.73)	-	-	-	-	-	-
Réservoir Manicouagan	-	-	-	-	-	-	-	-0.22 (0.09)	-	0.89 (0.23)
Monts Groulx	70.55 (5.13)	-	-32.81 (2.48)	-	-	-	-	-	-	-
Lac Grandmesnil	-	-	-	-	-	-	-	-0.45 (0.02)	-	-0.78 (0.05)
Lac Nipissis	-	6.65 (5.38)	-29.89 (14.40)	32.10 (7.80)	-	-	-	-	-	-
Havre-Saint Pierre	-	-	-	-	-	-	-0.16 (0.01)	-	-0.65 (0.05)	-
Lac Pécaudy	-	-	8.10 (1.10)	-11.96 (1.37)	-	-	-	-0.53 (0.06)	-	-
Petit lac Manicouagan	-	-	-	-	-	-	-	-0.53 (0.02)	-1.18 (0.05)	-

Source : Osse et al. (2025)

3.6. Results

Using the best-fitting ACAR model for each unit, we derived the estimated marginal effect of projected climate covariates over time (Figure 4.2). The estimation revealed marked heterogeneity in both the directionality and magnitude of climatic effects across space and scenarios. In some units (e.g., *Lac du Poisson Blanc*, *Lac Dionne*, *Sept-Îles*), climate effects was projected to intensify steadily under RCP8.5, indicating increasing pressure from climate-related drivers on defoliation risk. In contrast, other units exhibit non-monotonic (e.g., *Saint-Jérôme*, *Lac des Savanes*) or even declining trends (e.g., *Mont-Laurier*, *Lac Mékinac*), suggesting either buffering mechanisms or nonlinear thresholds in host–climate–insect interactions. This variability underscores that projected climatic effects were not uniform, but rather modulated by local ecological conditions.

The range of values projected for projected climatic effect was equally diverse. Some UPRs, such as *Lac la Blanche* and *Réservoir Pipmuacan*, display values oscillating around zero, suggesting comparatively stable or minimal sensitivity to climate. In contrast, other units– such as *Mont-Laurier*, *Lac Mékinac* and *Rivière Jupiter*– demonstrate substantial variability in effect magnitude, highlighting areas where climate changes could significantly influence future defoliation patterns. Moreover, inter-unit disparities tend to widen over time, particularly under RCP8.5, reflecting growing divergence in climate susceptibility.

These patterns are statistically confirmed by a three-way ANOVA (Table 5). The landscape unit factor accounts for the majority of explained variance, affirming the primacy of spatial heterogeneity. The effect of Year was also highly significant, as was the effect of the RCP scenario. All two-way interactions—UPR:Year, UPR:RCP, and Year:RCP —as well as the three-way interaction UPR:Year:RCP were significant. In particular, the strong UPR:RCP interaction reflects the context-dependent influence of emission trajectories on local defoliation risk, suggesting that the ecological consequences of climate change are both scenario-specific and landscape-contingent.

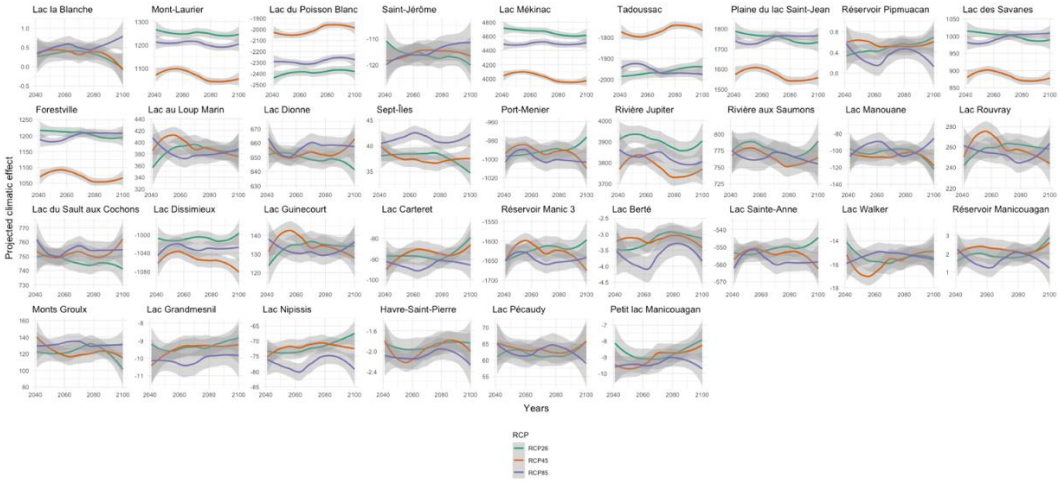

Figure 10
Projected climate-driven defoliation effect for 33 landscape units under RCP 2.6 (green), RCP 4.5 (orange), and RCP 8.5 (purple) from 2040 to 2100. Shaded ribbons indicate uncertainty intervals.

Table 5
Three-way ANOVA results for the projected climatic effect on defoliation

	Df	Sum Sq	Mean Sq	F value	Pr(>F)
UPR	32	9.74e+09	3.04e+08	2.90e+05	$< 2.2 \times 10^{-16}$ ***
Year	1	2.66e+04	2.66e+04	2.53e+01	4.99×10^{-7} ***
RCP	2	6.62e+05	3.31e+05	3.16e+02	$< 2.2 \times 10^{-16}$ ***
UPR:Year	32	3.44e+05	1.08e+04	1.03e+01	$< 2.2 \times 10^{-16}$ ***
UPR:RCP	64	2.25e+07	3.51e+05	3.34e+02	$< 2.2 \times 10^{-16}$ ***
Year:RCP	2	1.90e+04	9.49e+03	9.05e+00	1.19×10^{-4} ***
UPR:Year:RCP	64	2.68e+05	4.18e+03	3.99e+00	$< 2.2 \times 10^{-16}$ ***
Residuals	5742	6.02e+06	1.05e+03		
Signif. codes: 0 ‘***’ 0.001 ‘**’ 0.01 ‘*’ 0.05 ‘.’ 0.1 ‘ ’ 1					

3.7. Discussion

This study set out to quantify how climate change alone, isolated from autoregressive outbreak dynamics, may shape future defoliation patterns caused by SBW in Quebec's boreal forest. Using ordinal time-series modeling under ACAR and scenario-specific simulations, we demonstrated that climate variables exert heterogeneous and potentially intensifying effects on defoliation severity across ecological landscape units.

3.7.1. Spatial heterogeneity in climate-driven defoliation dynamics

Our results confirm that projected climatic effect patterns are highly contingent on landscape identity. This supports prior evidence that local climate–insect interactions modulate outbreak behavior (Candau and Fleming 2011a; De Grandpré et al. 2019). Units such as *Sept-Îles*, and *Monts Groulx* exhibit consistent increases in defoliation probability under RCP 8.5, suggesting strong climate sensitivity. These findings align with studies showing that elevated temperatures accelerate insect development and increase outbreak probability (Bouchard, Régnière, and Therrien 2018b; Pureswaran et al. 2019).

In contrast, units like *Lac au Loup Marin* or *Lac Pécaudy* show non-linear or flat trends, indicating potential climate buffering or ecological thresholds. Similar spatial buffering effects have been observed in other boreal systems where topographic complexity or microclimatic heterogeneity modulates insect impacts (Dale et al. 2001; D'orangeville et al. 2016). These unit-specific trajectories reinforce the notion that climate change will not have a uniform impact on insect outbreaks, a conclusion also drawn by Anderegg et al. (2022) in US forests.

3.7.2. Scenario-dependent intensification of risks

The widening divergence between RCP trajectories over time, especially under RCP 8.5, is a novel and robust signal emerging from our simulations. This intensification supports theoretical expectations that increased radiative forcing exacerbates outbreak risks by exceeding thermal development thresholds and desynchronizing host-insect phenology (Battisti 2008; Logan, Régnière, and Powell 2003). Our findings

parallel recent empirical analyses showing that high-emissions pathways are associated with expanded outbreak ranges and shorter recovery periods (Boucher et al. 2018; Boulanger et al. 2025).

Interestingly, we also observe occasional reversals where RCP 4.5 surpasses RCP 8.5 (e.g., *Lac du Poisson Blanc, Rivière Jupiter, Lac Mékinac, Mont-Laurier*), suggesting that mid-level emissions may interact differently with precipitation or humidity-driven variables. This type of non-monotonic response has been highlighted in pest–climate interaction models that incorporate nonlinear temperature–mortality functions (Bentz et al. 2010; Pureswaran, Roques, and Battisti 2018).

3.7.3. Unexpected results and variance sources

High uncertainty in certain units (e.g., *Rivière Jupiter*) stems from the interaction of multiple climatic variables without endogenous past outbreaks. Although these factors were excluded in our climate-only simulations, their past influence may be embedded in the parameter estimates. This supports previous modeling findings indicating that unmeasured ecological processes can amplify predictive uncertainty (Zinsou Max Debaly, Marchand, and Girona 2022; Haynes et al. 2022).

Some units show marginal or weak climate sensitivity (e.g., *Lac la Blanche*). This could reflect either true ecological inertia or a limitation in the climate data's ability to capture biologically meaningful variability. Recent work emphasizes the importance of fine-scale climate data (e.g., canopy-level humidity) to improve disturbance modeling (Braziunas et al. 2025; Wolf et al. 2021; Z. Li et al. 2024).

3.7.4. Significance and implications for forest management

Our results suggest that adaptive forest management must consider localized risk profiles. In areas where climate-driven effects intensify under RCP 8.5, preemptive strategies such as mixed-species planting, rotation adjustments, or proactive aerial suppression may be necessary (Tremblay et al. 2018; Raymond et al. 2023). Conversely, in climatically buffered areas, maintaining current regimes may suffice in the short term. Landscape-level heterogeneity in vulnerability implies that uniform policy responses may be inefficient or even maladaptive. Instead, targeted

interventions, such as host composition adjustment, site-specific silvicultural treatments, and early-warning systems, should be prioritized in high-risk areas identified through model-based projections.

From a policy perspective, these results support the idea of integrating spatially explicit insect risk maps into regional climate adaptation plans. Doing so would enhance resilience not only to SBW outbreaks but to other co-occurring stressors, such as drought and fire, which are increasingly correlated under warming scenarios (Boulanger and Pascual Puigdevall 2021).

3.8. Conclusion

This study demonstrates the differentiated and climate-contingent nature of SBW defoliation trajectories across Quebec's boreal forest under three projected emissions scenarios (RCP2.6, RCP4.5, and RCP8.5). By leveraging the adjacent-category autoregressive modeling framework, we isolated the marginal effect of climatic variables on annual transitions between ordinal defoliation classes, independent of past outbreaks. The analyses revealed strong spatial heterogeneity and divergent scenario-specific patterns of defoliation sensitivity across UPRs. In particular, we observed pronounced intensification of climate-driven defoliation risk under the RCP8.5 scenario in several UPRs, while others exhibited stable or even attenuated responses, suggesting differential local buffering capacities or nonlinear system responses.

These results reinforce the necessity of integrating spatially resolved climate-defoliation linkages into adaptive forest management strategies. Additionally, risk maps derived from climate-only defoliation simulations can serve as critical inputs to regional climate adaptation planning, particularly in anticipating and managing the compounding effects of fire, drought, and insect outbreaks.

In future work, enhancing predictive accuracy will depend significantly on incorporating endogenous feedback mechanisms into simulation models, particularly spatio-temporal autocorrelation and tree mortality processes, as well as examining compound disturbance interactions within integrated climate scenarios. These

developments will be crucial for creating robust forecasting tools capable of capturing the full complexity of disturbance dynamics in boreal forests under rapidly changing climate conditions. Such efforts will be essential for building robust forecasting tools that reflect the full complexity of boreal forest disturbance regimes in a rapidly changing climate.

Acknowledgments. We sincerely thank Yan Boulanger for generating and providing the climate data sets using BioSIM for our 33 ecological landscape units. His valuable support significantly contributed to this study.

Funding. PM and MMG obtained funding from the Natural Sciences and Engineering Research Council of Canada (NSERC) Alliance and the Québec Ministry of Natural Resources and Forests (MRNF) to understand the dynamics of spruce budworm (ALLRP 558267-20). MMG obtained additional funding from an NSERC Discovery grant to reconstruct the regime of natural disturbances in forest ecosystems (RGPIN-2022-05423).

Author contributions. OJFO: Conceptualization, Model development and data analysis, Software, Visualization, Writing – original draft, Writing – review and editing. PM: Conceptualization, Model development and data analysis, Funding acquisition, Software, Supervision, Validation, Writing – review and editing. MMG: Conceptualization, Funding acquisition, Supervision, Writing – review and editing. All authors gave their final approval for publication.

Ethics approval and consent to participate. Not applicable

Consent for publication. Not applicable

Availability of data and material. The datasets and R scripts used and/or analyzed during the current study are available from the corresponding author upon request.

Competing interest. The authors have no conflict of interest to declare

CONCLUSION GÉNÉRALE

Les trois chapitres de cette thèse dressent un portrait multidimensionnel de la dynamique des épidémies de TBE en forêt boréale québécoise, à travers le prisme de modèles statistiques innovants appliqués à des données temporelles et spatiales. En combinant des approches autorégressives, spatiales (indirectement) et prospectives, ce travail met en évidence les processus complexes qui régissent l'intensité, la fréquence et la distribution des défoliations, dans un contexte de changement climatique. L'intégration de données climatiques et géoréférencées permet de mieux comprendre la réponse de la TBE aux variations saisonnières de température et aux conditions environnementales locales (Osse, Marchand, and Girona 2025). Les résultats des chapitres II, III et IV soulignent notamment l'importance de la dépendance temporelle entre les années de défoliation, la variabilité régionale des réponses épidémiques, ainsi que l'effet différencié des scénarios climatiques futurs (RCP 2.6, 4.5 et 8.5) sur la dynamique de la TBE. De manière plus large, cette thèse illustre l'intérêt de modélisations adaptées à la nature ordinale des données de défoliation, et propose un cadre d'analyse robuste pour appuyer les décisions en aménagement forestier. En ce sens, elle contribue à renforcer les capacités de prévision et d'adaptation des gestionnaires forestiers face aux perturbations naturelles exacerbées par les changements climatiques.

Implications écologiques. Les résultats combinés des trois articles (chapitres II, III et IV) de cette thèse mettent en évidence la complexité, la variabilité et la sensibilité des écosystèmes boréaux face aux perturbations naturelles, en particulier celles causées par la TBE, dans un contexte de changement climatique. Chacun des volets méthodologiques développés, modélisation temporelle ordinale (chapitre 1), analyse spatialisée à l'échelle des unités de paysage (chapitre 2), et projections climatiques différenciées selon les trajectoires RCP (chapitre 3), converge vers un constat central : la réponse des écosystèmes boréaux aux stress biotiques est fortement conditionnée par des interactions non linéaires entre climat, l'hétérogénéité des conditions du peuplement forestier, et mémoire des perturbations passées (Osse, Marchand, and Girona 2025).

Les implications écologiques de ces travaux sont multiples. D'une part, les dynamiques de défoliation ne répondent pas de manière uniforme aux gradients climatiques : des effets seuils ont été détectés, suggérant que de légères augmentations de température ou des modifications dans les régimes saisonniers peuvent entraîner des basculements rapides dans les régimes de perturbation (Osse, Marchand, and Girona 2025). Cela a pour effet de compromettre les trajectoires de résilience naturelle des peuplements forestiers. D'autre part, l'hétérogénéité spatiale observée dans la réponse des unités de paysage montre que la gestion des épidémies ne peut plus être conçue selon des stratégies homogènes ou standardisées. Au contraire, elle doit intégrer la diversité des conditions écologiques locales, la variabilité des risques futurs, et les capacités différentielles des forêts à absorber ou amortir les perturbations.

Par ailleurs, les résultats soulignent le rôle central de la mémoire épidémique dans la structure temporelle des perturbations. Cette dimension, souvent négligée dans les approches classiques, conditionne la probabilité d'occurrence de défoliation sévère de manière cumulative. Les arbres déjà fragilisés par des épisodes antérieurs présentent une vulnérabilité accrue, ce qui renforce la possibilité d'un effet domino écologique à l'échelle du paysage. Cette observation appelle à une vigilance accrue dans les suivis post-épidémiques et la gestion du rétablissement des peuplements.

Enfin, les projections climatiques simulées dans le troisième chapitre laissent entrevoir une intensification des risques dans plusieurs régions du Québec boréal, en particulier sous les scénarios RCP 4.5 et RCP 8.5. Ces résultats invitent à considérer les futures épidémies non plus comme des événements exceptionnels, mais comme des éléments structurants du fonctionnement écosystémique, pouvant modifier profondément la composition, la structure et les services écologiques des forêts boréales.

Dans ce contexte, cette thèse offre des outils de modélisation robustes et des diagnostics régionaux précieux pour soutenir la transition vers une gestion écosystémique adaptative (Achim et al. 2022; D'Amato et al. 2023). Les cartes de

vulnérabilité, les typologies de réponse, et les analyses de trajectoires climatiques proposées ici constituent des leviers concrets pour anticiper les changements à venir, orienter les priorités de surveillance, et concevoir des stratégies d'aménagement forestier plus résilientes et plus sensibles à la complexité des régimes de perturbation en mutation.

Les limites de l'étude. Bien que les résultats présentés dans cette thèse apportent des contributions méthodologiques et empiriques importantes à la compréhension des dynamiques de défoliation par TBE, certaines limites doivent être reconnues, tant sur le plan des données que des approches de modélisation employées.

Premièrement, le modèle autorégressif à catégories adjacentes (ACAR), introduit dans le premier chapitre, repose sur une hypothèse de dépendance temporelle linéaire entre classes ordinales successives. Si ce cadre permet de représenter les effets de mémoire épidémique et les transitions de sévérité dans le temps, il ne tient pas compte des effets d'interactions entre plusieurs années passées ou de la durée des épisodes épidémiques continus, qui peuvent pourtant moduler fortement la réponse des peuplements forestiers. Par ailleurs, le modèle ACAR, dans sa forme actuelle, demeure unidimensionnel : il ne capture ni les effets spatiaux, ni les rétroactions écologiques complexes telles que la mortalité différée ou les modifications de la structure du peuplement après les événements de défoliation sévère.

Deuxièmement, bien que le deuxième chapitre introduise une régionalisation des modèles par unité de paysage (UPR), cette approche repose sur des ajustements locaux indépendants les uns des autres. Cela signifie que les corrélations spatiales et les effets de contagion potentiels entre unités voisines, pourtant bien documentés dans la dynamique des épidémies de TBE, ne sont pas explicitement intégrés dans l'inférence. De plus, la granularité spatiale retenue (les UPR) reflète des unités de planification forestière, mais ne coïncide pas nécessairement avec les gradients écologiques réels, ce qui peut introduire une part d'arbitraire dans la délimitation des zones homogènes.

Enfin, une limite transversale à l'ensemble des trois chapitres concerne la nature des données de défoliation elles-mêmes. Qu'il s'agisse de reconstructions dendrochronologiques ou de levés aériens, ces données comportent une incertitude inhérente liée à la subjectivité de la classification, à la résolution temporelle variable et à la difficulté de distinguer les effets d'autres agents de stress. L'absence de validation croisée systématique entre sources de données limite également la robustesse des inférences à grande échelle.

Malgré ces limites, les modèles développés ici constituent une avancée notable dans la représentation spatio-temporelle des régimes de défoliation, et offrent un socle méthodologique extensible pour des travaux futurs visant à intégrer de manière plus explicite les rétroactions écosystémiques, les interactions multi-agents et la dépendance spatiale.

Les perspectives de recherche. Les travaux présentés dans cette thèse ouvrent plusieurs pistes de recherche prometteuses, tant sur le plan méthodologique que sur celui de l'application à la gestion forestière et à la compréhension des régimes de perturbation en forêt boréale.

Une première avenue consiste à enrichir le cadre statistique utilisé en intégrant explicitement la dépendance spatiale entre unités de paysage. L'utilisation de modèles à effets spatiaux, tels que les modèles à équations différentielles stochastiques (SPDE) (Lindgren, Rue, and Lindström 2011; Sigrist, Künsch, and Stahel 2015) ou les modèles hiérarchiques bayésiens spatio-temporels (Song et al. 2024), permettrait de capter les processus de contagion épidémique, de propagation larvaire et de connectivité forestière qui sous-tendent les dynamiques régionales de la TBE. Cette approche renforcerait la précision des prédictions et améliorerait l'identification des zones tampons ou des barrières écologiques naturelles.

En parallèle, une perspective importante réside dans la modélisation multi-agents et la simulation éco-épidémiologique. En intégrant de manière dynamique les rétroactions entre végétation, climat, populations d'insectes, et perturbations multiples (ex. feux, sécheresse, exploitation du bois par l'homme), ces modèles permettraient

de mieux représenter les trajectoires couplées des forêts dans un contexte de changement global (Hof et al. 2021; Molina et al. 2022). Des environnements de simulation tels que LANDIS-II (Venable et al. 2024) ou SORTIE-ND (Sattler and LeMay 2011) pourraient être mobilisés à cette fin, en y intégrant des modules spécifiques de réponse aux défoliations ordinales.

Par ailleurs, la prise en compte des données multi-sources représente un autre levier majeur. L'intégration des levés aériens, des séries dendrochronologiques, des observations in situ et des données de télédétection à haute résolution (LiDAR, imagerie multispectrale) permettrait de raffiner la représentation des gradients de défoliation et de calibrer les modèles à différentes échelles spatiales et temporelles. Le recours à des techniques d'apprentissage automatique (e.g. forêt aléatoire (random forest) ordinal, réseaux bayésiens) pourrait compléter utilement les approches statistiques paramétriques, notamment pour explorer les non-linéarités complexes et les interactions de haut niveau.

En outre, une piste de développement conceptuel concerne la coupling des dynamiques épidémiques et des indicateurs de fonctionnement écosystémique, tels que la productivité primaire nette, la mortalité arborée, ou les bilans de carbone. Une telle intégration est essentielle pour relier les dynamiques de la TBE à des enjeux plus larges de résilience écosystémique, de régulation climatique et de biodiversité forestière. Ces travaux pourraient également éclairer les effets différenciés des épidémies sur les services écosystémiques et guider l'élaboration de stratégies de gestion forestière basées sur les seuils de tolérance écologique.

Enfin, sur le plan opérationnel, les résultats de cette thèse gagneraient à être traduits dans des outils d'aide à la décision co-construits avec les acteurs du territoire. Le développement d'indicateurs synthétiques de vulnérabilité, de tableaux de bord régionaux et de scénarios d'adaptation intégrés pourrait faciliter l'appropriation des connaissances scientifiques par les gestionnaires forestiers, les décideurs publics et les communautés locales. Une telle interface science-gestion est essentielle pour répondre aux défis croissants liés à l'adaptation des forêts boréales face aux

perturbations d’origine climatique et biologique. Ces travaux démontrent qu’une modélisation ordinale, temporelle et région-centrée renouvelle la lecture des épidémies de TBE et ouvre la voie à une gestion adaptative de la forêt boréale dans un contexte de changement climatique. Les avancées méthodologiques et empiriques présentées constituent un socle robuste pour les recherches futures.

ANNEXE A – INFORMATIONS SUPPLÉMENTAIRES CHAPITRE 1

A.1. Notations and conventions

For any sequence $(u_n)_{n\in\mathbb{N}}$, we adopt the convention $\sum_{i=0}^{-1} u_i = 0$. For a positive real number x, we set $\log^+(x) = \log(x)$ if $x \geq 1$ and 0 otherwise. When x is a vector of $\mathbb{R}^d$, $|x|_1$ is the standard norm-1 of x and for a (m,n) −matrix $A = \left(a_{i,j}\right)_{1\leq i\leq m, 1\leq j\leq n}$, $\| A \|_1 = \max_{1\leq j\leq n} \sum_{i=1}^{m} |a_{i,j}|$, $A^\top = \left(a_{j,i}\right)_{1\leq j\leq n, 1\leq i\leq m}$ is the (n,m) −matrix the transpose of A and $A[i\!:\!j, k\!:\!\ell]$ stands for the submatrix of A with entries $\left(a_{u,v}\right)_{i\leq u\leq j, k\leq v\leq \ell}$. For $A_1, \ldots, A_p$ matrices with r rows and $c_1, \ldots, c_p$ columns, $A = \left(A_1 | \cdots | A_p\right)$ is the column concatenation of $A_1, \ldots, A_p$. For two vectors $a = \left(a_1, \ldots, a_p\right)$ and $b = \left(b_1, \ldots, b_p\right)$ of $\mathbb{R}^p$, $a \odot b = \left(a_1 b_1, \ldots, a_p b_p\right)$ is the Hadamard product of a and b. For a $m \times m$ matrix A, the spectral radius of A will be denoted by $\rho(A)$.

A.2. ACAR model stability properties and statistical inference

The next result stands for the stability properties of [eq::model]-[eq::model_recursion].

Proposition 1. *Consider the model [eq::model]-[eq::model_recursion] and assume that* $(X_t, U_t)_{t\in\mathbb{Z}}$ *is stationary and ergodic with* $\mathbb{E}\log_+|X_0|_1 < \infty$. *We also suppose that* U_t *is independent from* $(U_{t-s}, X_{t-s})_{s>0}$. *If for* $k = 1, \ldots, K$, $|\beta_k| < 1$, *then there exists a unique non-anticipative, stationary and ergotic sequence* $(Y_t, X_t, \eta_t)_{t\in\mathbb{Z}}$ *solution of [eq::model]-[eq::model_recursion] when* $t \in \mathbb{Z}$. *In addition, for* $r \geq 1$, $\mathbb{E}|\eta_0|_1^r < \infty$ *provided that* $\mathbb{E}|X_0|_1^r < \infty$.

A.2.1. Statistical inference

From [eq::model_recursion],

$$\eta_t = \omega + \Gamma X_{t-1} + A\overline{Y}_{t-1} + B\eta_{t-1}$$

where $\omega = \left(\omega_j\right)_{1\leq j\leq K}$, $\Gamma^\top = (\gamma|\cdots|\gamma)$, $A^\top = (\alpha|\cdots|\alpha)$ and $B = \mathrm{diag}\left(\beta_j, 1 \leq j \leq K\right)$. The vector of the parameters of the model will be denoted by $\theta =$

$(\omega^\top, \mathrm{vec}(\Gamma)^\top, \alpha^\top, \beta_1, \dots, \beta_K)^\top$ and assume that $\Theta (\ni \theta)$ is a compact set. The true value of of the parameter will be θ_0. For what follows, we will write $\eta_t(\theta)$ (resp. $\eta_{j,t}(\theta), \pi_{j,t}(\theta), 1 \leq j \leq K$) to make the latent process depend on the parameter θ.

For $k = 1, \dots, K$,

$$\pi_{k,t}(\theta) = \frac{\mathrm{e}^{\sum_{j=1}^{k} \eta_{j,t}(\theta)}}{1 + \sum_{i=1}^{K} \mathrm{e}^{\sum_{j=1}^{i} \eta_{j,t}(\theta)}}, \quad \theta \in \Theta$$

and the parameter θ can by estimated by

$$\hat{\theta}_n = \underset{\theta \in \theta}{\mathrm{argmax}} \sum_{t=1}^{n} \left(\sum_{k=1}^{K} Y_{k,t} \left(\sum_{j=1}^{k} \eta_{j,t}\,(\theta) \right) - \log \left(1 + \sum_{k=1}^{K} \mathrm{e}^{\sum_{j=1}^{k} \eta_{j,t}(\theta)} \right) \right)$$

with initial values η_0(resp. $\overline{Y}_0$). This estimator corresponds to the conditional maximum likehood estimator of the model [eq::model]-[eq::model_recursion]. Let us set

$$\begin{aligned} s_t(\theta) = -\sum_{k=1}^K \left(\sum_{j\geq k} Y_{j,t} - \frac{\sum_{j\geq k} \mathrm{e}^{\sum_{i=1}^j \eta_{i,t}(\theta)}}{1+\sum_{k=1}^K \mathrm{e}^{\sum_{j=1}^k \eta_{j,t}(\theta)}}\right)\nabla_\theta \eta_{k,t}(\theta) \\ \%\dpartial{\eta_{k,t}(\theta)}{\theta} \end{aligned}$$

and

$$h_t(\theta) = \sum_{k=1}^{K} \left\{ \frac{1}{\left(1 + \sum_{k=1}^{K} \mathrm{e}^{\sum_{j=1}^{k} \eta_{j,t}(\theta)}\right)^2} \left[\left(\sum_{j \geq k} \mathrm{e}^{\sum_{i=1}^{j} \eta_{i,t}(\theta)} \right) \sum_{\ell=1}^{k-1} \left(1 + \sum_{j=1}^{\ell-1} \mathrm{e}^{\sum_{i=1}^{j} \eta_{i,t}(\theta)} \right) \nabla_\theta \eta_{\ell,t}(\theta) + \left(1 + \sum_{j=1}^{k-1} \mathrm{e}^{\sum_{i=1}^{j} \eta_{i,t}(\theta)} \right) \sum_{\ell=k}^{K} \left(\sum_{j \geq \ell} \mathrm{e}^{\sum_{i=1}^{j} \eta_{i,t}(\theta)} \right) \nabla_\theta \eta_{\ell,t}(\theta) \right] \right\} \nabla_\theta^\top \eta_{k,t}(\theta)$$

with $\nabla_\theta^\top \eta_{k,t}(\theta) = \left(\frac{\partial \eta_{k,t}}{\partial \theta_i} \right)_{1 \leq i \leq 3K+P}$.

Proposition 2.

Suppose that

the conditions of Proposition 6.1 hold for any $\theta \in \Theta$ with $\mathbb{E}|X_0|_1 < \infty$ and

$\eta_0(\theta) = \eta_0(\theta_0)\ \mathbb{P}_{\theta_0} - a.s \Rightarrow \theta = \theta_0$. Then, the estimator [eq::cmle] is consistent, i.e a.s $\lim_{n\to\infty} \hat{\theta}_n = \theta_0$.

If in addition, θ_0 is located in the interior of Θ, $\mathbb{E}|X_0|_1^2 < \infty$ and the matrix $\mathbb{E}h_0(\theta_0)$ is invertible, $\lim_{n\to\infty} \sqrt{n}\left(\hat{\theta}_n - \theta_0\right) = \mathcal{N}\left(0, J^{-1}LJ^{-1^\top}\right)$ where $L = \mathbb{E}s_0(\theta_0)s_0^\top(\theta_0)$ and $J = \mathbb{E}h_0(\theta_0)$.

A.2.2. Portmanteau-type tests for diagnostic checking

Portmanteau tests are used in time series analysis to assess whether the residuals from a fitted model exhibit autocorrelation. Essentially, they test the null hypothesis that the residuals are uncorrelated, which is a key assumption in many time series models. We used it here to test the adequacy of the model [eq::model]-[eq::model_recursion] and the set of assumptions of the Proposition 6.2. The null hypothesis is then that [eq::model]-[eq::model_recursion] hold with $\theta = \theta_0$. One can look at the residuals

$$e_t(\theta) = \left(\sum_{j\geq k} Y_{j,t} - \frac{\sum_{j\geq k} \mathrm{e}^{\sum_{i=1}^{j} \eta_{i,t}(\theta)}}{1 + \sum_{k=1}^{K} \mathrm{e}^{\sum_{j=1}^{k} \eta_{j,t}(\theta)}}\right)_{1\leq k\leq K}, t \in \mathbb{Z}, \theta \in \Theta,$$

and the autocorrelations

$$\rho_h(\theta) = \frac{1}{n}\sum_{t=1}^{n} e_t\,(\theta) \odot e_{t-h}(\theta), h = 1, \dots, n, \theta \in \Theta.$$

The vector of q successive autocorrelations is $\rho_{1:q}(\theta) = \mathrm{vec}\left(\left(\rho_1(\theta)|\cdots|\rho_q(\theta)\right)^\top\right)$ and its empirical counterpart $\rho_{1:q}(\hat{\theta}_n) = \mathrm{vec}\left(\left(\rho_1(\hat{\theta}_n)|\cdots|\rho_q(\hat{\theta}_n)\right)^\top\right)$. The vector $\rho_{1:q}(\theta)$ evaluated at θ_0 is denoted by $\rho_{1:q}$. Note that $\rho_{1:q} = n^{-1}\sum_{t=1}^{n} m_t$ and under the null hypothesis $\mathbb{E}(m_t|\mathcal{F}_{t-1}) = 0$, *i.e* $(m_t)_{t\in\mathbb{Z}}$ is a martingale difference sequence.

The Jacobian matrix ξ_t of e_t with respect to θ is

$$\xi_t(\theta)(k,\cdot)^\top = -\frac{1}{\left(1+\sum_{k=1}^{K}\mathrm{e}^{\sum_{j=1}^{k}\eta_{j,t}(\theta)}\right)^2}\left[\left(\sum_{j\geq k}\mathrm{e}^{\sum_{i=1}^{j}\eta_{i,t}(\theta)}\right)\sum_{\ell=1}^{k-1}\left(1+\sum_{j=1}^{\ell-1}\mathrm{e}^{\sum_{i=1}^{j}\eta_{i,t}(\theta)}\right)\nabla_\theta\eta_{\ell,t}(\theta) + \left(1+\sum_{j=1}^{k-1}\mathrm{e}^{\sum_{i=1}^{j}\eta_{i,t}(\theta)}\right)\sum_{\ell=k}^{K}\left(\sum_{j\geq \ell}\mathrm{e}^{\sum_{i=1}^{j}\eta_{i,t}(\theta)}\right)\nabla_\theta\eta_{\ell,t}(\theta)\right]$$

For the sake of readability, we will write $\hat{\rho}_{1:q}$ (resp. e_t and ξ_t) for $\rho_{1:q}(\hat{\theta}_n)$ (resp. $e_t(\theta_0)$ and $\xi_t(\theta_0)$).

Let us $C_q = \left(c_1|\cdots|c_q\right)^\top$ with $c_k = \left(c_{k,1}|\cdots|c_{k,q}\right)$. For $h = 1,\ldots,q, c_{k,h}^\top = \mathbb{E}e_{k,-h}\xi_0(k,\cdot), k = 1,\ldots,K$ and $\hat{C}_K$ its empirical counterpart. Let us set

$$d_{i,j}(u,v) = \mathbb{E}\mathrm{e}_{i+1,0}\mathrm{e}_{i+1,-u}\mathrm{e}_{j+1,0}\mathrm{e}_{j+1,-v}, i,j = 0,\ldots,K-1, u,v = 1,\ldots,q,$$

$G = (g_1|\cdots|g_K)^\top$, $g_k = \left(g_{k,1}^\top|\cdots|g_{k,q}^\top\right)$ with

$$g_{k,h} = \mathbb{E}e_{k,-h}e_{k,0}\sum_{\ell=1}^{K} e_{\ell,0}\,\nabla_{\theta_0}^\top\eta_{\ell,0}(\theta){J^{-1}}^\top, 1\leq h\leq q,$$

and D the $Kq\times Kq$ matrix with elements given by

$$D[(iq+1):(i+1)q,(jq+1):(j+1)q] = \left[d_{i,j}(u,v)\right]_{1\leq u,v\leq q}, 0\leq i,j\leq K-1,$$

where $\widehat{D}$, $\hat{G}$ and $\hat{S}$ stand for the empirical counterparts of D, G and S. Let us set $W = D + C_qJ^{-1}L{J^{-1}}^\top C_q^\top + GC_q^\top + C_qG^\top$ and $\widehat{W}$ its empirical counterpart.

We will need the following additional assumption which stands for the invertibility of W. For $k = 1, \dots, K$, let us set

$$\iota_{k,t} = \left(\underbrace{0_q^\top, \dots, 0_q^\top, e_{k,t-1}(\theta_0), \dots, e_{k,t-q}(\theta_0), 0_q^\top, \dots, 0_q^\top}_{\text{k-th block of q elements}} \right)^\top .$$

INV-1

For $\lambda \in \mathbb{R}^{Kq}$, if

$$\lambda^\top \sum_{k=1}^{K} e_{k,0} \left(\iota_{k,0} + C_q J^{-1} \nabla_{\theta_0} \eta_{k,0}(\theta) \right) = 0 \text{ a.s.}$$

then $\lambda = 0$.

Proposition 3. *Under the assumptions of Proposition 2 and INV-1, as n tends to ∞, $n\hat{\rho}_{1:q}^\top \widehat{W}^{-1} \hat{\rho}_{1:q} \Rightarrow \chi^2_{Kq}$ and the adequacy of the ACAR model [eq::model]-[eq::model_recursion] is then rejected at the asymptotic level α if $n\hat{\rho}_{1:q}^\top \widehat{W}^{-1} \hat{\rho}_{1:q} > \chi^2_{Kq}(1-\alpha)$.*

A.3. Comparison test of two adjacent-category time series models

When we are interested in modelling the same process at two or more sites, it may be useful to test whether the observed time series at different sites could plausibly be generated by the same model. Here, we propose a test for the comparison of two fitted models. For example, given two ecological sites, we suppose that the model at one site is driven by the parameter vector $\theta_0^{(1)}$ and that the second site follows parameter vector $\theta_0^{(2)}$. We want to test if the p-th covariate has the same effect at both sites, that is $\theta_{p,0}^{(1)} = \theta_{p,0}^{(2)}$ and also globally $\theta_0^{(1)} = \theta_0^{(2)}$. For $j = 1,2$, let us denote $\left(Y_t^{(j)}, X_t^{(j)}\right)_{t\in\mathbb{Z}}$ the process (Y_t, X_t) coinciding with site j. The problem of interest here is to test the equality of the distributions of $\left(Y_t^{(1)}, X_t^{(1)}\right)_{t\in\mathbb{Z}}$ and $\left(Y_t^{(2)}, X_t^{(2)}\right)_{t\in\mathbb{Z}}$.

For $\theta \in \Theta$, $\left(s_t^{(j)}(\theta)\right)_{t\in\mathbb{Z}}$ and $\left(h_t^{(j)}(\theta)\right)_{t\in\mathbb{Z}}$ are the score and hessian processes evaluated on θ for the process $\left(Y_t^{(j)}, X_t^{(j)}\right)_{t\in\mathbb{Z}}$. Under the conditions of proposition 6.2 for $\left(Y_t^{(j)}, X_t^{(j)}\right)_{t\in\mathbb{Z}}$,

$$\lim_{n\to\infty} \frac{1}{\sqrt{n}} \sum_{t=1}^{n} s_t^{(j)}\left(\theta_0^{(j)}\right) = \mathcal{N}\left(0, L_j\right)$$

and *a.s*

$$\lim_{n\to\infty} \frac{1}{n} \sum_{t=1}^{n} h_t^{(j)}\left(\theta_0^{(j)}\right) = J_j, j = 1,2.$$

Let us set $S = \mathbb{E} s_0^{(2)}\left(\theta_0^{(2)}\right) s_0^{(1)}\left(\theta_0^{(1)}\right)^{\top}$, $V = J_1^{-1} L_1 {J_1^{-1}}^{\top} + J_2^{-1} L_2 {J_2^{-1}}^{\top} + J_2^{-1} S {J_1^{-1}}^{\top} + J_1^{-1} S^{\top} {J_2^{-1}}^{\top}$ and $\hat{V}$ its empirical counterpart. We will denote $\hat{\theta}_n^{(1)}$ (resp. $\hat{\theta}_n^{(2)}$) the estimator of $\theta_0^{(1)}$ (resp. $\theta_0^{(2)}$) given by [eq::cmle] and $\hat{\theta}_{p,n}^{(1)}$ (resp. $\hat{\theta}_{p,n}^{(2)}$) the p-th element of $\theta_0^{(1)}$ (resp $\theta_0^{(2)}$).

We will need the following additional assumption, which stands for the invertibility of V.

INV-2

For $\lambda \in \mathbb{R}^{3K+P}$, if

$$\lambda^{\top}\left(J_1^{-1} s_t^{(1)}\left(\theta_0^{(1)}\right) + J_1^{-2} s_t^{(2)}\left(\theta_0^{(2)}\right)\right) = 0 \text{ a.s.}$$

then $\lambda = 0$.

Proposition 4. Suppose that $\left(s_t^{(1)}\left(\theta_0^{(1)}\right), s_t^{(2)}\left(\theta_0^{(2)}\right)\right)_{t\in\mathbb{Z}}$ is stationary and ergodic. Under the assumptions of Proposition 6.2 and INV-2.

As n tends to ∞, $n^{1/2}\frac{\widehat{\theta}_{p,n}^{(1)}-\widehat{\theta}_{p,n}^{(2)}}{\sqrt{\widehat{V}(p,p)}} \Rightarrow \mathcal{N}(0,1)$. The hypothesis $\theta_{p,0}^{(1)} = \theta_{p,0}^{(2)}$ is then rejected at the level α if $\left|n^{1/2}\frac{\widehat{\theta}_{p,n}^{(1)}-\widehat{\theta}_{p,n}^{(2)}}{\sqrt{\widehat{V}(p,p)}}\right| > q(1-\alpha/2)$.

As n tends to ∞, $n\left(\hat{\theta}_n^{(1)} - \hat{\theta}_n^{(2)}\right)^{\top} \hat{V}^{-1}\left(\hat{\theta}_n^{(1)} - \hat{\theta}_n^{(2)}\right) \Rightarrow \chi_P^2$. The hypothesis $\theta_0^{(1)} = \theta_0^{(2)}$ is then rejected at the level α if $n\left(\hat{\theta}_n^{(1)} - \hat{\theta}_n^{(2)}\right)^{\top} \hat{V}^{-1}\left(\hat{\theta}_n^{(1)} - \hat{\theta}_n^{(2)}\right) > \chi_P^2(1-\alpha)$.

On the stationary assumption on scores

Note that we require the joint process of scores $\left(s_t^{(1)}\left(\theta_0^{(1)}\right), s_t^{(2)}\left(\theta_0^{(2)}\right)\right)_{t\in\mathbb{Z}}$ to be stationary and ergodic. This assumption is satisfied as soon as the process $\left(X_t^{(1)}, X_t^{(2)}, U_t^{(1)}, U_t^{(2)}\right)_{t\in\mathbb{Z}}$, where $\left(U_t^{(1)}\right)_{t\in\mathbb{Z}}$ (resp. $\left(U_t^{(2)}\right)_{t\in\mathbb{Z}}$) is the uniform variable process that generates $\left(Y_t^{(1)}\right)_{t\in\mathbb{Z}}$ (resp. $\left(Y_t^{(2)}\right)_{t\in\mathbb{Z}}$, is stationary and ergodic. The case of independency of the processes $\left(X_t^{(1)}, U_t^{(1)}\right)_{t\in\mathbb{Z}}$ and $\left(X_t^{(2)}, U_t^{(2)}\right)_{t\in\mathbb{Z}}$ is particulary interesting because it entails S = 0. It can be also interesting to consider the case where $\left(X_t^{(1)}\right)_{t\in\mathbb{Z}}$ and $\left(X_t^{(2)}\right)_{t\in\mathbb{Z}}$ are independent but $\left(U_0^{(1)}, U_0^{(2)}\right)_{t\in\mathbb{Z}}$ is degenarate ; for example $U_0^{(1)} = U_0^{(2)}$ or $U_0^{(1)} = 1 - U_0^{(2)}$.

Propositions 1, 3, and 4 are supported by proofs that can be found in the supplementary materials

A.4. Supplementary materials

A.4.1. Proof of Proposition 1

Let us set $\lambda_t = \left(\lambda_{1,t}, \ldots, \lambda_{K,t}\right)^{\top}$. From Equation [eq::baseline_similarity],

$$\lambda_t = \widetilde{\omega} + \tilde{A}\overline{Y}_{t-1} + \tilde{B}\lambda_{t-1}, t \in \mathbb{Z},$$

where $\widetilde{\omega} = \left(\sum_{j=1}^{k} \omega_j, k = 1, \ldots, K\right), \tilde{A} = (\alpha|2\alpha| \cdots |K\alpha)^{\top}$ and

$$\tilde{B} = \begin{pmatrix} \beta_1 & 0 & \cdots & 0 \\ \beta_1 & \beta_2 & & 0 \cdots \\ \vdots & & \ddots & \ddots \\ \beta_1 & \beta_2 & \cdots & \beta_K \end{pmatrix}.$$

The result of Proposition 6.1 follows (Truquet 2020) Proposition 4 which provides stability conditions for category baseline multinomial autoregression. Indeed, for $k = 1, \ldots, K, |\beta_k| < 1$, the roots $1/\beta_k, k = 1, \ldots, K$ of polynomial

$$\mathcal{P}(z) = \det\left(I - \tilde{B}z\right) = \Pi_{j=1}^{K}\left(1 - \beta_j z\right)$$

are outside the unit disk. Moreover, the moments of latent process depend on that of $(X_t)_{t \in Z}$, as $Y_{k,t}$'s take only two values : 0 and 1.

A.4.2. Condition for identifiability of θ_0.

For any $\theta \in \Theta,\ |\beta_k|, k = 1, \ldots, K < 1$;

For any $v \in \mathbb{R}^P$,

$$v'X_1 \in \mathcal{F}_0 \vee \sigma(U_1) \Rightarrow v = 0;$$

The distribution of U_0 is non-degenerate;

If v is equal to any $\alpha_{0,k}\iota, k = 1, \ldots, K$ or $\gamma_{0,p}\iota, p = 1, \ldots, P$ with $\iota = (1, \ldots, 1)^{\top}$ has K components, the equalities $B^j v = B_0^j v, \quad j \geq 1$, entail $B = B_0$.

A.4.3. Derivative of latent process

For $k = 1, \ldots, K$,

$$
\begin{aligned}
\frac{\partial \eta_{k,t}(\theta)}{\partial \omega_\ell} &= 0, \ell \neq k, \\
\frac{\partial \eta_{k,t}(\theta)}{\partial \omega_k} &= 1 + \beta_k \frac{\partial \eta_{k,t-1}(\theta)}{\partial \omega_j} = 1 + \sum_{\ell \geq 1} \beta_k^\ell = \frac{1}{1-\beta_k}, \\
\frac{\partial \eta_{k,t}(\theta)}{\partial \gamma} &= X_{t-1} + \beta_k \frac{\partial \eta_{k,t-1}(\theta)}{\partial \gamma} = \sum_{\ell \geq 0} \beta_k^\ell X_{t-\ell-1}, \\
\frac{\partial \eta_{k,t}(\theta)}{\partial \alpha} &= \overline{Y}_{t-1} + \beta_k \frac{\partial \eta_{k,t-1}(\theta)}{\partial \alpha} = \sum_{\ell \geq 0} \beta_k^\ell \overline{Y}_{t-\ell-1}, \\
\frac{\partial \eta_{k,t}(\theta)}{\partial \beta_\ell} &= 0, \ell \neq k, and \\
\frac{\partial \eta_{k,t}(\theta)}{\partial \beta_k} &= \eta_{k,t-1}(\theta) + \beta_k \frac{\partial \eta_{k,t-1}(\theta)}{\partial \beta_k} = \sum_{\ell \geq 0} \beta_k^\ell \eta_{k,t-\ell-1}(\theta).
\end{aligned}
$$

A.4.4. Proof of Proposition 3

Let us denote by $\tilde{\rho}_h(\theta)$ the autocorrelation functions when the latent process is initialized at $t = 0$ and $\tilde{\rho}_h$ its value evaluate at $\theta = \theta_0$ and define $\rho_{1:q}(\theta)$ and $\tilde{\rho}_{1:q}(\theta)$ (resp. $\rho_{1:q}$ and $\tilde{\rho}_{1:q}$ accordingly. Under the conditions

$$
n^{1/2}\left|\rho_{1:q} - \tilde{\rho}_{1:q}\right|_1 = o_{\mathbb{P}}(1); \quad \sup_\theta \| \nabla_\theta \rho_{1:q}(\theta) - \nabla_\theta \tilde{\rho}_{1:q}(\theta) \| = o_{\mathbb{P}}(1) \text{ and } \lim_{n\to\infty} \mathbb{E} \sup_\theta \| \nabla_\theta^2 \rho_{1:q}(\theta) \| < \infty
$$

obtained with $\mathbb{E}|X_0|_2^r < \infty$ for r large enough.

$$
\sqrt{n}\hat{\rho}_{1:q} = \sqrt{n}\rho_{1:q} + C_q\sqrt{n}\left(\hat{\theta} - \theta_0\right) + o_{\mathbb{P}}(1)
$$

see (Francq and Zakoian 2019), proof of Theorem 8.2 for the case of GARCH model. From Proposition 6.2,

$$
\sqrt{n}\left(\hat{\theta}_n - \theta_0\right) = -J^{-1}\frac{1}{\sqrt{n}}\sum_{t=1}^{n} s_t\left(\theta_0\right) + o_{\mathbb{P}}(1).
$$

We also have

$$\sqrt{n}\rho_{1:q} = n^{-1/2}\sum_{t=1}^{n}\sum_{k=1}^{K} e_{k,t}\,\iota_k.$$

It follows that

$$\sqrt{n}\begin{pmatrix}\hat{\theta}_n - \theta_0\\ \rho_{1:q}\end{pmatrix} = \frac{1}{\sqrt{n}}\sum_{t=1}^{n}\sum_{k=1}^{K} e_{k,t}\begin{pmatrix}J^{-1}\nabla_{\theta_0}\eta_{k,t}(\theta)\\ \iota_{k,t}\end{pmatrix} + 0_{\mathbb{P}}(1).$$

Because the sequence $\left(\sum_{k=1}^{K} e_{k,t}\begin{pmatrix}\nabla_{\theta_0}\eta_{k,t}(\theta)\\ \iota_{k,t}\end{pmatrix}\right)_{t\in\mathbb{Z}}$ is a martingale difference sequence,

$$\sqrt{n}\begin{pmatrix}\hat{\theta}_n - \theta_0\\ \rho_{1:q}\end{pmatrix} \Rightarrow \mathcal{N}\left(0_{Kq+Q}, \begin{pmatrix}J^{-1}LJ^{-1^\top} & G^\top\\ G & D\end{pmatrix}\right).$$

From Equation [eq::hatrho],

$$\sqrt{n}\hat{\rho}_{1:q} \Rightarrow \mathcal{N}\left(0_{Kq}, D + C_qJ^{-1}LJ^{-1^\top}C_q^\top + GC_q^\top + C_qG^\top\right).$$

Under [ass::invertible] ,

$$D + C_qJ^{-1}LJ^{-1^\top}C_q^\top + GC_q^\top + C_qG^\top = \mathbb{E}ZZ^\top$$

with

$$Z = \sum_{k=1}^{K} e_{k,0}\left(\iota_k + C_qJ^{-1}\nabla_{\theta_0}\eta_{k,0}(\theta)\right)$$

is invertible. Then,

$$n\hat{\rho}_{1:q}^\top\left(D + C_qJ^{-1}LJ^{-1^\top}C_q^\top + GC_q^\top + C_qG^\top\right)^{-1}\hat{\rho}_{1:q} \Rightarrow \chi^2_{Kq}.$$

The result of the proposition follows from the continuous map theorem.

A.4.5. Proof of Proposition 4

From Proposition 6.2, $\begin{pmatrix} s_t^{(1)}\left(\theta_0^{(1)}\right) \\ s_t^{(2)}\left(\theta_0^{(2)}\right) \end{pmatrix}_{t\in\mathbb{Z}}$ is a square integrable martingale difference sequence. Then,

$$\sqrt{n}\begin{pmatrix} \hat{\theta}_n^{(1)} - \theta_0^{(1)} \\ \hat{\theta}_n^{(2)} - \theta_0^{(2)} \end{pmatrix} = -\frac{1}{\sqrt{n}}\sum_{t=1}^{n}\begin{pmatrix} J_1^{-1}s_t^{(1)}\left(\theta_0^{(1)}\right) \\ J_2^{-1}s_t^{(2)}\left(\theta_0^{(2)}\right) \end{pmatrix} + 0_{\mathbb{P}}(1)$$

$$\Rightarrow \quad \mathcal{N}\left(0_{2(3K+P)}, \begin{pmatrix} J_1^{-1}L_1{J_1^{-1}}^{\top} & J_1^{-1}S^{\top}{J_2^{-1}}^{\top} \\ J_2^{-1}S{J_1^{-1}}^{\top} & J_2^{-1}L_2{J_2^{-1}}^{\top} \end{pmatrix}\right).$$

It follows that, under the null hypothesis,

$$\sqrt{n}\left(\theta_n^{(1)} - \theta_n^{(2)}\right) = \sqrt{n}\left(\hat{\theta}_n^{(1)} - \theta_0^{(1)}\right) - \sqrt{n}\left(\hat{\theta}_n^{(2)} - \theta_0^{(2)}\right) \Rightarrow \mathcal{N}(0, V)$$

with

$$V = J_1^{-1}L_1{J_1^{-1}}^{\top} + J_2^{-1}L_2{J_2^{-1}}^{\top} + J_2^{-1}S{J_1^{-1}}^{\top} + J_1^{-1}S^{\top}{J_2^{-1}}^{\top} = \mathbb{E}UU^{\top},$$

and $U = J_1^{-1}s_t^{(1)}\left(\theta_0^{(1)}\right) + J_1^{-2}s_t^{(2)}\left(\theta_0^{(2)}\right)$. The matrix V is then invertible under [ass::invertible2]. The result of the proposition follows from the continuous map theorem.

A.4.6. Threshold estimate for the temperature effects

The thresholds are derived using the delta method (Van der Vaart 2000). Denoting $\theta_0(x)$ the regression parameter of covariate x, the threshold of the temperature effect in spring, for example, is $\mathrm{TS} = \frac{\theta_0(\Delta\text{temp. max. spring})}{2\times\theta_0(\text{Square of}\Delta\text{temp. max. spring})}$. Then, $\widehat{\mathrm{TS}}$ is obtained by replacing $\theta_0(x)$ by $\hat{\theta}(x)$. The variance of $\widehat{\mathrm{TS}} - \mathrm{TS}$ is $\hat{\mu}^{\top}\hat{\Sigma}_{spring}\hat{\mu}$, where

$$\hat{\mu}^{\top} = \left(\frac{1}{2 \times \hat{\theta}(\text{Square of}\Delta\text{temp. max. spring})}, -\frac{\hat{\theta}(\Delta\text{temp. max. spring})}{2 \times \hat{\theta}^{2}(\text{Square of}\Delta\text{temp. max. spring})} \right),$$

and $\hat{\Sigma}_{spring}$ is the estimate covariance matrix of

$$\left(\hat{\theta}(\Delta\text{temp. max. spring}), \hat{\theta}(\text{Square of}\Delta\text{temp. max. spring}) \right).$$

A.4.7. Results of the quasi-maximum likelihood estimation

Table 6
Results of the quasi-maximum likelihood estimation

n	θ_0	1.2	0.7	0.5	-0.8	1.5	-1.5	2.0	2.0	0.3	-0.3	0.5	0.8	-0.2	0.3
70	CMLE	3.616	3.311	1.687	-1.613	3.144	-3.108	4.252	4.165	-0.583	-1.507	-0.304	0.818	-0.132	0.298
	TSE	6.794	7.424	7.080	0.735	1.246	1.223	1.577	1.594	7.216	7.706	7.425	0.099	0.435	0.345
	MAE	3.482	3.985	3.058	2.154	2.716	3.597	3.773	3.692	3.208	3.912	3.659	0.824	0.970	0.806
	MSE	8.783	10.275	9.006	2.924	4.256	4.895	6.040	5.579	9.017	9.459	10.067	1.032	1.175	1.008
100	CMLE	1.642	0.854	0.625	-1.097	1.908	-1.966	2.581	2.577	0.180	-0.709	0.649	0.809	-0.171	0.273
	TSE	1.011	1.317	1.130	0.400	0.588	0.622	0.784	0.774	1.203	1.346	1.314	0.064	0.337	0.292
	MAE	0.756	0.641	0.646	1.200	0.925	2.122	1.258	1.258	0.903	1.646	0.819	0.736	0.537	0.097
	MSE	1.666	1.809	1.835	0.219	0.313	0.345	0.470	0.451	1.828	1.819	1.863	0.034	0.129	0.130
300	CMLE	1.237	0.636	0.580	-0.805	1.492	-1.531	1.997	2.012	0.250	-0.394	0.460	0.807	-0.207	0.308
	TSE	0.359	0.520	0.404	0.179	0.277	0.284	0.356	0.358	0.432	0.510	0.494	0.035	0.192	0.158
	MAE	0.843	0.191	0.123	0.979	1.223	1.784	1.644	1.642	0.134	0.810	0.103	0.765	0.392	0.143
	MSE	0.122	0.100	0.114	0.051	0.089	0.097	0.123	0.117	0.130	0.122	0.153	0.011	0.049	0.042
500	CMLE	1.182	0.578	0.518	-0.801	1.486	-1.492	1.973	1.966	0.277	-0.292	0.539	0.799	-0.207	0.291
	TSE	0.265	0.392	0.307	0.137	0.216	0.216	0.276	0.275	0.329	0.376	0.373	0.028	0.152	0.127
	MAE	0.935	0.308	0.193	0.937	1.284	1.716	1.724	1.725	0.060	0.676	0.137	0.772	0.352	0.173
	MSE	0.064	0.061	0.067	0.032	0.057	0.053	0.072	0.071	0.075	0.077	0.089	0.007	0.032	0.028
	θ_0	1.2	0.7	0.5	0.8	-1.5	1.5	-2.0	-2.0	-0.3	0.3	-0.5	-0.8	0.2	-0.3
70	CMLE	4.484	1.885	-0.373	2.239	-4.037	4.062	-5.408	-5.373	-0.289	1.602	-0.402	-0.804	0.116	-0.316
	TSE	2.937	1.474	1.459	0.761	1.290	1.265	1.638	1.668	1.543	2.348	1.500	0.061	0.376	0.329
	MAE	5.424	2.649	2.531	2.486	3.922	4.215	5.270	5.232	2.800	3.881	2.892	1.111	0.919	0.938
	MSE	11.246	4.721	5.134	4.489	6.677	6.917	8.772	8.434	5.974	9.647	6.247	1.271	1.137	1.121
100	CMLE	2.286	1.077	0.401	1.237	-2.345	2.356	-3.117	-3.186	-0.305	1.209	-0.686	-0.803	0.157	-0.298
	TSE	1.956	0.918	0.986	0.451	0.718	0.738	0.925	0.941	0.897	1.403	0.926	0.050	0.319	0.303
	MAE	1.808	0.889	0.956	0.547	0.932	0.946	1.205	1.274	0.842	1.492	1.111	0.043	0.151	0.127
	MSE	3.910	1.730	1.603	1.373	2.356	2.377	3.276	3.578	1.256	5.799	2.350	0.058	0.198	0.166
300	CMLE	1.171	0.638	0.401	0.849	-1.611	1.600	-2.123	-2.112	-0.198	0.490	-0.352	-0.808	0.189	-0.319
	TSE	0.803	0.378	0.480	0.171	0.273	0.271	0.348	0.347	0.365	0.438	0.360	0.028	0.184	0.167
	MAE	0.651	0.349	0.393	0.124	0.192	0.175	0.234	0.245	0.378	0.455	0.373	0.020	0.072	0.073
	MSE	0.845	0.461	0.513	0.162	0.260	0.252	0.318	0.324	0.472	0.578	0.459	0.026	0.092	0.094
500	CMLE	1.143	0.654	0.461	0.821	-1.538	1.556	-2.053	-2.065	-0.196	0.455	-0.389	-0.806	0.184	-0.310
	TSE	0.607	0.282	0.360	0.127	0.203	0.205	0.262	0.263	0.274	0.320	0.265	0.021	0.144	0.131
	MAE	0.601	0.266	0.280	0.093	0.136	0.155	0.176	0.190	0.268	0.346	0.264	0.018	0.056	0.053
	MSE	0.738	0.328	0.365	0.119	0.180	0.194	0.224	0.247	0.340	0.462	0.326	0.021	0.072	0.065
	θ_0	1.2	0.7	1.5	0.8	-1.5	-1.5	2.0	-2.0	0.3	-0.3	-0.5	-0.8	0.2	-0.3
70	CMLE	6.218	2.849	2.043	3.363	-6.405	-6.394	8.474	-8.528	2.311	0.434	0.235	-0.804	0.0742	-0.310
	TSE	3.610	1.817	1.786	0.968	1.551	1.603	2.042	2.103	2.1483	4.074	1.733	0.060	0.383	0.352
	MAE	7.506	4.794	3.945	3.563	6.421	6.409	8.480	8.530	4.885	6.469	4.185	1.179	1.002	1.033
	MSE	14.640	9.501	7.536	6.173	10.750	10.669	13.978	14.160	9.441	16.167	7.893	1.415	1.196	1.234
100	CMLE	1.870	0.861	1.385	1.249	-2.278	-2.265	2.965	-3.053	0.852	0.041	-0.284	-0.805	0.138	-0.319
	TSE	1.834	0.993	1.142	0.457	0.720	0.728	0.919	0.950	1.017	1.517	0.866	0.050	0.359	0.304
	MAE	1.542	0.886	0.922	0.524	0.837	0.828	1.025	1.107	1.101	1.413	0.950	0.043	0.162	0.134
	MSE	2.017	1.142	1.275	0.848	1.421	1.467	1.697	1.971	1.608	2.059	1.329	0.057	0.221	0.171
300	CMLE	1.324	0.795	1.448	0.874	-1.653	-1.650	2.196	-2.218	0.378	-0.247	-0.468	-0.802	0.183	-0.308
	TSE	0.853	0.438	0.545	0.181	0.293	0.292	0.379	0.381	0.378	0.499	0.371	0.028	0.192	0.181
	MAE	0.717	0.336	0.393	0.138	0.239	0.229	0.294	0.313	0.388	0.508	0.336	0.021	0.077	0.065
	MSE	0.861	0.451	0.504	0.188	0.332	0.311	0.406	0.418	0.490	0.647	0.422	0.027	0.096	0.083
500	CMLE	1.199	0.718	1.458	0.842	-1.580	-1.587	2.109	-2.116	0.380	-0.207	-0.431	-0.803	0.183	-0.307
	TSE	0.647	0.325	0.418	0.132	0.214	0.216	0.279	0.280	0.286	0.373	0.274	0.022	0.151	0.140
	MAE	0.537	0.298	0.353	0.103	0.161	0.168	0.207	0.201	0.313	0.364	0.264	0.017	0.060	0.051
	MSE	0.671	0.391	0.442	0.135	0.213	0.218	0.273	0.267	0.405	0.468	0.345	0.021	0.074	0.064

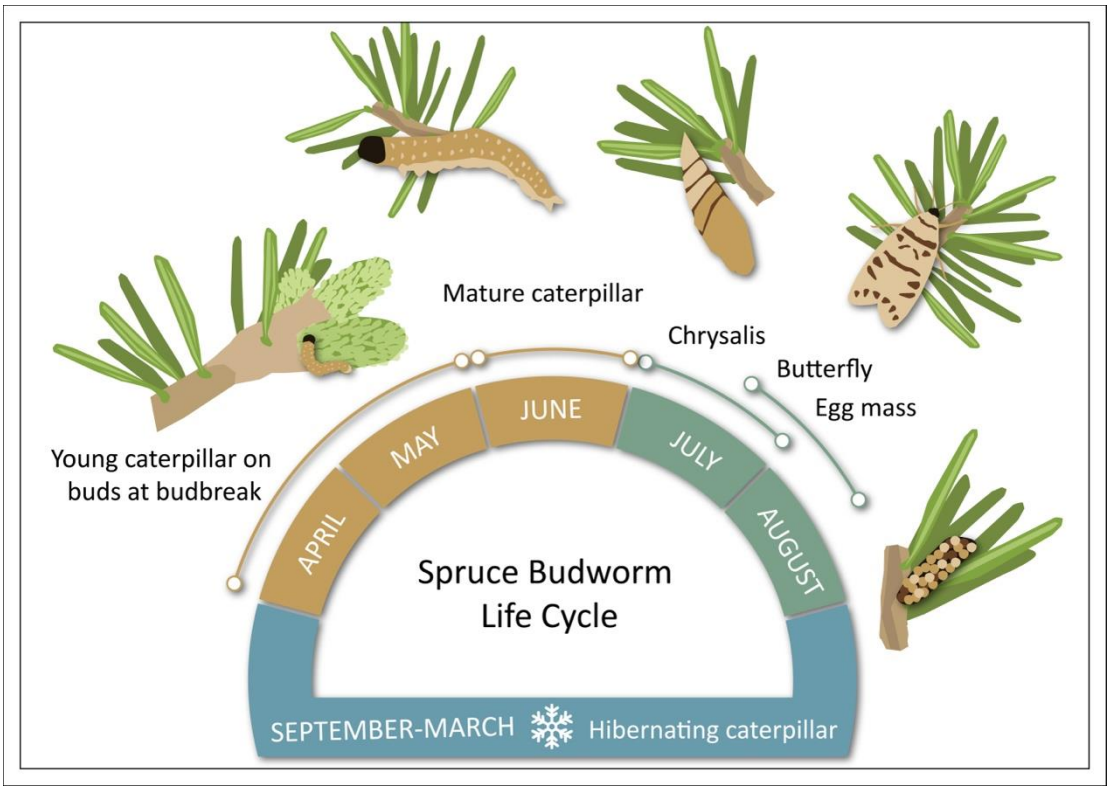

Figure 11
The life cycle of spruce budworm

LISTE DE RÉFÉRENCES

Aakala, Tuomas, Cécile C Remy, Dominique Arseneault, Hubert Morin, Martin P Girardin, Fabio Gennaretti, Lionel Navarro, et al. 2023. “Millennial-Scale Disturbance History of the Boreal Zone.” In Boreal Forests in the Face of Climate Change: Sustainable Management, 53–87. Springer.

Abarca, Mariana, and John T Lill. 2015. “Warming Affects Hatching Time and Early Season Survival of Eastern Tent Caterpillars.” *Oecologia* 179: 901–12.

Abdi, Hervé, and Lynne J Williams. 2010. “Tukey’s Honestly Significant Difference (HSD) Test.” *Encyclopedia of Research Design* 3 (1): 1–5.

Achim, Alexis, Guillaume Moreau, Nicholas C Coops, Jodi N Axelson, Julie Barrette, Steve Bédard, Kenneth E Byrne, et al. 2022. “The Changing Culture of Silviculture.” *Forestry* 95 (2): 143–52.

Agresti, Alan. 2010. *Analysis of Ordinal Categorical Data*. Vol. 656. John Wiley & Sons.

Akashi, F., M. Taniguchi, A. C. Monti, and T. Amano. 2021. *Diagnostic Methods in Time Series*. SpringerBriefs in Statistics. Springer Singapore.

Ameray, Abderrahmane, Yves Bergeron, Osvaldo Valeria, Miguel Montoro Girona, and Xavier Cavard. 2021. “Forest Carbon Management: A Review of Silvicultural Practices and Management Strategies Across Boreal, Temperate and Tropical Forests.” *Current Forestry Reports*, 1–22.

Ameray, Abderrahmane, Xavier Cavard, Dominic Cyr, Osvaldo Valeria, Miguel Montoro Girona, and Yves Bergeron. 2024. “One Century of Carbon Dynamics in the Eastern Canadian Boreal Forest Under Various Management Strategies and Climate Change Projections.” *Ecological Modelling* 498: 110894.

Anderegg, William RL, Oriana S Chegwidden, Grayson Badgley, Anna T Trugman, Danny Cullenward, John T Abatzoglou, Jeffrey A Hicke, Jeremy Freeman, and Joseph J Hamman. 2022. “Future Climate Risks from Stress, Insects and Fire Across US Forests.” *Ecology Letters* 25 (6): 1510–20.

Anderegg, William RL, Jeffrey A Hicke, Rosie A Fisher, Craig D Allen, Juliann Aukema, Barbara Bentz, Sharon Hood, et al. 2015. “Tree Mortality from Drought, Insects, and Their Interactions in a Changing Climate.” *New Phytologist* 208 (3): 674–83.

Anderson, D, and K Burnham. 2004. “Model Selection and Multi-Model Inference.” *Second. NY: Springer-Verlag* 63 (2020): 10.

Anderson, Dean P, and Brian R Sturtevant. 2011. “Pattern Analysis of Eastern Spruce Budworm Choristoneura Fumiferana Dispersal.” *Ecography* 34 (3): 488–97.

Balducci, Lorena, Angelo Fierravanti, Sergio Rossi, Sylvain Delzon, Louis De Grandpré, Daniel D Kneeshaw, and Annie Deslauriers. 2020. “The Paradox of Defoliation: Declining Tree Water Status with Increasing Soil Water Content.” *Agricultural and Forest Meteorology* 290: 108025.

Baskerville, G, and S Kleinschmidt. 1981. “A Dynamic Model of Growth in Defoliated Fir Stands.” *Canadian Journal of Forest Research* 11 (2): 207–15.

Battisti, Andrea. 2008. “Forests and Climate Change-Lessons from Insects.” *IFOREST-Biogeosciences and Forestry* 1 (1): 1.

Battisti, Andrea, Michael Stastny, Sigrid Netherer, Christelle Robinet, Axel Schopf, Alain Roques, and Stig Larsson. 2005. “Expansion of Geographic Range in the Pine Processionary Moth Caused by Increased Winter Temperatures.” *Ecological Applications* 15 (6): 2084–96.

Bauce, Éric, Michèle Crépin, and Nathalie Carisey. 1994. “Spruce Budworm Growth, Development and Food Utilization on Young and Old Balsam Fir Trees.” *Oecologia* 97 (4): 499–507.

Beckwith, Roy C, and Donald G Burnell. 1982. “Spring Larval Dispersal of the Western Spruce Budworm (Lepidoptera: Tortricidae) in North-Central Washington.” *Environmental Entomology* 11 (4): 828–32.

Bellemin-Noël, Bastien, Stéphane Bourassa, Emma Despland, Louis De Grandpré, and Deepa S Pureswaran. 2021. “Improved Performance of the Eastern Spruce Budworm on Black Spruce as Warming Temperatures Disrupt Phenological Defences.” *Global Change Biology* 27 (14): 3358–66.

Bentz, Barbara J, Jacques Régnière, Christopher J Fettig, E Matthew Hansen, Jane L Hayes, Jeffrey A Hicke, Rick G Kelsey, Jose F Negrón, and Steven J Seybold. 2010. “Climate Change and Bark Beetles of the Western United States and Canada: Direct and Indirect Effects.” *BioScience* 60 (8): 602–13.

Berchtold, André, and Adrian Raftery. 2002. “The mixture transition distribution model for high-order Markov chains and non-Gaussian time series.” *Statistical Science* 17 (3): 328–56. https://doi.org/10.1214/ss/1042727943.

Berguet, Cassy, Maxence Martin, Dominique Arseneault, and Hubert Morin. 2021. “Spatiotemporal Dynamics of 20th-Century Spruce Budworm Outbreaks in Eastern Canada: Three Distinct Patterns of Outbreak Severity.” *Frontiers in Ecology and Evolution* 8: 544088.

Black, Emily Nicole, Deepa S Pureswaran, and Katie Elizabeth Marshall. 2024. “Temperature Fluctuations Influence Predictions of Landscape-Scale Patterns of Spruce Budworm Defoliation.” *bioRxiv*, 2024–08.

Blais, Jean R. 1983. “Trends in the Frequency, Extent, and Severity of Spruce Budworm Outbreaks in Eastern Canada.” *Canadian Journal of Forest Research* 13 (4): 539–47.

Boakye, Emmanuel Amoah, Daniel Houle, Yves Bergeron, Martin P Girardin, and Igor Drobyshev. 2022. “Insect Defoliation Modulates Influence of Climate on the Growth of Tree Species in the Boreal Mixed Forests of Eastern Canada.” *Ecology and Evolution* 12 (3): e8656.

Bouchard, Mathieu, and Isabelle Auger. 2014. “Influence of Environmental Factors and Spatio-Temporal Covariates During the Initial Development of a Spruce Budworm Outbreak.” *Landscape Ecology* 29 (1): 111–26.

Bouchard, Mathieu, Daniel Kneeshaw, and Yves Bergeron. 2006. “Forest Dynamics After Successive Spruce Budworm Outbreaks in Mixedwood Forests.” *Ecology* 87 (9): 2319–29.

Bouchard, Mathieu, Jacques Régnière, and Pierre Therrien. 2018a. “Bottom-up Factors Contribute to Large-Scale Synchrony in Spruce Budworm Populations.” *Canadian Journal of Forest Research* 48 (3): 277–84.

Bouchard, Mathieu, Jacques Régnière, and Pierre Therrien. 2018b. “Bottom-up Factors Contribute to Large-Scale Synchrony in Spruce Budworm Populations.” *Canadian Journal of Forest Research* 48 (3): 277–84.

Boucher, Dominique, Yan Boulanger, Isabelle Aubin, Pierre Y Bernier, André Beaudoin, Luc Guindon, and Sylvie Gauthier. 2018. “Current and Projected Cumulative Impacts of Fire, Drought, and Insects on Timber Volumes Across Canada.” *Ecological Applications* 28 (5): 1245–59.

Boulanger, Yan, and Dominique Arseneault. 2004. “Spruce Budworm Outbreaks in Eastern Quebec over the Last 450 Years.” *Canadian Journal of Forest Research* 34 (5): 1035–43.

Boulanger, Yan, Adèle Desaint, Véronique Martel, Maryse Marchand, Salomon Massoda Tonye, Rémi Saint-Amant, and Jacques Régnière. 2025. “Recent Climate Change Strongly Impacted the Population Dynamic of a North American Insect Pest Species.” *PLOS Climate* 4 (2): e0000488.

Boulanger, Yan, Frédéric Fabry, Alamelu Kilambi, Deepa S Pureswaran, Brian R Sturtevant, and Rémi Saint-Amant. 2017. “The Use of Weather Surveillance Radar and High-Resolution Three Dimensional Weather Data to Monitor a Spruce Budworm Mass Exodus Flight.” *Agricultural and Forest Meteorology* 234: 127–35.

Boulanger, Yan, and Jesus Pascual Puigdevall. 2021. “Boreal Forests Will Be More Severely Affected by Projected Anthropogenic Climate Forcing Than Mixedwood and Northern Hardwood Forests in Eastern Canada.” *Landscape Ecology* 36: 1725–40.

Boulanger, Yan, Anthony R Taylor, David T Price, Dominic Cyr, Elizabeth McGarrigle, Werner Rammer, Guillaume Sainte-Marie, André Beaudoin, Luc Guindon, and Nicolas Mansuy. 2017. “Climate Change Impacts on Forest Landscapes Along the Canadian Southern Boreal Forest Transition Zone.” *Landscape Ecology* 32: 1415–31.

Brandt, James P, MD Flannigan, DG Maynard, Ian D Thompson, and WJA Volney. 2013. “An Introduction to Canada’s Boreal Zone: Ecosystem Processes, Health, Sustainability, and Environmental Issues.” *Environmental Reviews* 21 (4): 207–26.

Braziunas, Kristin H, Werner Rammer, Pieter De Frenne, Joan Díaz-Calafat, Per-Ola Hedwall, Cornelius Senf, Dominik Thom, Florian Zellweger, and Rupert Seidl. 2025. “Microclimate Temperature Effects Propagate Across Scales in Forest Ecosystems.” *Landscape Ecology* 40 (2): 37.

Brockerhoff, Eckehard G, Luc Barbaro, Bastien Castagneyrol, David I Forrester, Barry Gardiner, José Ramón González-Olabarria, Phil O’B Lyver, et al. 2017. “Forest Biodiversity, Ecosystem Functioning and the Provision of Ecosystem Services.” *Biodiversity and Conservation*. Springer.

Byrd, Richard H, Peihuang Lu, Jorge Nocedal, and Ciyou Zhu. 1995. “A Limited Memory Algorithm for Bound Constrained Optimization.” *SIAM Journal on Scientific Computing* 16 (5): 1190–1208.

Candau, Jean-Noël, and Richard A Fleming. 2005. “Landscape-Scale Spatial Distribution of Spruce Budworm Defoliation in Relation to Bioclimatic Conditions.” *Canadian Journal of Forest Research* 35 (9): 2218–32.

Candau, Jean-Noël, and Richard A Fleming. 2011a. “Forecasting the Response of Spruce Budworm Defoliation to Climate Change in Ontario.” *Canadian Journal of Forest Research* 41 (10): 1948–60.

Candau, Jean-Noël, and Richard A. Fleming. 2011b. “Forecasting the Response of Spruce Budworm Defoliation to Climate Change in Ontario.” *Canadian Journal of Forest Research* 41 (10): 1948–60. https://doi.org/10.1139/x11-134.

Candau, Jean-Noël, Richard A Fleming, and Xianli Wang. 2018. “Ecoregional Patterns of Spruce Budworm—Wildfire Interactions in Central Canada’s Forests.” *Forests* 9 (3): 137.

Chagnon, Catherine, Mathieu Bouchard, and David Pothier. 2022. “Impacts of Spruce Budworm Defoliation on the Habitat of Woodland Caribou, Moose, and Their Main Predators.” *Ecology and Evolution* 12 (3): e8695.

Chang, Wei-Yew, Van A Lantz, Chris R Hennigar, and David A MacLean. 2012a. “Benefit-Cost Analysis of Spruce Budworm (Choristoneura Fumiferana Clem.) Control: Incorporating Market and Non-Market Values.” *Journal of Environmental Management* 93 (1): 104–12.

Chang, Wei-Yew, Van A Lantz, Chris R Hennigar, and David A MacLean. 2012b. “Economic Impacts of Forest Pests: A Case Study of Spruce Budworm Outbreaks and Control in New Brunswick, Canada.” *Canadian Journal of Forest Research* 42 (3): 490–505.

Chavardès, Raphaël D, Fabio Gennaretti, Pierre Grondin, Xavier Cavard, Hubert Morin, and Yves Bergeron. 2021. “Role of Mixed-Species Stands in Attenuating the Vulnerability of Boreal Forests to Climate Change and Insect Epidemics.” *Frontiers in Plant Science* 12: 658880.

Chen, Cen, Parinaz Rahimzadeh-Bajgiran, and Aaron Weiskittel. 2021. “Assessing Spatial and Temporal Dynamics of a Spruce Budworm Outbreak Across the Complex Forested Landscape of Maine, USA.” *Annals of Forest Science* 78 (2): 33.

Chen, Cen, Aaron Weiskittel, Mohammad Bataineh, and David A MacLean. 2017a. “Evaluating the Influence of Varying Levels of Spruce Budworm Defoliation on Annualized Individual Tree Growth and Mortality in Maine, USA and New Brunswick, Canada.” *Forest Ecology and Management* 396: 184–94.

Chen, Cen, Aaron Weiskittel, Mohammad Bataineh, and David A. MacLean. 2017b. “Even Low Levels of Spruce Budworm Defoliation Affect Mortality and Ingrowth but Net Growth Is More Driven by Competition.” *Canadian Journal of Forest Research* 47 (11): 1546–56. https://doi.org/10.1139/cjfr-2017-0012.

Cooke, Barry J. 2022. “Forest Landscape Effects on Dispersal of Spruce Budworm Choristoneura Fumiferana (Clemens, 1865)(lepidoptera, Tortricidae) and Forest Tent Caterpillar Malacosoma Disstria hübner, 1820 (Lepidoptera, Lasiocampidae) Female Moths in Alberta, Canada.” *Insects* 13 (11): 1013.

Cooke, Barry J. 2024. “On the Characterization of Patterning in Spruce Budworm Time-Series Data.” *Canadian Journal of Forest Research*.

Cox, David R, Gudmundur Gudmundsson, Georg Lindgren, Lennart Bondesson, Erik Harsaae, Petter Laake, Katarina Juselius, and Steffen L Lauritzen. 1981. “Statistical Analysis of Time Series: Some Recent Developments [with Discussion and Reply].” *Scandinavian Journal of Statistics*, 93–115.

Crozier, Lisa, and Greg Dwyer. 2006. “Combining Population-Dynamic and Ecophysiological Models to Predict Climate-Induced Insect Range Shifts.” *The American Naturalist* 167 (6): 853–66.

D’Amato, Anthony W, Brian J Palik, Patricia Raymond, Klaus J Puettmann, and Miguel Montoro Girona. 2023. “Building a Framework for Adaptive Silviculture Under Global Change.” In *Boreal Forests in the Face of Climate Change: Sustainable Management*, 359–81. Springer.

D’orangeville, L, Louis Duchesne, Daniel Houle, Daniel Kneeshaw, Benoît Côté, and Neil Pederson. 2016. “Northeastern North America as a Potential Refugium for Boreal Forests in a Warming Climate.” *Science* 352 (6292): 1452–55.

Dale, Virginia H, Linda A Joyce, Steve McNulty, Ronald P Neilson, Matthew P Ayres, Michael D Flannigan, Paul J Hanson, et al. 2001. “Climate Change and Forest Disturbances: Climate Change Can Affect Forests by Altering the Frequency, Intensity, Duration, and Timing of Fire, Drought, Introduced Species, Insect and Pathogen Outbreaks, Hurricanes, Windstorms, Ice Storms, or Landslides.” *BioScience* 51 (9): 723–34.

Davis, Richard A, Scott H Holan, Robert Lund, and Nalini Ravishanker. 2016. *Handbook of Discrete-Valued Time Series*. CRC Press.

De Grandpré, Louis, Daniel D Kneeshaw, Sophie Perigon, Dominique Boucher, Maryse Marchand, Deepa Pureswaran, and Martin P Girardin. 2019. “Adverse Climatic Periods Precede and Amplify Defoliator-Induced Tree Mortality in Eastern Boreal North America.” *Journal of Ecology* 107 (1): 452–67.

De Grandpré, Louis, Kaysandra Waldron, Mathieu Bouchard, Sylvie Gauthier, Marilou Beaudet, Jean-Claude Ruel, Christian Hébert, and Daniel D. Kneeshaw. 2018. “Incorporating Insect and Wind Disturbances in a Natural Disturbance-Based Management Framework for the Boreal Forest.” *Forests*.

Debaly, Zinsou Max, Philippe Marchand, and Miguel Montoro Girona. 2022. “Autoregressive Models for Time Series of Random Sums of Positive Variables: Application to Tree Growth as a Function of Climate and Insect Outbreak.” *Ecological Modelling* 471: 110053. https://doi.org/10.1016/j.ecolmodel.2022.110053.

Debaly, Zinsou-Max, and Lionel Truquet. 2023. “Multivariate Time Series Models for Mixed Data.” *Bernoulli* 29 (1): 669–95.

Delisle, Johanne, Michèle Bernier-Cardou, and Alain Labrecque. 2022. “Cold Tolerance and Winter Survival of Seasonally-Acclimatised Second-Instar Larvae of the Spruce Budworm, Choristoneura Fumiferana.” *Ecological Entomology* 47 (4): 553–65.

Deslauriers, Annie, Marie-Pier Fournier, Fabrizio Cartenì, and John Mackay. 2019. “Phenological Shifts in Conifer Species Stressed by Spruce Budworm Defoliation.” *Tree Physiology* 39 (4): 590–605.

Despland, Emma, Maria Gundersen, Simon P Daoust, Brian J Mader, Nathalie Delvas, Paul J Albert, and Eric Bauce. 2011. “Taste Receptor Activity and Feeding Behaviour Reveal Mechanisms of White Spruce Natural Resistance to Eastern Spruce Budworm Choristoneura Fumiferana.” *Physiological Entomology* 36 (1): 39–46.

Doran, Olivia, David A MacLean, and John A Kershaw. 2017. “Needle Longevity of Balsam Fir Is Increased by Defoliation by Spruce Budworm.” *Trees* 31: 1933–44.

Dudek, Andrzej. 2020. “Silhouette Index as Clustering Evaluation Tool.” In *Classification and Data Analysis: Theory and Applications 28*, 19–33. Springer.

Dwyer, Greg, Jonathan Dushoff, and Susan Harrell Yee. 2004. “The Combined Effects of Pathogens and Predators on Insect Outbreaks.” *Nature* 430 (6997): 341–45.

Eickenscheidt, N, NH Augustin, and N Wellbrock. 2019. “Spatio-Temporal Modelling of Forest Monitoring Data: Modelling German Tree Defoliation Data Collected Between 1989 and 2015 for Trend Estimation and Survey Grid Examination Using GAMMs.” *iForest-Biogeosciences and Forestry* 12 (4): 338.

Eveleigh, Eldon S, and Rob C Johns. 2014. “Intratree Variation in the Seasonal Distribution and Mortality of Spruce Budworm (Lepidoptera: Tortricidae) from the Peak to Collapse of an Outbreak.” *Annals of the Entomological Society of America* 107 (2): 435–44.

Ferland, René, Alain Latour, and Driss Oraichi. 2006. “Integer-Valued GARCH Process.” *Journal of Time Series Analysis* 27 (6): 923–42.

Fierravanti, Angelo, Claudia Cocozza, Caterina Palombo, Sergio Rossi, Annie Deslauriers, and Roberto Tognetti. 2015. “Environmental-Mediated Relationships Between Tree Growth of Black Spruce and Abundance of Spruce Budworm Along a Latitudinal Transect in Quebec, Canada.” *Agricultural and Forest Meteorology* 213: 53–63.

Fierravanti, Angelo, S. Rossi, D. Kneeshaw, L. De Grandpré, and A. Deslauriers. 2019. “Low Non-Structural Carbon Accumulation in Spring Reduces Growth and Increases Mortality in Conifers Defoliated by Spruce Budworm.” *Frontiers in Forests and Global Change*. https://doi.org/10.3389/ffgc.2019.00015.

Flower, A, DG Gavin, EK Heyerdahl, RA Parsons, and GM Cohn. 2014. “Drought-Triggered Western Spruce Budworm Outbreaks in the Interior Pacific Northwest: A Multi-Century Dendrochronological Record.” *Forest Ecology and Management* 324: 16–27.

Fokianos, Konstantinos, and Benjamin Kedem. 2003. “Regression Theory for Categorical Time Series.” *Statistical Science* 18 (3): 357–76.

Fokianos, Konstantinos, Bard Stove, Dag Tjostheim, and Paul Doukhan. 2020. “Multivariate Count Autoregression.” *Bernoulli*.

Fokianos, Konstantinos, and Dag Tjøstheim. 2012. “Nonlinear Poisson Autoregression.” *Annals of the Institute of Statistical Mathematics* 64 (6): 1205–25.

Fortin, Mathieu, Jean-François Lavoie, Jacques Régnière, and Rémi Saint-Amant. 2022. “A Web API for Weather Generation and Pest Development Simulation in North America.” *Environmental Modelling & Software* 157: 105476. https://doi.org/10.1016/j.envsoft.2022.105476.

Francq, Christian, and Jean-Michel Zakoian. 2019. “Estimating GARCH Models by Quasi-Maximum Likelihood.” In *GARCH Models: Structure, Statistical Inference and*

Financial Applications, 175–215. John Wiley & Sons, Ltd. https://doi.org/10.1002/9781119313472.ch7.

Frelich, Lee E, Jill Johnstone, and Timo Kuuluvainen. 2024. “Boreal Forests.” In *Future Forests*, 221–42. Elsevier.

Fuentealba, A, and É Bauce. 2012. “Carry-over Effect of Host Nutritional Quality on Performance of Spruce Budworm Progeny.” *Bulletin of Entomological Research* 102 (3): 275–84.

Fuentealba, Alvaro, Alain Dupont, Roberto Quezada-Garcia, and Eric Bauce. 2022. “Efficacy of Insecticide Aerial Spraying Programs to Reduce Tree Mortality During a Spruce Budworm Outbreak (1967–1992) in the Province of Quebec.” *Agricultural and Forest Entomology* 24 (4): 586–99. https://doi.org/https://doi.org/10.1111/afe.12523.

Fuentealba, Alvaro, Deepa Pureswaran, Éric Bauce, and Emma Despland. 2017. “How Does Synchrony with Host Plant Affect the Performance of an Outbreaking Insect Defoliator?” *Oecologia* 184: 847–57.

Gauthier, Sylvie, Pierre Bernier, Timo Kuuluvainen, Anatoly Z Shvidenko, and Dmitry G Schepaschenko. 2015. “Boreal Forest Health and Global Change.” *Science* 349 (6250): 819–22.

Gauthier, Sylvie, Louis De Grandpré, and Yves Bergeron. 2000. “Differences in Forest Composition in Two Boreal Forest Ecoregions of Quebec.” *Journal of Vegetation Science* 11 (6): 781–90.

Gauthier, Sylvie, Timo Kuuluvainen, S Ellen Macdonald, Ekaterina Shorohova, Anatoly Shvidenko, Annie-Claude Bélisle, Marie-Andrée Vaillancourt, et al. 2023. “Ecosystem Management of the Boreal Forest in the Era of Global Change.” In *Boreal Forests in the Face of Climate Change: Sustainable Management*, 3–49. Springer.

Germain, Marion, Daniel Kneeshaw, Louis De Grandpré, Mélanie Desrochers, Patrick James, Udayalakshmi Vepakomma, Jean-François Poulin, and Marc-André Villard. 2021. “Insectivorous Songbirds as Early Indicators of Future Defoliation by Spruce Budworm.” *Landscape Ecology* 36 (10): 3013–27.

Girardin, Martin P, Edward H Hogg, Pierre Y Bernier, Werner A Kurz, Xiao Jing Guo, and Guillaume Cyr. 2016. “Negative Impacts of High Temperatures on Growth of Black Spruce Forests Intensify with the Anticipated Climate Warming.” *Global Change Biology* 22 (2): 627–43.

Girona, Miguel Montoro, Tuomas Aakala, Núria Aquilué, Annie-Claude Bélisle, Emeline Chaste, Victor Danneyrolles, Olalla Díaz-Yáñez, et al. 2023. “Challenges for the Sustainable Management of the Boreal Forest Under Climate Change.” In *Boreal Forests in the Face of Climate Change: Sustainable Management*, 773–837. Springer.

Goodhue, Joseph, Sarah Ervin, John Reese Hatheway, Jie Ren, et al. 2017. “Cockroaches’ Increasing Metabolic Rate with Rising Temperatures.” *Journal of Introductory Biology Investigations* 6 (1).

Goodsell, Robert M, Dylan Z Childs, Matthew Spencer, Shaun Coutts, Remi Vergnon, Tom Swinfield, Simon A Queenborough, and Robert P Freckleton. 2021. “Developing Hierarchical Density-Structured Models to Study the National-Scale Dynamics of an Arable Weed.” *Ecological Monographs* 91 (3): e01449.

Gray, David R. 2013. “The Influence of Forest Composition and Climate on Outbreak Characteristics of the Spruce Budworm in Eastern Canada.” *Canadian Journal of Forest Research* 43 (12): 1181–95.

Grondin, P, C Ansseau, L Bélanger, JF Bergeron, Y Bergeron, A Bouchard, J Brisson, et al. 1996. “Écologie Forestière.” *Manuel de Foresterie*, 133–279.

Hance, Thierry, Joan van Baaren, Philippe Vernon, and Guy Boivin. 2007. “Impact of Extreme Temperatures on Parasitoids in a Climate Change Perspective.” *Annu. Rev. Entomol.* 52 (1): 107–26.

Hansen, Matthew C, Stephen V Stehman, and Peter V Potapov. 2010. “Quantification of Global Gross Forest Cover Loss.” *Proceedings of the National Academy of Sciences* 107 (19): 8650–55.

Hassell, DC, DJ Allwright, and AC Fowler. 1999. “A Mathematical Analysis of Jones’s Site Model for Spruce Budworm Infestations.” *Journal of Mathematical Biology* 38: 377–421.

Hastie, Trevor J. 2017. “Generalized Additive Models.” In *Statistical Models in s*, 249–307. Routledge.

Hastie, Trevor, Robert Tibshirani, and Jerome Friedman. 2009. “The Elements of Statistical Learning.” *Cited on* 33.

Hayes, Matthew B, Lihong Jiao, Tsu-hsuan Tsao, Ian King, Michael Jennings, and Chen Hou. 2015. “High Temperature Slows down Growth in Tobacco Hornworms (Manduca Sexta Larvae) Under Food Restriction.” *Insect Science* 22 (3): 424–30.

Haynes, Kyle J, Andrew M Liebhold, Jonathan S Lefcheck, Randall S Morin, and Guiming Wang. 2022. “Climate Affects the Outbreaks of a Forest Defoliator Indirectly Through Its Tree Hosts.” *Oecologia* 198 (2): 407–18.

Hébert, Christian, and Conrad Cloutier. 1990. “Temperature-Dependent Development of Eggs and Larvae of *Winthemia Fumiferanae* Toth.(diptera: Tachinidae), a Larval–Pupal Parasitoid of the Spruce Budworm (Lepidoptera: Tortricidae).” *The Canadian Entomologist* 122 (2): 329–41.

Hennigar, Chris R, and David A MacLean. 2010. “Spruce Budworm and Management Effects on Forest and Wood Product Carbon for an Intensively Managed Forest.” *Canadian Journal of Forest Research* 40 (9): 1736–50.

Heyde, C. C. 2013. *Quasi-Likelihood and Its Application: A General Approach to Optimal Parameter Estimation*. Springer Series in Statistics. Springer New York. https://books.google.fr/books?id=MhzVnQEACAAJ.

Hof, Anouschka R, Miguel Montoro Girona, Marie-Josée Fortin, and Junior A Tremblay. 2021. “Using Landscape Simulation Models to Help Balance Conflicting Goals in Changing Forests.” *Frontiers in Ecology and Evolution*. Frontiers Media SA.

Houndode, Djidjoho Julien, Cornelia Krause, and Hubert Morin. 2021. “Predicting Balsam Fir Mortality in Boreal Stands Affected by Spruce Budworm.” *Forest Ecology and Management* 496: 119408.

Howe, Michael, Sarah J Hart, and Amy M Trowbridge. 2024. “Budworms, Beetles and Wildfire: Disturbance Interactions Influence the Likelihood of Insect-Caused Disturbances at a Subcontinental Scale.” *Journal of Ecology* 112 (11): 2567–84.

Jacobs, Patricia A, and Peter AW Lewis. 1978. “Discrete Time Series Generated by Mixtures. I: Correlational and Runs Properties.” *Journal of the Royal Statistical Society: Series B (Methodological)* 40 (1): 94–105.

Jactel, Hervé, Julia Koricheva, and Bastien Castagneyrol. 2019. “Responses of Forest Insect Pests to Climate Change: Not so Simple.” *Current Opinion in Insect Science* 35: 103–8.

Jahn, Malte, and Christian H Weiß. 2024. “Nonlinear GARCH-Type Models for Ordinal Time Series.” *Stochastic Environmental Research and Risk Assessment* 38 (2): 637–49.

James, Patrick MA, M-J Fortin, BR Sturtevant, A Fall, and D Kneeshaw. 2011. “Modelling Spatial Interactions Among Fire, Spruce Budworm, and Logging in the Boreal Forest.” *Ecosystems* 14: 60–75.

Jamieson, Mary A, Ezra G Schwartzberg, Kenneth F Raffa, Peter B Reich, and Richard L Lindroth. 2015. “Experimental Climate Warming Alters Aspen and Birch Phytochemistry and Performance Traits for an Outbreak Insect Herbivore.” *Global Change Biology* 21 (7): 2698–2710.

Jardon, Yves, Hubert Morin, and Pierre Dutilleul. 2003. “Périodicité Et Synchronisme Des épidémies de La Tordeuse Des Bourgeons de l’épinette Au Québec.” *Canadian Journal of Forest Research* 33 (10): 1947–61.

Jennings, Daniel T, Mark W Houseweart, and John B Dimond. 1983. “Dispersal Losses of Early-Instar Spruce Budworm (*Lepidoptera: Tortricidae*) Larvae in Strip Clearcut and Dense Spruce-Fir Forests of Maine.” *Environmental Entomology* 12 (6): 1787–92.

Jepsen, Jane U, Snorre B Hagen, Stein-Rune Karlsen, and Rolf A Ims. 2009. “Phase-Dependent Outbreak Dynamics of Geometrid Moth Linked to Host Plant Phenology.” *Proceedings of the Royal Society B: Biological Sciences* 276 (1676): 4119–28.

Kabir, M Humayun. 2021. “Reaction-Diffusion Modeling of the Spread of Spruce Budworm in Boreal Ecosystem.” *Journal of Applied Mathematics and Computing* 66 (1): 203–19.

Kassambara, Alboukadel, and Fabian Mundt. 2017. “Package ‘Factoextra’.” *Extract and Visualize the Results of Multivariate Data Analyses* 76 (2).

Kayes, Imrul, and Azim Mallik. 2020. “Boreal Forests: Distributions, Biodiversity, and Management.” *Life on Land*. Springer International Publishing.

Kneeshaw, Daniel D, Louis De Grandpré, Loïc D’Orangeville, Maryse Marchand, Jeanne Moisan-Perrier, Louis-Etienne Robert, and Mathieu Bouchard. 2022. “Forest Structure and Composition Diverge Following Harvesting Compared to a Spruce Budworm *Choristoneura Fumiferana* (Clem.) Outbreak.” *Frontiers in Forests and Global Change* 5: 680262.

Kottek, Markus, Jürgen Grieser, Christoph Beck, Bruno Rudolf, and Franz Rubel. 2006. “World Map of the köppen-Geiger Climate Classification Updated.” *Meteorologische Zeitschrift* 15 (3): 259–63.

Krause, Cornelia, and Hubert Morin. 1995. “Changes in Radial Increment in Stems and Roots of Balsam Fir [*Abies Balsamea* (l.) Mill.] After Defoliation Spruce Budworm.” *The Forestry Chronicle* 71 (6): 747–54. https://doi.org/10.5558/tfc71747-6.

Kumbasli, Meric, and Eric Bauce. 2013. “Spruce Budworm Biological and Nutritional Performance Responses to Varying Levels of Monoterpenes.” *iForest-Biogeosciences and Forestry* 6 (6): 310.

Larroque, Jeremy, Julian Wittische, and Patrick MA James. 2022. “Quantifying and Predicting Population Connectivity of an Outbreaking Forest Insect Pest.” *Landscape Ecology* 37 (3): 763–78.

Lavoie, Janie, Miguel Montoro Girona, Guillaume Grosbois, and Hubert Morin. 2021. “Does the Type of Silvicultural Practice Influence Spruce Budworm Defoliation of Seedlings?” *Ecosphere* 12 (4): e03506.

Lavoie, Janie, Miguel Montoro Girona, and Hubert Morin. 2019. “Vulnerability of Conifer Regeneration to Spruce Budworm Outbreaks in the Eastern Canadian Boreal Forest.” *Forests* 10 (10): 850.

Lemay, Audrey, Julie Barrette, and Cornelia Krause. 2022. “Balsam Fir (Abies Balsamea (l.) Mill.) Wood Quality After Defoliation by Spruce Budworm (Choristoneura Fumiferana Clem.) In the Boreal Forest of Quebec, Canada.” *Forests* 13 (11): 1926.

Li, Mingke, David A MacLean, Chris R Hennigar, and Jae Ogilvie. 2020. “Previous Year Outbreak Conditions and Spring Climate Predict Spruce Budworm Population Changes in the Following Year.” *Forest Ecology and Management* 458: 117737.

Li, Zhengjie, Zhiwei Wu, Shihao Zhu, Xiang Hou, and Shun Li. 2024. “Estimation of Understory Fine Dead Fuel Moisture Content in Subtropical Forests of Southern China Based on Landsat Images.” *Forests* 15 (11): 2002.

Liebhold, Andrew, Walter D Koenig, and Ottar N Bjørnstad. 2004. “Spatial Synchrony in Population Dynamics.” *Annu. Rev. Ecol. Evol. Syst.* 35 (1): 467–90.

Lindgren, Finn, Håvard Rue, and Johan Lindström. 2011. “An Explicit Link Between Gaussian Fields and Gaussian Markov Random Fields: The Stochastic Partial Differential Equation Approach.” *Journal of the Royal Statistical Society Series B: Statistical Methodology* 73 (4): 423–98.

Liu, Eric Ye, Van A Lantz, David A MacLean, and Chris Hennigar. 2019. “Economics of Early Intervention to Suppress a Potential Spruce Budworm Outbreak on Crown Land in New Brunswick, Canada.” *Forests* 10 (6): 481.

Liu, Mengya, Qi Li, and Fukang Zhu. 2022. “Modeling Air Quality Level with a Flexible Categorical Autoregression.” *Stochastic Environmental Research and Risk Assessment*, 1–11.

Liu, Mengya, Fukang Zhu, and Ke Zhu. 2022. “Modeling Normalcy-Dominant Ordinal Time Series: An Application to Air Quality Level.” *Journal of Time Series Analysis* 43 (3): 460–78.

Liu, Meng, and Yu Zhu. 2018. “Stability of a Budworm Growth Model with Random Perturbations.” *Applied Mathematics Letters* 79: 13–19.

Liu, Qiuyu, Changhui Peng, Robert Schneider, Dominic Cyr, Nate G McDowell, and Daniel Kneeshaw. 2023. “Drought-Induced Increase in Tree Mortality and Corresponding Decrease in the Carbon Sink Capacity of Canada’s Boreal Forests from 1970 to 2020.” *Global Change Biology* 29 (8): 2274–85.

Liu, Zelin, Changhui Peng, Louis De Grandpré, Jean-Noël Candau, Timothy Work, Chunbo Huang, and Daniel Kneeshaw. 2019. “Simulation and Analysis of the Effect of a Spruce Budworm Outbreak on Carbon Dynamics in Boreal Forests of Québec.” *Ecosystems* 22 (8): 1838–51.

Liu, Zelin, Changhui Peng, Louis De Grandpré, Jean-Noël Candau, Timothy Work, Xiaolu Zhou, and Daniel Kneeshaw. 2020. “Aerial Spraying of Bacterial Insecticides to Control Spruce Budworm Defoliation Leads to Reduced Carbon Losses.” *Ecosphere* 11 (1): e02988.

Liu, Zelin, Changhui Peng, David A MacLean, Louis De Grandpré, Jean-Noël Candau, and Daniel Kneeshaw. 2022. “Evaluating and Quantifying the Effect of Various Spruce

Budworm Intervention Strategies on Forest Carbon Dynamics in Atlantic Canada." *Forest Ecosystems* 9: 100052.

Logan, Jesse A, Jacques Régnière, and James A Powell. 2003. "Assessing the Impacts of Global Warming on Forest Pest Dynamics." *Frontiers in Ecology and the Environment* 1 (3): 130–37.

Ludwig, Donald, Dixon D Jones, Crawford S Holling, et al. 1978. "Qualitative Analysis of Insect Outbreak Systems: The Spruce Budworm and Forest." *Journal of Animal Ecology* 47 (1): 315–32.

Luo, Yong, and Han YH Chen. 2015. "Climate Change-Associated Tree Mortality Increases Without Decreasing Water Availability." *Ecology Letters* 18 (11): 1207–15.

MacCarthy, James, Jessica Richter, Sasha Tyukavina, Mikaela Weisse, and Nancy Harris. 2023. "The Latest Data Confirms: Forest Fires Are Getting Worse." *World Resources Institute* 29.

Mackey, Brendan, Carly Campbell, Patrick Norman, Sonia Hugh, Dominick A DellaSala, Jay R Malcolm, Mélanie Desrochers, and Pierre Drapeau. 2023. "Assessing the Cumulative Impacts of Forest Management on Forest Age Structure Development and Woodland Caribou Habitat in Boreal Landscapes: A Case Study from Two Canadian Provinces." *Land* 13 (1): 6.

MacLean, David A. 2016. "Impacts of Insect Outbreaks on Tree Mortality, Productivity, and Stand Development." *The Canadian Entomologist* 148 (S1): S138–59.

MacLean, David A, Joe Collier, Wayne E MacKinnon, and Kevin B Porter. 2024. "Defoliation Level Interacts with Tree Species and Soil Richness to Determine Volume Increment Reduction and Recovery from Simulated Spruce Budworm Attack." *Canadian Journal of Forest Research* 54 (10): 1155–69.

Maechler, Martin, Peter Rousseeuw, Anja Struyf, Mia Hubert, Kurt Hornik, Matthias Studer, Pierre Roudier, and Juan Gonzalez. 2013. "Package 'Cluster'." *Dosegljivo Na* 980.

Mattson, William J, Robert A Haack, Robert K Lawrence, and Scott S Slocum. 1991. "Considering the Nutritional Ecology of the Spruce Budworm in Its Management." *Forest Ecology and Management* 39: 183–210.

McNie, Pierce, Daniel Kneeshaw, and Élise Filotas. 2024. "Increased Unpredictability in Spruce Budworm Outbreaks Following Habitat Loss and Landscape Fragmentation." *Ecological Modelling* 491: 110675.

Messier, Christian C, Klaus J Puettmann, and K Dave Coates. 2013. *Managing Forests as Complex Adaptive Systems: Building Resilience to the Challenge of Global Change*. Routledge.

MFFP. 2022. “Données sur les perturbations naturelles - Insecte: Tordeuse des bourgeons de l’épinette.” https://www.donneesquebec.ca/recherche/dataset/donnees-sur-les-perturbations-naturelles-insecte-tordeuse-des-bourgeons-de-lepinette.

Moise, Eric RD, Michael B Lavigne, and Rob C Johns. 2019. “Density Has More Influence Than Drought on Spruce Budworm (*Choristoneura Fumiferana*) Performance Under Outbreak Conditions.” *Forest Ecology and Management* 433: 170–75.

Moise, Eric RD, Jamie Warren, and Joseph J Bowden. 2024. “Impacts of Winter Warming Events on Spruce Budworm: The Importance of Timing.” *Journal of Insect Science* 24 (2): 17.

Molina, Eliana, Osvaldo Valeria, Maxence Martin, Miguel Montoro Girona, and Jorge Andrés Ramirez. 2022. “Long-Term Impacts of Forest Management Practices Under Climate Change on Structure, Composition, and Fragmentation of the Canadian Boreal Landscape.” *Forests* 13 (8): 1292.

Montoro Girona, Miguel, Lionel Navarro, and Hubert Morin. 2018. “A Secret Hidden in the Sediments: Lepidoptera Scales.” *Frontiers in Ecology and Evolution* 6: 2.

Moysiadis, T., and K. Fokianos. 2014. “On Binary and Categorical Time Series Models with Feedback.” *Journal of Multivariate Analysis* 131: 209–28.

MRNF. 2022. “Ministère des Ressources naturelles et des Forêts. Données sur les perturbations naturelles - Insecte : Tordeuse des bourgeons de l’épinette.” https://www.donneesquebec.ca/recherche/dataset/donnees-sur-les-perturbations-naturelles-insecte-tordeuse-des-bourgeons-de-lepinette.

Murtagh, Fionn, and Pierre Legendre. 2014. “Ward’s Hierarchical Agglomerative Clustering Method: Which Algorithms Implement Ward’s Criterion?” *Journal of Classification* 31: 274–95.

Natcher, David C. 2001. “Land Use Research and the Duty to Consult: A Misrepresentation of the Aboriginal Landscape.” *Land Use Policy* 18 (2): 113–22.

Navarro, Lionel, Hubert Morin, Yves Bergeron, and Miguel Montoro Girona. 2018. “Changes in Spatiotemporal Patterns of 20th Century Spruce Budworm Outbreaks in Eastern Canadian Boreal Forests.” *Frontiers in Plant Science* 9: 1905.

Nealis, VG, and J Régnière. 2004. “Insect Host Relationships Influencing Disturbance by the Spruce Budworm in a Boreal Mixedwood Forest.” *Canadian Journal of Forest Research* 34 (9): 1870–82.

Nealis, Vincent, and Jacques Régnière. 2021. “Ecology of Outbreak Populations of the Western Spruce Budworm.” *Ecosphere* 12 (7): e03667.

Nenzen, Hedvig K, Elise Filotas, Pedro Peres-Neto, and Dominique Gravel. 2017. “Epidemiological Landscape Models Reproduce Cyclic Insect Outbreaks.” *Ecological Complexity* 31: 78–87.

Nenzén, Hedvig K, Pedro Peres-Neto, and Dominique Gravel. 2018. “More Than Moran: Coupling Statistical and Simulation Models to Understand How Defoliation Spread and Weather Variation Drive Insect Outbreak Dynamics.” *Canadian Journal of Forest Research* 48 (3): 255–64.

Nie, Zhuoyi, David A MacLean, and Anthony R Taylor. 2018. “Forest Overstory Composition and Seedling Height Influence Defoliation of Understory Regeneration by Spruce Budworm.” *Forest Ecology and Management* 409: 353–60.

Noor, Sabina, Zahra Gozalzadeh, Allison Pamela Yataco, Miguel Montoro Girona, and Emma Despland. 2025. “Bottom-up and Top-down Forces Regulate Spruce Budworm (Lepidoptera: Tortricidae) Biological Performance on Regenerating White Spruce.” *Forest Ecology and Management* 593: 122883.

O’Connell, Benjamin P, and Erin Wiley. 2024. “Heatwaves Do Not Limit Recovery Following Defoliation but Alter Leaf Drought Tolerance Traits.” *Plant, Cell & Environment* 47 (2): 482–96.

Osse, Olaloudé Judicaël Franck, Zinsou Max Debaly, Philippe Marchandb, and Miguel Montoro Girona. 2023. “Adjacent-Category Models for Ordinal Time Series and Their Application to Climate-Dependent Spruce Budworm Defoliation Dynamics.” *arXiv Preprint arXiv:2309.04688*.

Osse, Olaloudé Judicaël Franck, Philippe Marchand, and Miguel Montoro Girona. 2025. “Spatial Variability in Defoliation Dynamics During Spruce Budworm Outbreaks: A Landscape Perspective.” *Ecological Modelling* 510: 111337.

Overpeck, Jonathan T, David Rind, and Richard Goldberg. 1990. “Climate-Induced Changes in Forest Disturbance and Vegetation.” *Nature* 343 (6253): 51–53.

Paixao, Carlos, Cornelia Krause, Hubert Morin, and Alexis Achim. 2019. “Wood Quality of Black Spruce and Balsam Fir Trees Defoliated by Spruce Budworm: A Case Study in the Boreal Forest of Quebec, Canada.” *Forest Ecology and Management* 437: 201–10.

Pan, Yude, Richard A Birdsey, Jingyun Fang, Richard Houghton, Pekka E Kauppi, Werner A Kurz, Oliver L Phillips, et al. 2011. “A Large and Persistent Carbon Sink in the World’s Forests.” *Science* 333 (6045): 988–93.

Park, Andrew, Klaus Puettmann, Edward Wilson, Christian Messier, Susanne Kames, and Amalesh Dhar. 2014. “Can Boreal and Temperate Forest Management Be Adapted to the Uncertainties of 21st Century Climate Change?” *Critical Reviews in Plant Sciences* 33 (4): 251–85.

Pebesma, Edzer. 2018. “Simple Features for r: Standardized Support for Spatial Vector Data.” *R Journal* 10 (1).

Perrier, Jeanne Moisan, Daniel Kneeshaw, Martin-Hugues St-Laurent, Peter Pyle, and Marc-André Villard. 2021. “Budworm-Linked Warblers as Early Indicators of Defoliation by Spruce Budworm: A Field Study.” *Ecological Indicators* 125: 107543.

Ponder, BM, LR Kipp, C Bergh, GC Lonergan, and WD Seabrook. 1986. “Factors Affecting Spruce Budworm (*Choristoneura Fumiferana*)(clem.) Mating and Mating Disruption with Pheromone in the Laboratory.” *The Canadian Entomologist* 118 (8): 797–805.

Portalier, SMJ, J-N Candau, and F Lutscher. 2024. “Larval Mortality from Phenological Mismatch Can Affect Outbreak Frequency and Severity of a Boreal Forest Defoliator.” *Ecological Modelling* 493: 110724.

Pureswaran, Deepa S, Louis De Grandpré, David Paré, Anthony Taylor, Martin Barrette, Hubert Morin, Jacques Régnière, and Daniel D Kneeshaw. 2015. “Climate-Induced Changes in Host Tree–Insect Phenology May Drive Ecological State-Shift in Boreal Forests.” *Ecology* 96 (6): 1480–91.

Pureswaran, Deepa S, Mathieu Neau, Maryse Marchand, Louis De Grandpré, and Dan Kneeshaw. 2019. “Phenological Synchrony Between Eastern Spruce Budworm and Its Host Trees Increases with Warmer Temperatures in the Boreal Forest.” *Ecology and Evolution* 9 (1): 576–86.

Pureswaran, Deepa S, Alain Roques, and Andrea Battisti. 2018. “Forest Insects and Climate Change.” *Current Forestry Reports* 4: 35–50.

R Core Team. 2022. *R: A Language and Environment for Statistical Computing*. Vienna, Austria: R Foundation for Statistical Computing.

Ramachandran, R. 1987. “Influence of Host-Plants on the Wind Dispersal and the Survival of an Australian Geometrid Caterpillar.” *Entomologia Experimentalis Et Applicata* 44 (3): 289–94.

Ranta, Esa, Veijo Kaitala, Jan Lindström, and Harto Linden. 1995. “Synchrony in Population Dynamics.” *Proceedings of the Royal Society of London. Series B: Biological Sciences* 262 (1364): 113–18.

Raymond, Patricia, Magnus Löf, Phil Comeau, Lars Rytter, Miguel Montoro Girona, and Klaus J Puettmann. 2023. “Silviculture of Mixed-Species and Structurally Complex Boreal Stands.” In *Boreal Forests in the Face of Climate Change: Sustainable Management*, 403–16. Springer.

Régnière, Jacques, Johanne Delisle, Brian R Sturtevant, Matthew Garcia, and Rémi Saint-Amant. 2019. “Modeling Migratory Flight in the Spruce Budworm: Temperature Constraints.” *Forests* 10 (9): 802.

Régnière, Jacques, and Vincent G Nealis. 2019a. “Density Dependence of Egg Recruitment and Moth Dispersal in Spruce Budworms.” *Forests* 10 (8): 706.

Régnière, Jacques, and Vincent G Nealis. 2019b. “Influence of Temperature on Historic and Future Population Fitness of the Western Spruce Budworm, Choristoneura Occidentalis.” *International Journal of Pest Management* 65 (3): 228–43.

Régnière, Jacques, James Powell, Barbara Bentz, and Vincent Nealis. 2012. “Effects of Temperature on Development, Survival and Reproduction of Insects: Experimental Design, Data Analysis and Modeling.” *Journal of Insect Physiology* 58 (5): 634–47.

Régnière, Jacques, M Lukas Seehausen, and Véronique Martel. 2020. “Modeling Climatic Influences on Three Parasitoids of Low-Density Spruce Budworm Populations. Part 1: *Tranosema Rostrale* (Hymenoptera: Ichneumonidae).” *Forests* 11 (8): 846.

Régnière, Jacques, Rémi St-Amant, and Pierre Duval. 2012. “Predicting Insect Distributions Under Climate Change from Physiological Responses: Spruce Budworm as an Example.” *Biological Invasions* 14: 1571–86.

Régnière, J, and VG Nealis. 2007. “Ecological Mechanisms of Population Change During Outbreaks of the Spruce Budworm.” *Ecological Entomology* 32 (5): 461–77.

Reichenbach, Norman G, and Gordon R Stairs. 1985. “Bioenergetics of the Western Spruce Budworm (Lepidoptera: Tortricidae) with Comments on Endotherm and Ectotherm Population Energetics.” *Canadian Journal of Zoology* 63 (6): 1330–38.

Ren, Ping, Valérie Néron, Sergio Rossi, Eryuan Liang, Mathieu Bouchard, and Annie Deslauriers. 2020. “Warming Counteracts Defoliation-Induced Mismatch by Increasing Herbivore-Plant Phenological Synchrony.” *Global Change Biology* 26 (4): 2072–80.

Rhainds, Marc, and Stephen B Heard. 2015. “Sampling Procedures and Adult Sex Ratios in Spruce Budworm.” *Entomologia Experimentalis Et Applicata* 154 (2): 91–101.

Rose, AH, and JR Blais. 1954. “A Relation Between April and May Temperatures and Spruce Budworm Larval Emergence1.” *The Canadian Entomologist* 86 (4): 174–77.

Royama, T. 1984. “Population Dynamics of the Spruce Budworm Choristoneura Fumiferana.” *Ecological Monographs* 54 (4): 429–62.

Royama, T, WE MacKinnon, EG Kettela, NE Carter, and LK Hartling. 2005. “Analysis of Spruce Budworm Outbreak Cycles in New Brunswick, Canada, Since 1952.” *Ecology* 86 (5): 1212–24.

Safranyik, L, Allan L Carroll, J Régnière, DW Langor, WG Riel, TL Shore, BJCB Peter, BJ Cooke, VG Nealis, and SW Taylor. 2010. “Potential for Range Expansion of

Mountain Pine Beetle into the Boreal Forest of North America." *The Canadian Entomologist* 142 (5): 415–42.

Salisbury, F. B., P. F. Wareing, and A. W. Galston. 2013. *The Flowering Process*. Elsevier Science.

Sato, Hiromitsu, Emeline Chaste, Martin P Girardin, Jed O Kaplan, Christelle Hély, Jean-Noël Candau, and Stephen J Mayor. 2023. "Dynamically Simulating Spruce Budworm in Eastern Canada and Its Interactions with Wildfire." *Ecological Modelling* 483: 110412.

Sattler, Derek F, and Valerie LeMay. 2011. "A System of Nonlinear Simultaneous Equations for Crown Length and Crown Radius for the Forest Dynamics Model SORTIE-ND." *Canadian Journal of Forest Research* 41 (8): 1567–76.

Saucier, Jean-Pierre, Jocelyn Gosselin, Claude Morneau, and Pierre Grondin. 2010. "Utilisation de La Classification de La végétation Dans l'aménagement Forestier Au Québec." *Revue Forestière Française* 62 (3-4): 428–38.

Schowalter, Timothy D. 2022. *Insect Ecology: An Ecosystem Approach*. Academic Press.

Scott, Lisa N, Sean M Smith, John S Gunn, Marek Petrik, Mark J Ducey, Thomas S Buchholz, and Ethan P Belair. 2023. "Salvage Decision-Making Based on Carbon Following an Eastern Spruce Budworm Outbreak." *Frontiers in Forests and Global Change* 6: 1062176.

Seehausen, M Lukas, Éric Bauce, Jacques Régnière, and Richard Berthiaume. 2014. "Influence of Partial Cutting on Parasitism of Endemic Spruce Budworm (Lepidoptera: Tortricidae) Populations." *Environmental Entomology* 43 (3): 626–31.

Seehausen, M Lukas, Jacques Régnière, Véronique Martel, and Sandy M Smith. 2017. "Developmental and Reproductive Responses of the Spruce Budworm (Lepidoptera: Tortricidae) Parasitoid *Tranosema Rostrale* (Hymenoptera: Ichneumonidae) to Temperature." *Journal of Insect Physiology* 98: 38–46.

Seidl, Rupert, Marie-Josée Fortin, Juha Honkaniemi, and Melissa Lucash. 2023. "Modeling Natural Disturbances in Boreal Forests." In *Boreal Forests in the Face of Climate Change: Sustainable Management*, 591–612. Springer.

Seidl, Rupert, Juha Honkaniemi, Tuomas Aakala, Alexey Aleinikov, Per Angelstam, Mathieu Bouchard, Yan Boulanger, et al. 2020. "Globally Consistent Climate Sensitivity of Natural Disturbances Across Boreal and Temperate Forest Ecosystems." *Ecography* 43 (7): 967–78.

Seidl, Rupert, Dominik Thom, Markus Kautz, Dario Martin-Benito, Mikko Peltoniemi, Giorgio Vacchiano, Jan Wild, et al. 2017. "Forest Disturbances Under Climate Change." *Nature Climate Change* 7 (6): 395–402.

Shalev-Shwartz, Shai, and Shai Ben-David. 2014. *Understanding Machine Learning: From Theory to Algorithms*. Cambridge University Press.

Sidhu, HK, KA Kidd, EJS Emilson, M Stastny, L Venier, BW Kielstra, and CPR McCarter. 2024. “Increasing Spruce Budworm Defoliation Increases Catchment Discharge in Conifer Forests.” *Science of the Total Environment* 912: 168561.

Sigrist, Fabio, Hans R Künsch, and Werner A Stahel. 2015. “Stochastic Partial Differential Equation Based Modelling of Large Space–Time Data Sets.” *Journal of the Royal Statistical Society Series B: Statistical Methodology* 77 (1): 3–33.

Simard, Isabelle, Hubert Morin, and Claude Lavoie. 2006. “A Millennial-Scale Reconstruction of Spruce Budworm Abundance in Saguenay, Quéebec, Canada.” *The Holocene* 16 (1): 31–37.

Smith, SM, M Hubbes, and JR Carrow. 1986. “Factors Affecting Inundative Releases of *Trichogramma Minutum* Ril. Against the Spruce Budworm 1.” *Journal of Applied Entomology* 101 (1-5): 29–39.

Song, Jianxiang, Jiafu Liu, Xinyue Zhang, Xin Chen, Yingtao Shang, and Fengjie Gao. 2024. “Spatio-Temporal Fluctuation Analysis of Ecosystem Service Values in Northeast China over Long Time Series: Based on Bayesian Hierarchical Modeling.” *Land* 13 (6): 833.

Soti, Valérie, Ibrahima Thiaw, Zinsou Max Debaly, Ahmadou Sow, Mously Diaw, Souleymane Fofana, Mouhamadou Diakhate, Cheikh Thiaw, and Thierry Brévault. 2019. “Effect of Landscape Diversity and Crop Management on the Control of the Millet Head Miner, *Heliocheilus Albipunctella* (Lepidoptera: Noctuidae) by Natural Enemies.” *Biological Control* 129: 115–22.

Stahle, Lars, Svante Wold, et al. 1989. “Analysis of Variance (ANOVA).” *Chemometrics and Intelligent Laboratory Systems* 6 (4): 259–72.

Sturtevant, Brian R, Barry J Cooke, Daniel D Kneeshaw, and David A MacLean. 2015. “Modeling Insect Disturbance Across Forested Landscapes: Insights from the Spruce Budworm.” In *Simulation Modeling of Forest Landscape Disturbances*, 93–134. Springer.

Subedi, Anoj, Philippe Marchand, Yves Bergeron, Hubert Morin, and Miguel Montoro Girona. 2023. “Climatic Conditions Modulate the Effect of Spruce Budworm Outbreaks on Black Spruce Growth.” *Agricultural and Forest Meteorology* 339: 109548.

Tai, Amberly R, and Allan L Carroll. 2022. “In the Pursuit of Synchrony: Northward Shifts in Western Spruce Budworm Outbreaks in a Warming Environment.” *Frontiers in Forests and Global Change* 5: 895579.

Thiffault, Nelson, Pierre Grondin, Jean Noël, and Véronique Poirier. 2015. “Ecological Gradients Driving the Distribution of Four Ericaceae in Boreal Quebec, Canada.” *Ecology and Evolution* 5 (9): 1837–53.

Tiné, Mariana, Liliana Perez, Roberto Molowny-Horas, and Marcel Darveau. 2019. “Hybrid Spatiotemporal Simulation of Future Changes in Open Wetlands: A Study of the Abitibi-Témiscamingue Region, Québec, Canada.” *International Journal of Applied Earth Observation and Geoinformation* 74: 302–13. https://doi.org/10.1016/j.jag.2018.10.001.

Tremblay, Junior A, Yan Boulanger, Dominic Cyr, Anthony R Taylor, David T Price, and Martin-Hugues St-Laurent. 2018. “Harvesting Interacts with Climate Change to Affect Future Habitat Quality of a Focal Species in Eastern Canada’s Boreal Forest.” *PLoS One* 13 (2): e0191645.

Truquet, Lionel. 2020. “Coupling and perturbation techniques for categorical time series.” *Bernoulli* 26 (4): 3249–79. https://doi.org/10.3150/20-BEJ1225.

Van der Vaart, Aad W. 2000. *Asymptotic Statistics*. Vol. 3. Cambridge University Press.

Venable, Kar’retta, John M Johnston, Stephen D LeDuc, and Lourdes Prieto. 2024. “Model Linkage to Assess Forest Disturbance Impacts on Water Quality: A Wildfire Case Study Using LANDIS (II)-VELMA.” *Environmental Modelling & Software* 180: 106134.

Venier, LA, and SB Holmes. 2010. “A Review of the Interaction Between Forest Birds and Eastern Spruce Budworm.” *Environmental Reviews* 18 (NA): 191–207.

Venier, Lisa A, Ian D Thompson, Richard Fleming, J Malcolm, Isabelle Aubin, John A Trofymow, David Langor, et al. 2014. “Effects of Natural Resource Development on the Terrestrial Biodiversity of Canadian Boreal Forests.” *Environmental Reviews* 22 (4): 457–90.

Volney, W Jan A, and Richard A Fleming. 2000. “Climate Change and Impacts of Boreal Forest Insects.” *Agriculture, Ecosystems & Environment* 82 (1-3): 283–94.

Volney, W.J.A., Fleming, R.A., 2007. “Spruce Budworm (Choristoneura Spp.) Biotype Reactions to Forest and Climate Characteristics.” *Global Change Biology* 13 (8): 1630–43.

Walker, Xanthe J, Jennifer L Baltzer, Steven G Cumming, Nicola J Day, Christopher Ebert, Scott Goetz, Jill F Johnstone, et al. 2019. “Increasing Wildfires Threaten Historic Carbon Sink of Boreal Forest Soils.” *Nature* 572 (7770): 520–23.

Wang, Yan. 2019. “Analysis of a Budworm Growth Model with Jump–Diffusion.” *Physica A: Statistical Mechanics and Its Applications* 531: 121763.

Wang, Yonghe. 2024. “The Effect of Climate Change on Forest Fire Danger and Severity in the Canadian Boreal Forests for the Period 1976–2100.” *Journal of Geophysical Research: Atmospheres* 129 (4): e2023JD039118.

Wang, Zhaoguo, Zhenghu Zhou, and Chuankuan Wang. 2021. “Defoliation-Induced Tree Growth Declines Are Jointly Limited by Carbon Source and Sink Activities.” *Science of the Total Environment* 762: 143077.

Ward, Samuel F, Roger D Moon, and Brian H Aukema. 2019. “Implications of Seasonal and Annual Heat Accumulation for Population Dynamics of an Invasive Defoliator.” *Oecologia* 190: 703–14.

Watha-Ndoudy, Noël, Claude Mélaine Dipakama, JD Nzila, Isidore Nguelet-Moukaha, and Victor Kimpouni. 2022. “Impact de l’orpaillage Sur Les écosystèmes Forestiers Du Secteur de Souanké, république Du Congo.” *European Scientific Journal, ESJ* 18: 169.

Watt, Graham A, Brian J Stocks, Richard A Fleming, and Sandy M Smith. 2020. “Stand Breakdown and Surface Fuel Accumulation Due to Spruce Budworm (Choristoneura Fumiferana) Defoliation in the Boreal Mixedwood Forest of Central Canada.” *Canadian Journal of Forest Research* 50 (6): 533–41.

Weiß, Christian H. 2018. “An Introduction to Discrete-Valued Time Series.” In, 73–94. John Wiley & Sons.

Weiß, Christian. 2020. “Regime-Switching Discrete ARMA Models for Categorical Time Series.” *Entropy* 22 (4): 458.

Wickham, H, R François, L Henry, and K Müller. 2023. “Vaughan, d. Dplyr: A Grammar of Data Manipulation.” *R Package Version* 1 (2).

Wilson, Jake, and John Graham. 2005. “Relationships Between First Nations and the Forest Industry: The Legal and Policy Context.”

Wolf, Kyra D, Philip E Higuera, Kimberley T Davis, and Solomon Z Dobrowski. 2021. “Wildfire Impacts on Forest Microclimate Vary with Biophysical Context.” *Ecosphere* 12 (5): e03467.

Wyatt, Stephen. 2008. “First Nations, Forest Lands, and ‘Aboriginal Forestry’ in Canada: From Exclusion to Comanagement and Beyond.” *Canadian Journal of Forest Research* 38 (2): 171–80.

Xu, Wenhuan, and Masumi Hisano. 2024. “Spatial Variation in Boreal Forest Responses to Global Environmental Change in Western Canada.” *Agricultural and Forest Meteorology* 355: 110140.

Yataco, Allison Pamela, Sabina Noor, Miguel Montoro Girona, Timothy Work, and Emma Despland. 2024. “Limited Differences in Insect Herbivory on Young White Spruce Growing in Small Open Plantations and Under Natural Canopies in Boreal Mixed Forests.” *Insects* 15 (3): 196.

Zhang, Bo, David A MacLean, Rob C Johns, and Eldon S Eveleigh. 2018. “Effects of Hardwood Content on Balsam Fir Defoliation During the Building Phase of a Spruce Budworm Outbreak.” *Forests* 9 (9): 530.

Zhu, Chenghao, Xiaoli Zhang, Ning Zhang, Mohammed Abdelmanan Hassan, and Lin Zhao. 2018. “Assessing the Defoliation of Pine Forests in a Long Time-Series and Spatiotemporal Prediction of the Defoliation Using Landsat Data.” *Remote Sensing* 10 (3). https://doi.org/10.3390/rs10030360.